The Effects of Aging on EGFR/pSTAT3-Dependent Gliovascular Structural Plasticity

By

William A. Mills III

Dissertation submitted to the Faculty of the Virginia Polytechnic Institute and State University in Partial fulfillment of the requirements for the degree of

Doctor of Philosophy

In

Translational Biology, Medicine, & Health

Committee Members:

Harald Sontheimer, Chairmen

Michelle Olsen

Michael Fox

John Chappelle

May 10th, 2021

Roanoke, VA

Keywords: astrocytes, aging, pSTAT3, EGFR, gliovascular unit, neurovascular coupling, blood-brain barrier, astrogliosis, gliosis

The Effects of Aging on EGFR/pSTAT3-Dependent Gliovascular Structural Plasticity

William A. Mills III

Academic Abstract

Astrocytes comprise the most abundant cell population in human brain (1). First described by Virchow as being 'glue' of the brain (2), modern research has truly extended our knowledge and understanding regarding the vast array of roles these cells execute under normal physiological conditions. Examples include neurotransmitter reuptake at the synapse (3), the regulation of blood flow at capillaries to meet neuronal energy demand (4), and maintenance/repair of the blood-brain barrier (BBB) (5), which is comprised, in part, of tight junction proteins such zonula-occludens-1 (ZO1) (6) and Claudin-5 (7). Underlying the execution of these processes is the morphological and spatial arrangement of astrocytes between neurons and endothelial cells comprising blood vessels, where comprehensively speaking, these cells form what is known as the gliovascular unit (8). Astrocytes extend large processes called endfeet that intimately associate with and enwrap up to 99% of the cerebrovascular surface (9). Disruptions to this association can occur in the form of retracted endfeet, and this has been characterized in several disease states such as major depressive disorder (10-12), ischemia (13-15), and normal biological aging (16-18). Disruption can also take the form of cellular/protein aggregate intercalation, which our lab previously characterized in a human-derived glioma model (19) and vascular amyloidosis human Amyloid Precursor Protein J20 (hAPPJ20) animal model (20). In both models, focal astrocyte-vascular disruptions coincided with perturbations to astrocyte control of blood flow, with deficits in BBB integrity present in the glioma model as well.

These findings lead to the preliminary work in this dissertation where we aimed to extend BBB findings in the glioma model to the hAPPJ20 vascular amyloidosis model. Immunohistochemical analysis in two-year old hAPPJ20 animal arterioles revealed that indeed in locations of vascular amyloid buildup and endfoot separation, there was a significant reduction in a tight junction protein critical for BBB maintenance, ZO1. This reduction in ZO1 expression was accompanied by extravasation of 70kDa FITC and the ~1kDa Cadaverine, suggesting that BBB integrity was compromised. These findings led to the **objective of this dissertation**, which was to determine if focal ablation of an astrocyte is sufficient to disrupt BBB integrity. By utilizing the *in vivo* 2Phatal single-cell apoptosis induction method (21), we found that 1) focal loss of astrocyte-vascular coverage does not result in barrier deficits, but rather induces a plasticity response whereby

surrounding astrocytes extend processes to reinnervate vascular vacancies no longer occupied by previously ablated astrocytes. 2) Replacement astrocytes are capable of inducing vasocontractile responses in blood vessels, and that 3) aging significantly attenuates the kinetics of this process. We then tested the ***hypothesis*** that focal loss of astrocyte-vascular coverage leads to a gliovascular structural plasticity response, in part, through the phosphorylation of signal transducer and activator of transcription 3 (STAT3) by Janus Kinase 2 (JAK2). This dissertation found that 4), this was indeed the case, and finally, 5) we determined that gliovascular structural plasticity occurs after reperfusion post-focal photothrombotic stroke. Together, the work presented in this dissertation sheds light on a novel plasticity response whereby astrocytes maintain continual cerebrovascular coverage and therefore physiological control. Future studies should aim to determine if 1) astrocytes also replace the synaptic contacts with neighboring neurons once held by a previous astrocyte, and 2) what therapeutic opportunity gliovascular structural plasticity may present regarding BBB repair following stroke.

The Effects of Aging on EGFR/pSTAT3-Dependent Gliovascular Structural Plasticity

William A. Mills III

General Audience Abstract

Astrocytes are the most abundant cell type in the brain. Their anatomical relationship to neurons and endothelial cells allows them to execute many vital brain functions, and comprehensively speaking, these cells form what is known as the gliovascular unit. Important for maintaining the expression of proteins preventing vascular leakage in the brain are molecules released from astrocytes processes called endfeet. These endfeet intimately enwrap blood vessels, and disruptions to endfeet-vascular coverage often coincide with vascular leakage in the brain. This dissertation therefore aimed to determine if astrocyte-vascular coverage is necessary in preventing vascular leakage. State-of-the art imaging in live animals determined this not to be the case, and rather found that focal loss of astrocyte-vascular coverage induces a plasticity response wherein neighboring astrocytes extend new endfeet to reinnervate vascular vacancies. Furthermore, we found that the kinetics of endfoot replacement are significantly reduced in aging, and that the phosphorylation of signal transducer and activator of transcription 3 (STAT3) is a critical arbiter underlying this response. Finally, given that we found endfoot replacement to occur in locations of lost astrocyte-vascular contact following reperfusion post-focal photothrombotic stroke, these findings may have implications regarding repair of the blood-brain barrier following CNS insults such as stroke.

References

1. Herculano-Houzel S. The human brain in numbers: a linearly scaled-up primate brain. *Frontiers in Human Neuroscience*. 2009. doi: 10.3389/neuro.09.031.2009
2. Virchow R. Uber das granulierte ansehen der Wandungen der Gerhirnventrikel. *Allg Z Psychiatr*. 1846; 3:242-250.
3. Kimelberg H & Nedergaard M. Functions of Astrocytes and their Potential as Therapeutic Targets. *Neurotherapeutics: The Journal of the American Society for Experimental Neurotherapeutics*. 2010; 7: 338-353. doi: 10.1016/j.nurt.2010.07.006
4. Mishra A, Reynolds JP, Chen Y, Gourine AV, Rusakov DA, Attwell D. Astrocytes mediate neurovascular signaling to capillary pericytes but not to arterioles [published correction appears in Nat Neurosci. 2017 Jul 26;20(8):1189] [published correction appears in Nat Neurosci. 2020 Sep;23(9):1176]. *Nat Neurosci*. 2016;19(12):1619-1627. doi:10.1038/nn.4428
5. Faulkner JR, Herrmann JE, Woo MJ, Tansey KE, Doan NB, & Sofroniew MV. Reactive astrocytes protect tissue and preserve function after spinal cord injury.Journal of Neuroscience, 24(9), 2143 2155.https://doi.org/10.1523/JNEUROSCI.3547-03.2004
6. Nitta T et al. Size-selective loosening of the blood-brain barrier in claudin-5 deficient mice. *The Journal of Cell Biology*. 2003; 161: 653-660. doi: 10.1083/jcb.200302070.
7. Hagan N & Ben-Zvi A. The molecular, cellular, and morphological components of blood-brain barrier developing during embryogenesis. *Seminars in cell & developmental biology*. 2015; 38:7-15. doi: 10.1016/j.semcdb.2014.12.006.
8. Abbott NJ, Rönnbäck L, & Hansson E. Astrocyte-endothelial interactions at the blood-brain barrier. *Nature Reviews Neuroscience.* 2006; 7: 41-53. doi: 10.1038/nrn1824
9. Watanabe K, Takeishi H, Hayakawa T, Sasaki H. Three-dimensional organization of the perivascular glial limiting membrane and its relationship with the vasculature: a scanning electron microscope study. Okajimas folia anatomica Japonica. 2010; 87: 109-121
10. Rajkowska, G., Hughes, J., Stockmeier, C. A., Javier Miguel-Hidalgo, J., & Maciag, D.(2013). Coverage of blood vessels by astrocytic endfeet is reduced in major depressivedisorder.Biological psychiatry,73(7), 613–621.https://doi.org/10.1016/j.biopsych.2012.09.02411.
11. Gudmundsson P, Skoog I, Waern M, Blennow K, P·lsson S, Rosengren L, Gustafson D. Therelationship between cerebrospinal fluid biomarkers and depression in elderly women.Am J Geriatr Psychiatry. 2007;15:832. doi: 10.1097/JGP.0b013e3180547091.12.
12. Bechter K, Reiber H, Herzog S, Fuchs D, Tumani H, Maxeiner HG. Cerebrospinal fluidanalysis in affective and schizophrenic spectrum disorders: identification of subgroups with immune responses and blood-CSF barrier dysfunction. J Psychiatr Res.2010;44:321–330. doi: 10.1016/j.jpsychires.2009.08.008.
13. Frydenlund, D. S., Bhardwaj, A., Otsuka, T., Mylonakou, M. N., Yasumura, T., Davidson,K. G., et al. (2006). Temporary loss of perivascular aquaporin-4 in neocortex after transient middle cerebral artery occlusion in mice.Proc. Natl. Acad. Sci. U S A103,13532–13536. doi: 10.1073/pnas.060579610314.
14. Steiner, E., Enzmann, G. U., Lin, S., Ghavampour, S., Hannocks, M. J., Zuber, B., et al.(2012). Loss of astrocyte polarization upon transient focal brain ischemia as a possible mechanism to counteract early edema formation.Glia60, 1646–1659. doi:10.1002/glia.2238315.
15. Wang, Y. & Parpura, V. Central Role of Maladapted Astrocytic Plasticity in Ischemic Brain Edema Formation.Front. Cell. Neurosci10,129 (129)
16. Chen A, Akinyemi RO, Hase Y, Firbank MJ, Ndung'u MN, Foster V, Craggs LJ, Washida K,Okamoto Y, Thomas AJ, Polvikoski TM, Allan LM, Oakley AE, O'Brien JT, Horsburgh K,Ihara M, Kalaria RN. Frontal white matter hyperintensities, clasmatodendrosis andgliovascular abnormalities in ageing and poststroke dementia. Brain. 2016; 139(Pt 1):242-258. doi: 10.1093/brain/awv32817.
17. Montagne A, Barnes SR, Sweeney MD, Halliday MR, Sagare AP, Zhao Z, Toga AW, JacobsRE, Liu CY,Amezcua L, Harrington MG, Chui HC, Law M, Zlokovic BV. Blood-Brain Barrier Breakdown in the Aging Human Hippocampus. Neuron; 85(2): 296-302.18.

18. Elahy M, Jackaman C, Mamo JCL, Lam V, Dhaliwal SS, Giles C, Nelson D, Takechi R. Blood-brain barrier dysfunction developing during normal aging is associated with inflammation and loss of tight junctions but not with leukocyte recruitment. ImmunAgeing. 2015; 12:2. doi: 10.1186/s11979-015-0029-9.
19. Watkins S, Robel S, Kimbrough IF, Robert SM, Ellis-Davies G, Sontheimer H. Disruption of astrocyte-vascular coupling and the blood-brain barrier by invading glioma cells. Nature Communications, 5, 4196. doi: 10.1038/ncomms5196
20. Kimbrough IF, Robel S, Roberson ED, Sontheimer H. Vascular amyloidosis impairs the gliovascular unit in a mouse model of Alzheimer's disease. Brain, 138(12). doi: 10.1093/brain/awv327.
21. Hill RA, Damisah EC, Chen F, Kwan AC, Grutzendler J. Targeted two-photon chemical apoptotic ablation of defined cell types in vivo. Nature Communications. 2017; 8, 15837. doi: 10.1016/j.bbrc.2016.08.088.

Dedication

To my mother, grandmothers, dear friend Megan, and father. I *think* you would have been proud mom, and you too memaw, though I'm not entirely sure. How I wish all of you could have made it to the end! Dad, you modeled for me what it meant to be 'sorrowful, yet always rejoicing.' There's never been a time in my life where I needed to understand how to live that more than these past six years. Thanks for being the rock that you are.

Acknowledgements

Harry, I remember most of our early conversations and doubt I'll ever forget them. The first time I sat in your office you told me I would be successful wherever I went. Nobody of your status had ever expressed that confidence in me, and that conversation inspired me to press on when things got bad. It inspired me to press on when things got really bad. Thanks for allowing me to learn how to be independent and also enabling me to acquire a healthy dose of confidence in myself.

Ian, I could not have asked for a better secondary mentor in graduate school. We accomplished many things together in the laboratory and classroom. Thanks for being patient with me in this graduate school journey and for investing so much in my professional and personal development.

Rachel, you are my best friend. Nobody understands me quite like you, and I know I could not have made this journey without you.

Mike, I have often looked out at academia and wondered who I could be like. You are an incredible scientist, mentor, leader, and person. Thanks for caring about me even when my training wasn't your responsibility.

Dr. Theus, thanks for offering mentorship when I needed it.

Sujith, thank you for those early-morning basketball sessions filled with great advice and camaraderie. Maybe it was just fun exercise for you, but it was much more to me.

James, Tate, Brett, Ryan, Wesley, Wes, Joe, and Dan- thanks for being my brothers and for caring about me.

Troy and Sparsh, thank you for listening to me discuss the same topics over and over and for being great friends.

Table of Contents

Chapter 1

Introduction and Preliminary Work

Introduction

Astrocytes extend processes called endfeet that are thought to encapsulate more than 99% of the cerebrovascular surface (1). Due to this intimate association, astrocyte endfeet are situated in a nexus that enables interaction with endothelial cells as well as the surrounding vascular mural cells (pericytes on capillaries and smooth muscle cells on arterioles/venules) (**Figure 1A**). Through the release of angiogenic signals (2-6), astrocytes induce expression of tight junction proteins that form the blood-brain barrier (BBB), and can regulate local blood flow ("functional hyperemia") through the release of vasoactive molecules such as Prostaglandin E2 (7-8). Consequently, any condition that compromises the structure or function of endfeet can cause impairments in blood flow or the BBB. In a previous study (9), we demonstrated that invading glioma cells along the vasculature peel endfeet away, resulting in reduced expression of tight junction proteins Zonula-Occludens 1 (ZO-1) and Claudin 5 along with the extravasation of various molecular weight dyes. Additionally, using the hAPPJ20 model of familial Alzheimer disease (AD) we demonstrated (10), vascular amyloid deposits aggregate between the astrocytic endfeet and vessel wall (**Figure 1C-D**). These amyloid laden vessels showed an impaired ability to regulate vascular tone and blood flow upon stimulation.

Given the observed BBB deficits in the glioma model, this dissertation initially aimed to determine if BBB breaches also occurred in locations of amyloid deposition and perturbed endfoot-vascular interactions. Initial studies demonstrated that three-dimensional accumulation of vascular amyloid occurs over time—a phenotype that presented with significant reductions in the expression of tight junction protein ZO-1. This was further accompanied by extravasation of 70kDa and ~1kDa molecules. Taken together, the aforementioned results led us to ask if the focal ablation of an astrocyte is sufficient to induce breaches in BBB integrity. While numerous *in vitro* cell culture studies suggested this could be the case (11,12), *in vivo* evidence was lacking. We therefore adopted the targeted two-photon chemical apoptotic (2Phatal) single-cell ablation method (13) to focally strip penetrating arterioles of astrocyte coverage *in vivo*. Furthermore, we utilized aged mice in our study to determine what aspect of the BBB phenotype in the J20 model was due solely to endfoot separation and/or the process of normal biological aging.

In contrary to anticipated results, evidence revealed that focal removal of astrocyte-vascular coverage was not sufficient to induce breaches in BBB integrity. It was, however, sufficient to induce a plasticity response in which surrounding astrocytes extend processes to reinnervate vascular vacancies. For the sake of this dissertation, this process will be referred to as gliovascular structural plasticity (GSP). In continued studies we determined that GSP remained intact at all levels of the vascular tree and that normal biological aging significantly reduces GSP kinetics. Furthermore, we determined that replacement astrocytes are capable of vasoconstricting pre-capillary arterioles and that GSP occurs following reperfusion post-focal photothrombotic stroke. We then pharmacologically tested the ***hypothesis*** that focal loss of astrocyte-vascular coverage leads to gliovascular structural plasticity through the phosphorylation of Signal Transducer and Activator of Transcription 3 (STAT3) by Janus Kinase 2 (JAK2) and observed this to be the case.

Significance: These studies have characterized a novel aspect of gliovascular biology and the consequences of normal biological aging on this physiological process. Though our studies determined that astrocytes are not necessary for BBB maintenance in the young and aged brain, astrocytes have been shown to be necessary for BBB repair. This has relevance given that GSP occurs in response to the loss of astrocyte-vascular coverage following reperfusion post-focal photothrombotic stroke, a CNS insult accompanied by BBB breakdown. Future studies should aim to determine if elimination of GSP following stroke prolongs the time to BBB repair in regions of lost vascular coverage. They should also clarity if replacement astrocytes integrate into sites of synaptic contact occupied by previous astrocytes and what relevance this may have for neurovascular coupling at precapillary arterioles.

Preliminary Work

What is Alzheimer Disease?

Alzheimer Disease (AD) is a neurodegenerative disease that causes progressive dementia and can be uniquely identified by amyloid β (Aβ) plaques and neurofibrillary tangles (NFTs) (14). NFTs are composed of the hyper-phosphorylated microtubule-associated protein tau (pTau) (15); amyloid plaques form from Aβ protein

aggregation (16)-a process that begins when type I transmembrane amyloid precursor protein (APP) (17-18) is sequentially cleaved by β- and γ-secretases (19) (**Figure 2**). Following intramembrane cleavage at the γ-secretase site, amyloid exists as a monomer, the most common variants of which are $A\beta_{40}$ and $A\beta_{42}$ (20,21). From this monomeric form, amyloid accumulation continues through an oligomerization and fibrillogenesis stage until finally reaching the terminal plaque phase (22). It is this step-wise process of amyloid accumulation that constitutes the foundation of the amyloid cascade hypothesis. Here, all of the pathological phenotypes documented in AD—including neuronal loss, synaptic failure, synapse loss, and dementia—are postulated to occur as a result of APP processing, Aβ oligomerization and fibrillogenesis (14,23). Definitive evidence showing that amyloid accumulation is causative of AD pathogenesis, however, is currently lacking (14).

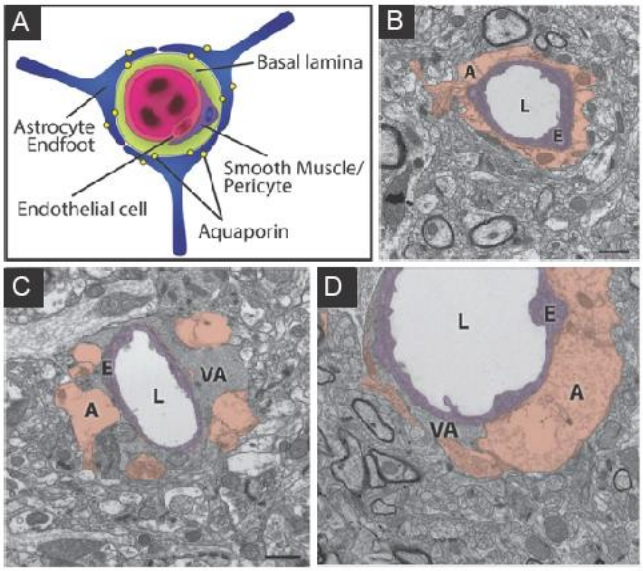

Figure 1: (A) The gliovascular unit (B) EM showing intact vascular coverage of the vasculature (C) EM showing astrocyte completely or (D) partially displaced from the blood vessel by vascular amyloid (VA). E: endothelial cell, L: lumen. A: astrocyte. Scale bar 1µm. Reproduced with permission from Kimbrough et. al 2015

Epidemiological studies reveal that AD is the most common form of dementia in the elderly (24) and the sixth leading cause of death in the United States (25). It affects females twice as often as males (24), and an estimated 14 million Americans will live with AD by 2050 (24). This could easily overwhelm our health care systems and result in a total cost of 1.1 trillion dollars (24). In light of this, research efforts have aimed to develop therapeutic interventions capable of slowing or preventing this disease. However, currently there are only five FDA-approved drugs aimed at helping treat symptomology such as memory loss and mood and sleep disorders. These drugs, however, have limited efficacy, and their effects have been shown to diminish over time with long-term use (24).

Given this slow therapeutic progress and the expected doubling in disease prevalence to occur by 2030 (24), the National Institute on Aging and Alzheimer's Association (NIA-AA) recently developed a biomarker-

based classification system to aid researchers in developing hypotheses that address the underlying pathological processes of AD (14). This AT(N) classification system is based off the evidence-based belief that Aβ deposition (A), pathologic tau (T), and neurodegeneration (N) allow for a definitive diagnosis of AD (26). The advent of technology capable of measuring peptide levels in cerebrospinal fluid (CSF) or brain imaging of live patients has enabled the formulation of this biological definition of AD. Specifically, Aβ plaques are indicated by cortical amyloid positron emission tomography (PET) ligand binding (27,28), or low CSF $A\beta_{42}$ (29-31). Elevated CSF phosphorylated tau (P-tau) and cortical tau PET ligand binding denote fibrillar tau presence (30, 32-34). Finally, CSF T-tau (35), fluorodeoxyglucose (FDG) PET hypometabolism, and atrophy on magnetic resonance imaging (MRI) (36-42) all indicate neurodegeneration or neuronal injury.

Binarizing these biomarkers gives eight possible categorizations for patients (**Table 1**), and thus AD is now viewed as a continuum rather than the three distinct clinical phases proposed in 2011 (43). Having evidence of Aβ deposition alone results in a label of "Alzheimer's pathologic change". A diagnosis of AD is given when positive biomarker evidence for both A and T, or A, T, and N are detected. Testing negative for A but positive for the other two categories is deemed a non-AD pathologic change. Finally, having biomarker evidence for A and N without T represents pathologic changes indicative of AD and other dementias (14).

The use of biomarkers now allows for a definitive diagnosis in living individuals and officially sever clinical symptoms from disease classification, which has been a major milestone for AD research. Historically, AD was only definitively diagnosed at autopsy or was classified as probable AD in living patients (44), which effectively meant that the disease burden was likely too great for any hope of therapeutic intervention by the time a diagnostic decision was reached. Taken together, advances in biomarker research offer hope for therapeutic intervention aimed at slowing disease progression long before symptoms present themselves, and future research will continue to address hypotheses developed from the AT(N) framework.

Mouse models of Alzheimer Disease

Mouse models of autosomal dominant AD are based on mutations to the amyloid precursor protein (APP) along with presinilin 1 and 2 genes (PSEN1 and PSEN2) (45-48). These three mutations all directly impact Aβ

AT(N) profiles	Biomarker Category	
A-T-(N)-	Normal AD biomarkers	
A+T-(N)-	Alzheimer's pathologic change	Alzheimer's continuum
A+T+(N>	Alzheimer's disease	
A+T+(N)+	Alzheimer's disease	
A+T-(N)+	Alzheimer's and concomitant suspected non-Alzheimer's pathologic change	
A-T+(N)-	Non-AD pathologic change	
A-T-(N)+	Non-AD pathologic change	
A-T+(N)+	Non-AD pathologic change	

Table 1- Eight different AD biomarker profiles are possible based on binarizing the AT(N) system. Patients are placed into one of three possible categories based on their biomarker profile: patients with normal biomarker profiles, patients with a non-AD pathologic change (green), and patients in the Alzheimer's continuum (blue). Table modified from Jack et. al 2018 (14).

Mouse Models of Alzheimer Disease continued

production through the processing of APP (49-52). As mentioned above, APP is a type 1 transmembrane protein with a large extracellular amino-terminal domain. β-secretase cleaves APP at a site in the extracellular space whereas γ-secretase cleaves APP at a site within the membrane (53-54). Most AD-inducing mutations in the APP gene occur at these two sites and are named according to the geographic location from which the first family reported to have the mutation originated (55) (**Figure 2**). Other APP mutations such as the Dutch and Arctic variants occur within the amino acid sequence comprising the Aβ portion of the APP gene (56-57). The aforementioned point mutations are not the only AD-causing changes, and as such, increasing APP gene copy number has been one other method used to model AD. Such changes have also been found in multiple families (58) along with down's syndrome patients. Given APP's position on chromosome 21, individuals with down's syndrome possess three APP gene copy numbers and develop early-onset AD, typically in their 40s (59). Finally, the presinilin genes encode the catalytic subunit of γ-secretase (53-54), and AD-inducing mutations to these genes result in an increased $A\beta_{42}/A\beta_{40}$ ratio (48, 60-62).

Our studies from **Figure 1** specifically utilized the hAPPJ20 mouse model of AD, which expresses the human version of APP (hAPP) under the control of the Platelet Derived Growth Factor-subunit B promoter (63-64). This model possesses two mutations, the K670N/M671L double mutation at the β-secretase cleavage site and the V717F mutation at the γ-secretase cleavage site (63) (**Figure 2**). Physiologically speaking, the double mutation (known as the Swedish mutation) results in both increased $A\beta_{40}$ and $A\beta_{42}$ production due to increase β-secretase activity (50,52). The other mutation (known as the Indiana mutation) results in production of more $A\beta_{42}$ relative to $A\beta_{40}$, with $A\beta_{42}$ considered the more toxic of the two (49, 51-52). Relevant to our studies, this model presents with robust vascular amyloidosis and gliosis, and mice possess cognitive deficits as well (10, 63).

Finally, two considerations should be kept in mind regarding the use of AD animal models in research. First, though familial forms of AD comprise only a modicum of total cases, clinicians agree that the similarities to the sporadic form of AD captured in these models are more notable than their differences. Second, while it would be desirable for AD mouse models to express every cognitive and pathological feature documented within the disease, this is not the case. Mouse models of AD should therefore be viewed as reductionist tools best suited to test therapeutic approaches aimed at inhibiting genes and proteins implicated in AD as well as elucidating their effects on basic brain function (55).

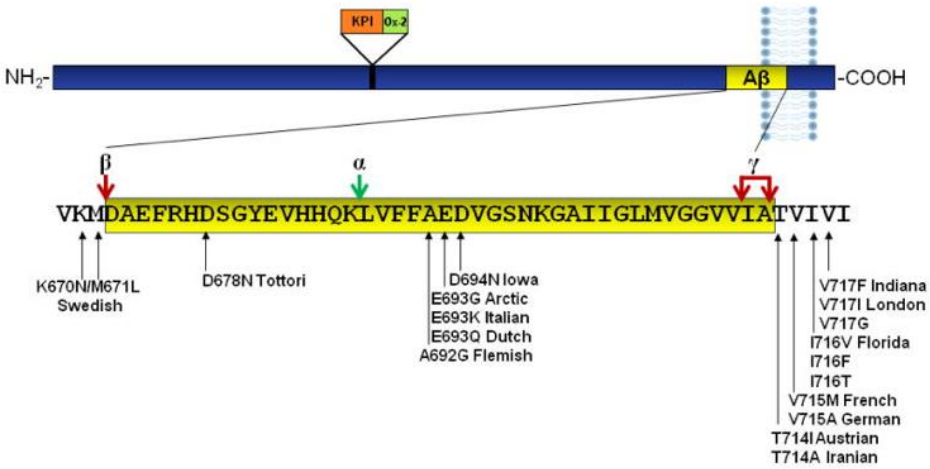

Figure 2-$A\beta_{42}$ production and APP mutations. Amino acids 672-713 of APP compose $A\beta_{42}$, which is produced through sequential cleavage by β-secretase, then γ-secretase. The production of $A\beta_{40}$ or $A\beta_{42}$ occurs depending on which site γ-secretase cleaves at. Aβ is not produced when α-secretase processes APP. Common mutations at the β- and γ-secretase cleavage sites along with intra-Aβ mutations are shown. Reproduced with permission from Hall et. al 2012.

Cerebral Amyloid Angiopathy: a vascular pathology marked by amyloid deposition

The two-hit vascular hypothesis of AD stands in opposition to the amyloid cascade hypothesis. In this paradigm, it is speculated that cerebrovascular damage occurring prior to detectable levels of Aβ is sufficient to induce neuronal injury and subsequent neurodegeneration (65-70). Documented examples of cerebrovascular damage include BBB breakdown and cerebral blood flow (CBF) reductions, and this 'first hit' can result from various vascular risk factors, such as hypertension and diabetes, as well as genetic risk factors, such as apolipoprotein E ε4 (APOE4) (70-75).

Neuronal injury is initiated by the accumulation of neurotoxic molecules that enter the brain due to BBB breakdown and due to hypoperfusion and the subsequent hypoxia from CBF reductions that exacerbate this condition (66,70). The onset of vascular damage can further engender the genesis of amyloid accumulation in the brain, which constitutes the 'second hit' (65-70). Thus, vascular damage can induce neuronal injury independent from or in association with Aβ.

Typically, 70-85% of Aβ levels in the brain are maintained through degradation and elimination via a transvascular route across the BBB (76-78). This transvascular route is maintained by the low-density lipoprotein receptor-related protein-1 (LRP1) (70-71, 76,78-80), which has decreased expression reported in aged endothelial cells (81). The remaining 15% of Aβ is removed by cerebrospinal fluid (CSF) absorption in the circulatory and lymphatic systems, the accumulation of which occurs via interstitial fluid bulk flow along penetrating arteries (76-78). Interestingly, one study found that partial endothelial nitric oxide synthase (eNOS) deficiency results in increased accumulation of $A\beta_{40}$ in the cerebrovasculature (82). Mice in this study go on to develop cerebral amyloid angiopathy (CAA) and CAA-associated pathology, including smooth muscle cell degeneration, microhemorrhages, and cognitive impairment (83). The findings from this model are relevant given that major cardiovascular risk factors, including hypertension, hypercholesterolemia, aging, and diabetes impair the production and/or biological activity of endothelial nitric oxide. Such inhibition can lead to the upregulation of both APP and β-secretase expression, as well as β-secretase activity (84). Taken together, any perturbation to

vascular function can exacerbate and lead to amyloid-induced pathology, as well as independently induce neuronal injury and degeneration.

As just mentioned, CAA is the accumulation of amyloid in the vascular wall of a blood vessel, typically the tunica media (85) and is found in 85-95% of AD patients (86-87). **Figure 3** depicts the appearance of amyloid deposits in pial vessels along the surface of the brain. This constitutes one of the pathological hallmarks first described by Stefanos Pantelakis, namely the selective accumulation of amyloid along leptomeningeal and cortical small arterioles and capillaries. Pantelakis further determined that amyloid deposition is primarily found in posterior lobar brain regions, particularly the occipital lobes (88), and that CAA is associated with aging and dementia. It lacks association, however, with white matter small vessels, systemic amyloidosis, as well as hypertension and arteriosclerosis (88). Clinically speaking, CAA can present with spontaneous lobar ICH and transient focal neurological episodes (89). In addition, it presents with cognitive impairment and dementia, with the cognitive profile resembling more of what is seen in classic vascular cognitive impairment rather than AD. Here, episodic memory remains preserved while executive function and processing speed are impaired (89). On a diagnostic level, key neuroimaging features of CAA include white matter hyperintensities, cortical superficial siderosis, cortical microinfarcts, multiple strictly lobar cerebral microbleeds, and MRI-visible perivascular spaces in the centrum semiovale (90).

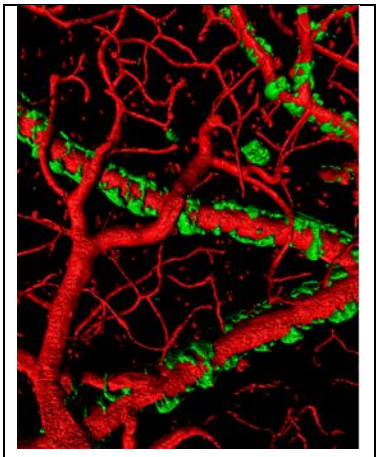

Fig 3- High-resolution 3D rendering created from *in vivo* multi-photon optical sections of a 15-month-old hAPPJ20 mouse. Amyloid deposits are shown in green. Reproduced with permission from Ian Kimbrough, PhD

Taken together, CAA stands as a unique pathological entity from AD that warrants further research. Its accumulation results from perivascular drainage failure (91-92), and given the toxic nature of amyloid accumulation, CAA only serves to further exacerbate pre-existing vascular deficits. **Given the shared molecular entity with AD, however, understanding CAA would provide an opportunity for both vascular and neurodegenerative pathways in AD to be united** (93)**.** This outcome could further foster therapeutic

developments that improve health in aging and avoids the looming economic impact that aging and AD will have on the population due to the expected doubling of AD-related dementias by 2060 (94).

Astrocytes, the BBB and CAA: loss of trophic support or toxic gain of function?

The BBB is a continuous structure localized to the membranes of adjacent endothelial cells (95). Composed of transmembrane tight junction proteins (96) such as Claudin-5 (97) and Zonula Occludens-1 (98), the BBB is impermeable to blood-born molecules including glucose and amino acids as well as immune cells (95). Such properties ensure that the central nervous system (CNS) internal milieu is continually maintained. Though CNS endothelial cells inherently express tight junction proteins in development, pericytes regulate their formation (99), and astrocytes stabilize expression through the release of soluble factors such as angiopoietin -1 (Ang1) (2-3) and Sonic Hedgehog (Shh) (4-6). Furthermore, contact between the astrocytic endfoot and endothelial cell has been shown to enhance barrier properties *in vitro* (100).

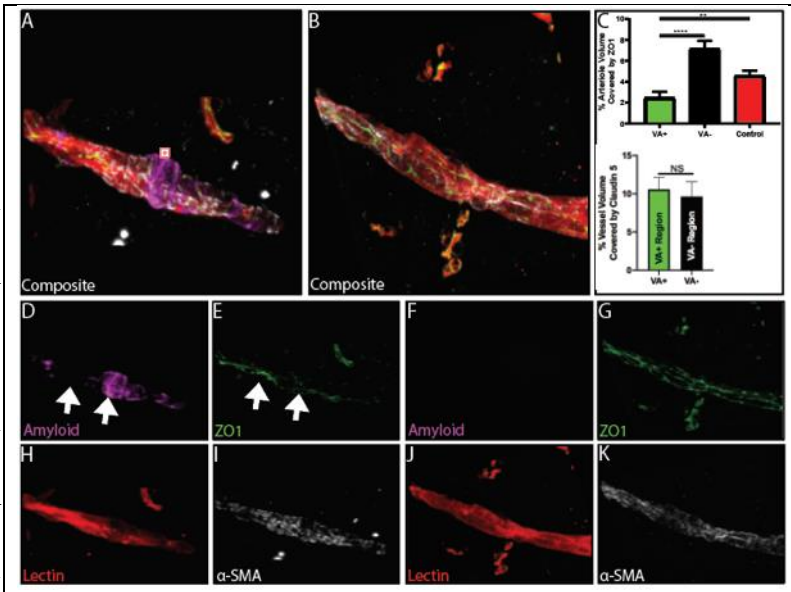

Fig. 4- ZO1 but not Claudin-5 is significantly reduced in regions of amyloid deposition (A) arteriole with amyloid deposition in center of vessel (B) arteriole without amyloid deposition (C) Quantitative volumetric analysis of ZO1 levels in arterioles of hAPPJ20+ mice with amyloid deposition relative to vessels without (green and black bar), or hAPPJ20+ arterioles with amyloid deposition relative to age-matched control vessels without (green and red bar) ***p<0.0001, **p<0.0016, n=41 arterioles/7 mice for each group (D, E, H, I) Individual channels for the larger representative image shown in A. Arrows indicate amyloid laden and free regions (F, G, J, K) Individual channels for the larger representative control image shown in B

Interestingly, a previous study demonstrated that hypoxic conditions lead to downregulation of Src-suppressed C Kinase Substrate (SSeCKS) (3). It was further shown that SSeCKS regulates the upregulation of Ang1 and downregulation Vascular Endothelial Growth Factor (VEGF). Onset of hypoxia therefore results in significant reductions to ZO-1 due to decreased activity of SSeCKS and downstream reduction of Ang1/increased production of VEGF. Thus, taken together with the results from **Figure 1** (10), we speculated that amyloid

deposition impaired the astrocytic endfoot from providing trophic support to the underlying vessel. This could occur either due to disruption of the normal gliovascular interface (lost contact) or a reduced activity of Ang1 due to hypoxic conditions known to coincide with CAA deposition. Most studies that have focused on astrocytes in AD have done so either in the context of amyloid production and clearance (102) or toxic gain-of-functions amyloid may induce in astrocytes, such as pro-inflammatory cytokine release (103-104). A focus on loss of trophic support therefore provided a novel direction in which to understand how CAA may affect the ability of astrocytes to regulate BBB integrity.

Results-Vascular amyloid accumulation over time results in three-dimensional encapsulation of blood vessels leading to subsequent reductions in ZO-1 and extravasation of various molecular weight molecules.

Using the hAPPJ20 familial mouse model of AD, we first wanted to determine if the tight junction proteins ZO-1 and Claudin 5 were significantly reduced in regions of amyloid deposition at penetrating arterioles. Previous work had already examined tight junction protein expression in capillaries laden with amyloid (101), and immunolabeling for α smooth actin allowed for definitive arteriole identification. Volumetric fluorescent image analysis from immunohistochemical studies revealed ZO1 but not Claudin 5 to be significantly reduced in regions of amyloid deposition relative to regions without, as well as amyloid laden vessels relative to age-matched control arterioles (**Figure 4A-C**).

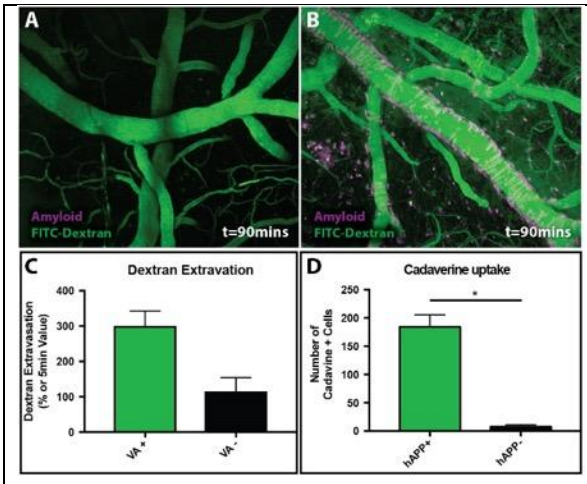

Fig. 5- Impaired BBB detected by infusion of 70kD FITC-dextran and Cadaverine. A. in vivo 19 mo hAPPJ20 mouse after IP administration of Methoxy-XO4. B. Substantial dye extravasation after only 1.5 h. C. Quantitative analyses of FITC- dextran extravasation p=0.0247 n=3/group. D. Quantitative analyses of Cadaverine uptake shows significant enhancement in hAPP+ compared to hAPP- mice. ***p=0.0001,****p=<0.0001 n=3 biological replicates/ group

In light of this, we next wanted to determine if breaches to BBB integrity accompanied ZO1 reductions. To do so, we retro-orbitally injected 70kDa FITC in hAPPJ20 mice and performed two-photon imaging through a cranial window. Upon injection, we measured the average intensity at baseline and 1.5 hours post-injection by placing

an ROI at locations adjacent to amyloid-laden or age-matched control vessels (**Figure 5A-B**). Preliminary results revealed that amyloid laden vessels exemplified a much larger increase in intensity 1.5 hours post-injection relative to age-matched control vessels (**Figure 5C**). We then retro-orbitally injected the ~1kDa Cadaverine in these same mice and harvested PFA fixed brains for further immunohistochemical analysis. Counting Cadaverine positive cells is a reliable method of determining dye extravasation as this dye is taken up into surrounding cells following extravasation from the vasculature. Following this methodology, our preliminary data revealed a significantly higher number of Cadaverine positive cells in the somatosensory cortex of hAPPJ20 mice relative to age-matched controls (**Figure 5D**).

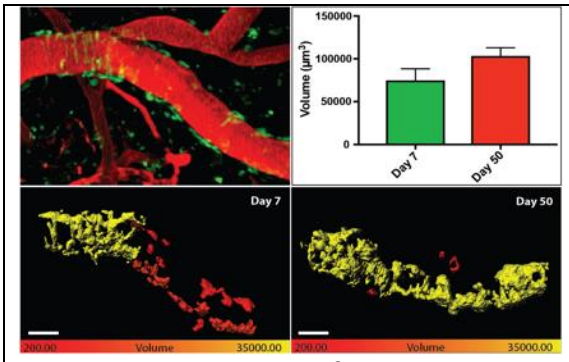

Fig. 6. Accumulation of vascular amyloid visualized through *in vivo* imaging of hAPPJ20 mice using the amyloid marker Methoxy-XO4. The exact same vessels were repeatedly imaged for 50 days respectively and coverage determined through statistical volume coding in Imaris with more yellow equating to more amyloid. n=3 biological replicates. Scale bar 20 µm.

In considering how astrocyte dysfunction may contribute to the observed BBB impairments, we hypothesized that the accumulation of amyloid leads to reduced expression of ZO1 by decreasing expression of Ang1, a molecule previously shown to regulate ZO1 expression (3). As a first step in addressing this hypothesis, we wanted to determine if vascular amyloid accumulated over time. To do so, we implanted cranial windows in hAPPJ20 mice following previously established methodology (10). Vascular amyloid was labeled by intraperitoneal injections of the congophilic dye Methoxy-XO4, which binds β-sheet rich structures found in fibrillogenic vascular amyloid. Arterioles were identified by retro-orbitally injecting Alexa-633 hydrazide. Repeatedly imaging vessels starting at day 7 post-operation (dpo) until dpo50 revealed that amyloid accumulates quite extensively over time (**Figure 6**). We then turned to immunohistochemistry to determine if Ang1 would be significantly reduced in amyloid laden regions relative to those without. Preliminary studies revealed this to indeed be the case (**Figure 7**), but future studies are needed to determine if the quantified fluorescence is derived from astrocytes or endothelial cells.

In light of the aforementioned data, we wanted to definitively determine if the focal ablation of an astrocyte is sufficient to disrupt blood-brain barrier integrity. To do so, we utilized the 2Phatal method of single-cell

ablation (13). This method utilizes the focal illumination properties of a femto-second pulsed laser to bleach the nucleic-acid binding Hoechst dye, which then induces apoptosis presumably through reactive oxygen species (ROS)-induced DNA damage. By repeatedly imaging at the time of endfoot retraction, we surprisingly found that focal removal of astrocyte-vascular coverage resulted in a plasticity response wherein neighboring astrocytes innervate vascular vacancies left by the previously ablated astrocyte (**Figure 8**). We therefore aimed to determine if this response occurred at all levels of the vascular tree as well as its physiological relevance. We also wanted to determine how normal biological aging would impact GSP. This was relevant as a study in aging would allow us to dissect apart how endfoot retraction from the vasculature impacts BBB integrity on an aged vessel versus amyloid accumulation. By eliminating one variable, we could begin to more reliably attribute causality to one entity versus the other (amyloid deposition versus endfoot retraction). Furthermore, given that both endfoot retraction and BBB breakdown have been shown to occur later in life (105), the results from this study could directly link these two phenotypes together. The following specific aims were therefore proposed to address this newfound direction.

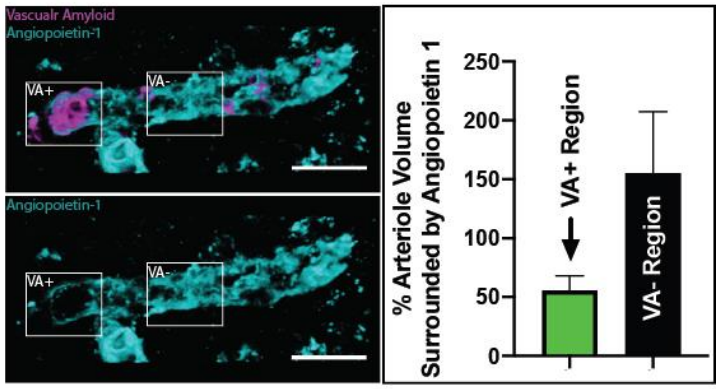

Fig. 7-Preliminary quantitative volumetric image analysis showing that Angiopoietin 1 is significantly reduced in regions of amyloid deposition relative to regions without.

Aim 1: Determine the effects of normal biological aging on gliovascular structural plasticity. Determine if replacement endfeet are able to restore BBB integrity and/or vasocontractile ability. It is unknown if astrocyte endfeet demonstrate structural plasticity in aging. Data from laser-ablation studies of individual astrocytes suggests that endfeet are dynamic, where endfeet from neighboring astrocytes can re-occupy vacated spaces on arterioles. Whether or not these endfeet are functional, however, remains to be determined. Recent studies have demonstrated that astrocytic processes become short and stubby with increasing age (106-111). Considering this and our data, we therefore proposed and expected to demonstrate through observational studies using 2-photon imaging through cranial windows that astrocytic endfeet innervate vascular vacancies at all levels

of the vascular tree in the adult brain. We further expected to demonstrate that the process of normal biological aging perturbed some aspect of GSP, either resulting in its loss altogether or perhaps reducing the kinetics of the response. Additionally, we expected to demonstrate that replacement endfeet in the adult brain are functional, either by restoring lost BBB integrity post-ablation and/or inducing a vasocontractile response upon laser-stimulation.

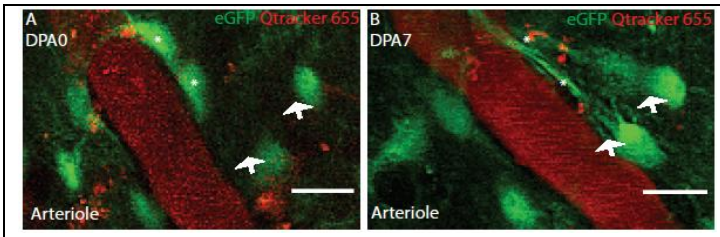

Fig. 8- A) 2Phatal ablation of astrocytes at an ateriole interface induces a replacement response from surrounding astrocytes B) 7 days later. Scale 20µm. * indicates ablated cells and arrows replacement astrocytes

Aim 2: Determine if the phosphorylation of signal transducer and activator of transcription 3 (STAT3) by Janus Kinase 2 (JAK2) is necessary for gliovascular structural plasticity. We ***hypothesized*** that the focal ablation of astrocyte would lead to GSP, in part, through the phosphorylation of STAT3 by JAK2. Many of the signaling molecules underlying changes in astrocyte morphology, such as Heparin-Binding Epidermal Growth Factor (112), Ciliary Neurotrophic Factor (113), Leukemia Inhibitory Factor (114), and Transforming growth factor β (115), all converge on the JAK-STAT pathway (116). This pathway is known to be a critical mediator of astrogliosis (20), and the morphology of replacement astrocytes from our preliminary data were suggestive of a focal astrogliosis response. We therefore turned to the JAK2 pharmacological inhibitor AG490 to test this hypothesis and quantified the ratio of increased astrocyte volume at day five post-ablation relative to baseline. Furthermore, we aimed to determine if breaches in BBB integrity would occur in regions of reduced endfoot replacement.

Overall, these studies have allowed us to determine that astrocyte endfoot replacement does occur at all levels of the vascular tree- and though the kinetics of replacement are significantly attenuated in aging- it occurs at a timescale whereby blood-brain barrier integrity is maintained. We have further determined that replacement endfeet are capable of vasoconstricting primary capillaries and that pSTAT3 is a necessary arbiter of the gliovascular structural plasticity response. Combined, these studies reveal a novel cellular and molecular

mechanism whereby astrocytes maintain cerebrovascular physiological integrity and have implications for how perturbed gliovascular interactions in various disease states contribute to cerebrovascular pathology.

References

1. Watanabe K, Takeishi H, Hayakawa T, Sasaki H. Three-dimensional organization of the perivascular glial limiting membrane and its relationship with the vasculature: a scanning electron microscope study. Okajimas folia anatomica Japonica. 2010; 87: 109-121

2. Obermeier B, Daneman R, & Ransohoff RM. Development, maintenance and disruption of the blood-brain barrier. Nat Medicine. 2013; 19: 1584-1596. Doi: 10.1038/nm.3407.

3. Lee SW, et al. SSeCKS regulates angiogenesis and tight junction formation in the blood-brain barrier. Nat Medicine. 2003;9:900-906.

4. Wang Y, Imitola J, Rasmussen S, O'Connor KC, & Khoury, SJ. Paradoxical dysregulation of the neural stem cell pathway sonic hedgehog-Gli1 in autoimmune encephalomyelitis and multiple sclerosis. Ann Neurol. 2008; 64: 417-427. Doi: 10.1002/ana.21457.

5. Alvarez JI, et. Al. The Hedgehog pathway promotes blood-brain barrier integrity and CNS immune quiescence. Science. 2011; 334: 1727-1731. Doi: 10.1126/science.1206936.

6. Daneman R, & Engelhardt B. Brain barriers in health and disease. Neurobiol Dis. 2017; 107: 1-3.doi: 10.1016/j.nbd.2017.05.008.

7. Gordon GR, Mulligan SJ, & MacVicar BA. Astrocyte control of the cerebrovasculature. Glia. 2007; 55:1214-1221.

8. Metea MR, & Newman EA. Glial cells dilate and constrict blood vessels: a mechanism of neurovascular coupling. J Neurosci. 2006; 26: 2862-2870.

9. Watkins S, Robel S, Kimbrough IF, Robert SM, Ellis-Davies G, Sontheimer H. Disruption of astrocyte-vascular coupling and the blood-brain barrier by invading glioma cells. Nature Communications, 5, 4196. doi: 10.1038/ncomms5196

10. Kimbrough IF, Robel S, Roberson ED, Sontheimer H. Vascular amyloidosis impairs the gliovascular unit in a mouse model of Alzheimer's disease. Brain, 138(12). doi: 10.1093/brain/awv327.

11. Tao-Cheng JH, Nagy Z, Brightman MW. Tight junctions of brain endothelium *in vitro* are enhanced by astroglia. Journal of Neuroscience. 1987; 7(10): 3293-3299. doi: 10.1523/jneurosci.07-10-03293

12. Rubin LL, Hall DE, Porter S, Barbu K, Cannon C, Homer HC, Janatpour M, Liaw CW, Manning K, Morales J. A cell culture model of the blood-brain barrier. Journal of Cell Biology. 1991; 115(6): 1725-1735. doi: 10.1083/jcb.115.6.1725

13. Hill RA, Damisah EC, Chen F, Kwan AC, Grutzendler J. Targeted two-photon chemical apoptotic ablation of defined cell types in vivo. Nature Communications. 2017; 8, 15837. doi: 10.1016/j.bbrc.2016.08.088.

14. Jack CR Jr, Bennett DA, Blennow K, et al. NIA-AA Research Framework: Toward a biological definition of Alzheimer's disease. *Alzheimers Dement*. 2018;14(4):535-562. doi:10.1016/j.jalz.2018.02.018

15. Grundke-Iqbal I, Iqbal K, Tung YC, Quinlan M, Wisniewski HM, Binder LI. Abnormal phosphorylation of the microtubule-associated protein tau (tau) in Alzheimer cytoskeletal pathology. *Proc Natl Acad Sci U S A*. 1986;83(13):4913-4917. doi:10.1073/pnas.83.13.4913

16. Colvin MTet al. Atomic resolution structure of monomorphic A beta(42) amyloid fibrils. *J. Am. Chem. Soc.* 2016 **138**: 9663–9674. doi:10.1021/jacs.6b05129

17. Glenner GG, and Wong CW. Alzheimer's disease: initial report of the purification and characterization of a novel cerebrovascular amyloid protein. *Biochem. Biophys. Res. Commun.* 1984b; 120:885–890. doi: 10.1016/s0006-291x(84)80190-4

18. Goedert, M., and Spillantini, M. G. A century of Alzheimer's disease. *Science* 2006; 314:777–781. doi: 10.1126/science.1132814

19. Acx, H., Chávez-Gutiérrez, L., Serneels, L., Lismont, S., Benurwar, M., Elad, N., et al. Signature amyloid β profiles are produced by different γ-secretase complexes. *J. Biol. Chem.* 2014;289:4346–4355. doi: 10.1074/jbc.m113.530907

20. Olsson F, Schmidt S, Althoff V, Munter LM, Jin S, Rosqvist S, *et al*. Characterization of intermediate steps in amyloid beta (Abeta) production under near-native conditions. *J Biol Chem* 2014; **289**: 1540–50.

21. Takami M, Nagashima Y, Sano Y, Ishihara S, Morishima-Kawashima M, Funamoto S, *et al*. Gamma-secretase: successive tripeptide and tetrapeptide release from the transmembrane domain of beta-carboxyl terminal fragment. *J Neurosci* 2009; **29**: 13042–52.
22. Jan A, Hartley DM, Lashuel HA. Preparation and characterization of toxic Abeta aggregates for structural and functional studies in Alzheimer's disease research. *Nat Protoc*. 2010;5(6):1186-1209. doi:10.1038/nprot.2010.72
23. Hardy J, & Selkoe DJ. The Amyloid Hypothesis of Alzheimer's Disease: Progress and Problems on the Road to Therapeutics. Science. 19 Jul 2002; 297(5580): 353-356. doi: 10.1126/science.1072994.
24. Alzheimer's Association Report. 2020 Alzheimer's disease facts and figures. Alzheimer's & Dementia. 10 Mar 2020; 16(3): 3910460. doi: 10.1002/alz.12068
25. Xu JQ, Murphy SL, Kochanek KD, Arias E. Mortality in the United States, 2018. NCHS Data Brief; No. 355. Hyattsville, MD: National Center for Health Statistics. 2020.
26. Jack CR Jr, Bennett DA, Blennow K, et al. A/T/N: An unbiased descriptive classification scheme for Alzheimer disease biomarkers. *Neurology*. 2016;87(5):539-547. doi:10.1212/WNL.0000000000002923
27. Klunk WE, Engler H, Nordberg A, Wang Y, Blomqvist G, Holt DP, et al. Imaging brain amyloid in Alzheimer's disease with Pittsburgh Compound-B. *Ann Neurol.* 2004;55:306–19.
28. Villain N, Chetelat G, Grassiot B, Bourgeat P, Jones G, Ellis KA, et al. Regional dynamics of amyloid-beta deposition in healthy elderly, mild cognitive impairment and Alzheimer's disease: a voxelwise PiB-PET longitudinal study. *Brain.* 2012;135:2126–39.
29. Fagan AM, Roe CM, Xiong C, Mintun MA, Morris JC, Holtzman DM. Cerebrospinal fluid tau/beta-amyloid(42) ratio as a prediction of cognitive decline in nondemented older adults. *Arch Neurol.* 2007;64:343–9.
30. Mattsson N, Zetterberg H, Hansson O, Andreasen N, Parnetti L, Jonsson M, et al. CSF biomarkers and incipient Alzheimer disease in patients with mild cognitive impairment. *JAMA.* 2009;302:385–93.
31. Visser PJ, Verhey F, Knol DL, Scheltens P, Wahlund LO, Freund-Levi Y, et al. Prevalence and prognostic value of CSF markers of Alzheimer's disease pathology in patients with subjective cognitive impairment or mild cognitive impairment in the DESCRIPA study: a prospective cohort study. *Lancet Neurol.* 2009;8:619–27.
32. Buerger K, Ewers M, Pirttila T, Zinkowski R, Alafuzoff I, Teipel SJ, et al. CSF phosphorylated tau protein correlates with neocortical neurofibrillary pathology in Alzheimer's disease. *Brain.* 2006;129:3035–41.
33. Brier MR, Gordon B, Friedrichsen K, McCarthy J, Stern A, Christensen J, et al. Tau and Aβ imaging, CSF measures, and cognition in Alzheimer's disease. *Sci Transl Med.* 2016;8 338ra66.
34. Chhatwal JP, Schultz AP, Marshall GA, Boot B, Gomez-Isla T, Dumurgier J, et al. Temporal T807 binding correlates with CSF tau and phospho-tau in normal elderly. *Neurology.* 2016;87:920–6.
35. Blennow K, Hampel H, Weiner M, Zetterberg H. Cerebrospinal fluid and plasma biomarkers in Alzheimer disease. *Nat Rev Neurol.* 2010;6:131–44.
36. Seab JP, Jagust WJ, Wong ST, Roos MS, Reed BR, Budinger TF. Quantitative NMR measurements of hippocampal atrophy in Alzheimer's disease. *Magn Reson Med.* 1988;8:200–8.
37. Fox NC, Cram WR, Scahill RI, Stevens JM, Janssen JC, Rossor MN. Imaging of onset and progression of Alzheimer's disease with voxel-compression mapping of serial magnetic resonance images. *Lancet.* 2001;358:201–5.
38. Minoshima S, Giordani B, Berent S, Frey KA, Foster NL, Kuhl DE. Metabolic reduction in the posterior cingulate cortex in very early Alzheimer's disease. *Ann Neurol.* 1997;42:85–94.
39. Besson FL, La Joie R, Doeuvre L, Gaubert M, Mezenge F, Egret S, et al. Cognitive and brain profiles associated with current neuroimaging biomarkers of preclinical Alzheimer's disease. *J Neurosci.* 2015;35:10402–11.
40. Dickerson BC, Bakkour A, Salat DH, Feczko E, Pacheco J, Greve DN, et al. The cortical signature of Alzheimer's disease: regionally specific cortical thinning relates to symptom severity in very mild to mild AD dementia and is detectable in asymptomatic amyloid-positive individuals. *Cereb Cortex.* 2009;19:497–510.

41. Knopman DS, Jack CR, Jr, Wiste HJ, Weigand SD, Vemuri R, Lowe VJ, et al. Selective worsening of brain injury biomarker abnormalities in cognitively normal elderly persons with beta-amyloidosis. *JAMA Neurol.* 2013;70:1030–8.
42. Landau SM, Harvey D, Madison CM, Koeppe RA, Reiman EM, Foster NL, et al. Associations between cognitive, functional, and FDG-PET measures of decline in AD and MCI. *Neurobiol Aging.* 2011;32:1207–18.
43. Dubois B, Hampel H, Feldman HH, Scheltens P, Aisen P, Andrieu S, et al. Preclinical Alzheimer's disease: definition, natural history, and diagnostic criteria. *Alzheimers Dement.* 2016;12:292–323.
44. McKhann G, Drachman D, Folstein M, Katzman R, Price D, Stadlan EM. Clinical diagnosis of Alzheimer's disease: report of the NINCDS-ADRDA Work Group under the auspices of Department of Health and Human Services Task Force on Alzheimer's Disease. *Neurology.* 1984;34:939–44
45. Goate A, Chartier-Harlin MC, Mullan M , Brown J, Crawford F, Fidani L, Giuffra L, Haynes A, Irving N, James L, Mant R, Newton P, Rooke K, Roques P, Talbot C, Pericak-Vance M, Roses A, Williamson R, Rossor M, Owen M, & Hardy J. Segregation of a missense mutation in the amyloid precursor protein gene with familial Alzheimer's disease. *Nature*. 1991; 349: 704-706. doi: 10.1038/349704a0
46. Levy-Lahad E, Wijsman EM, Nemens E, Anderson L, Goddard KA, Weber JL, Bird TD, Schellenberg GD. A familial Alzheimer's disease locus on chromosome 1. *Science*. 18 Aug 1995; 269(5226): 970-973. doi: 10.1126/science.7638621
47. Rogaev EI, Sherrington R, Rogaeva EA, Levesque G, Ikeda M, Liang Y, Chi H, Lin C, Holman K, Tsuda T, Mar L, Sorbi S, Nacmias B, Piacentini S, Amaducci L, Chumakov I, Cohen D. Lannfelt L, Fraser PE, Rommens JM, & St George-Hyslop PH. *Nature*. 31 Aug 1995: 376; 775-778. doi: 10.1038/376775a0
48. Sherrington R, Rogaev EI, Liang Y, Rogaeva EA, Leveseque G, Ikeda M, Chi H, Lin C, Li G, Holman K, Tsuda T, Mar L, Foncin JF, Bruni AC, Montesi MP, Sorbi S, Rainero I, Pinessi L, Nee L, Chumakov I, Pollen D, Brookes A, Sanseau P, Polinsky RJ, Wasco W, Da Silva HAR, Haines JL, Pericak-Vance MA, Tanzi RE, Roses AD, Fraser PE, Rommens JM, & St George-Hyslop PH. Cloning of a gene bearing missense mutations in early-onset familial Alzheimer's disease. *Nature*. 1995;375:754-760. doi: 10.1038/375754a0.
49. Chartier-Harlin MC< Crawford F, Houlden H, Warren A, Hughes D, Fidani L, Goate A, Rosssor M, Roques P, Hardy J, & Mullan M. Early-onset Alzheimer's disease caused by mutations at codon 717 of the β-amyloid precursor protein gene. *Nature*. 1991;353:844-846. doi: 10.1038/353844a0
50. Citron M, Oltersdorf T, Haass C, McConlogue L, Hung AY, Seubert P, Vigo-Pelfrey C, Lieberburg I, & Selkoe DJ. Mutation of the β-amyloid precursor protein in familial Alzheimer's disease increases β-protein production. *Nature*. 1992; 360:672-674. doi:10.1038/360672a0.
51. Price DL, Sisodia SS. Mutant genes in familial Alzheimer's disease and transgenic models. *Annu Rev Neurosci*. 1998;21:479-505. doi:10.1146/annurev.neuro.21.1.479
52. Suzuki N, Cheung TT, Cai XD, et al. An increased percentage of long amyloid beta protein secreted by familial amyloid beta protein precursor (beta APP717) mutants. *Science*. 1994;264(5163):1336-1340. doi:10.1126/science.8191290
53. De Strooper B, Saftig P, Craessaerts K, et al. Deficiency of presenilin-1 inhibits the normal cleavage of amyloid precursor protein. *Nature*. 1998;391(6665):387-390. doi:10.1038/34910
54. Edbauer D, Winkler E, Regula JT, Pesold B, Steiner H, Haass C. Reconstitution of gamma-secretase activity. *Nat Cell Biol.* 2003;5(5):486-488. doi: 10.1038/ncb960
55. Hall AM, Roberson ED. Mouse models of Alzheimer's disease. *Brain Res Bull*. 2012;88(1):3-12. doi:10.1016/j.brainresbull.2011.11.017
56. Massi F, Klimov D, Thirumalai D, Straub JE. Charge states rather than propesntiy for beta-structure determine enhanced fibrillogensis in wild-type Alzheimer's beta-amyloid peptide compared to E22Q Dutch mutant. *Protein Sci*. 2002;11(7): 1639-1647. doi: 10.1110/ps.3150102
57. Nilsberth C, Westlind-Danielsson A, Eckman CB, et al. The 'Arctic' APP mutation (E693G) causes Alzheimer's disease by enhanced Abeta protofibril formation. *Nat Neurosci*. 2001;4(9):887-893. doi:10.1038/nn0901-887

58. Cabrejo L, Guyant-Maréchal L, Laquerrière A, Vercelletto M, De La Fournière F, Thomas-Antérioin C, Verny C, Letournel F, Pasquier F, Vital A, Frédéric C, Frebourg T, Campion D, & Hannequin D. Phenotype associated with APP duplication in five families. *Brain*. 2006; 129(11): 2966-2976. doi: 10.1093/brain/awl237.
59. Heston LL. Down's syndrome and Alzheimer's dementia: defining an association. Psychiatr Dev. 1984; 2(4): 287-294.
60. Duff K. Alzheimer transgenic mouse models come of age. *Trends Neurosci*. 1997;20(7):279-280. doi:10.1016/s0166-2236(97)01093-x
61. Oyama F, Sawamura N, Kobayashi K, Morishima-Kawashima M, Kuramochi T, Ito M, Tomita T, Maruyama K, Saido TC, Iwatsubo T, Capell A, Walter J, Grünberg J, Ueyama Y, Haass C, & Ihara Y. Mutant presinilin 2 transgenic mouse: effect on an age-dependent increase of amyloid beta-protein 42 in the brain. *J Neurochemistry*. 1998; 71(1): 313-322. doi: 10.1046/j.1471-4159.1998.71010313.x.
62. Sherrington R, Froelich S, Sorbi S, Campion D, Chi H, Rogaeva EA, Levesque G, Rogaev EI, Lin C, Liang Y, Ikeda M, Mar L, Brice A, Agid Y, Percy ME, Clerget-Darpoux F, Piacentini S, Marcon G, Canmias B, Amaducci L, Frebourg T, Lannfet L, Rommens JM, & St George-Hyslop PH. Alzheimer's Disease Associated with Mutations in Presinilin 2 is Rare and Variably Penetrant. *Human Molecular Genetics*. 1996; 5(7): 985-988. doi: 10.1093/hmg/5.7.985.
63. Mucke L, Masliah E, Yu GQ, Mallory M, Rockenstein EM, Tatsuno G, Hu K, Kholodenko D, Johnson-Wood K, & McConlogue L. High-Level Neuronal Expression of $A\beta_{1-42}$ in Wild-Type Human Amyloid Protein Precursor Transgenic Mice: Synaptotoxicity with Plaque Formation. *Journal of Neuroscience*. 2000; 20(11): 4050-4058. doi: 10.1523/JNEUROSCI.20-11-04050.2000
64. Palop, JJ, Jones B, Kekonius L, Chin J, Yu GQ, Raber J, Masliah E, & Mucke L. Neuronal depletion of calcium-dependent proteins in the dentate gyrus is tightly linked to Alzheimer's disease-related cognitive deficits. *Proceedings of the National Academy of Sciences of the United States of America*. 5 Aug 2003; 100(16): 9572-9577. doi: 10.1073/pnas.1133381100
65. Winkler EA, Sagare AP, Zlokovic BV. The pericyte: a forgotten cell type with important implications for Alzheimer's disease? *Brain Pathol Zurich Switz*. 2014;24:371-386.
66. Sagare AP, Bell RD, Zlokovic BV. Neurovascular defects and faulty amyloid-β vascular clearance in Alzheimer's disease. *J Alzheimers Dis JAD*. 2013;33(Suppl 1): S87-100.
67. Sagare AP, Bell RD, Zlokovic BV. Neurovascular dysfunction and faulty amyloid β-peptide clearance in Alzheimer disease. *Cold Spring Harb Perspect Med*. 2012;2.
68. Zlokovic BV. Neurovascular mechanisms of Alzheimer's neurodegeneration. *Trends Neurosci*. 2005;28:202-208.
69. Sweeney MD, Sagare AP, Zlokovic BV. Cerebrospinal fluid biomarkers of neurovascular dysfunction in mild dementia and Alzheimer's disease. *J Cereb Blood Flow Metab.* 2015;35:1055-1068.
70. Zlokovic BV. Neurovascular pathways to neurodegeneration in Alzheimer's disease and other disorders. *Nat Rev Neurosci.* 2011;12:723-738.
71. Zlokovic BV. The blood-brain barrier in health and chronic neurodegenerative disorders. *Neuron*. 2008;57:178-201.
72. Alzheimer's Association. 2015 Alzheimer's disease facts and figures. *Alzheimers Dement J Alzheimers Assoc.* 2015;11:332-384.
73. Tanzi RE. The genetics of Alzheimer disease. *Cold Spring Harb Perspect Med*. 2012;2
74. Corder EH, Saunders AM, Strittmatter WJ, Schmechel DE, Gaskell PC, Small GW, Roses AD, Haines JL, Pericak-Vance MA. Gene dose of apolipoprotein E type 4 allele and the risk of Alzheimer's disease in late onset families. *Science*. 1993; 261:921-923.
75. Verghese PB, Castellano JM, Holtzman DM. Apolipoprotein E in Alzheimer's disease and other neurological disorders. *Lancet Neurol.* 2011;10:241-252.
76. Ramanathan A, Nelson AR, Sagare AP, Zlokovic BV. Impaired vascular-mediated clearance of brain amyloid beta in Alzheimer's disease: the role, regulation and restoration of LRP1. *Front Aging Neurosci.* 2015;7:136.

77. Deane R, Wu Z, Sagare A, Davis J, S Yan D, Hamm K, Xu F, Parisi M, LaRue B, Hu HW, Spijkers P, Guo H, Song X, Lenting PJ, Van Nostrand WE, Zlokovic BV. LRP/amyloid beta-peptide interaction mediates differential brain efflux of Abeta isoforms. *Neuron*. 2004;43:333-344.
78. Tarasoff-Conway JM, Carare RO, Osorio RS, Glodzik L, Butler T, Fieremans E. Axel L, Rusinek H, Nicholson C, Zlokovic BV, Frangione B, Blennow K, Méard J, Zetterberg H, Wisniewski T, de Leon MJ. Clearance systems in the brain-implications for Alzheimer disease. *Nat Rev Neurol.*2015.
79. Zlokovic BV, Deane R, Sagare AP, Bell RD, Winkler EA. Low-density lipoprotein receptor-related protein-1: a serial clearance homeostatic mechanism controlling Alzheimer's amyloid β-peptide elimination from the brain. *J Neurochem*. 2010; 115:1077-1089.
80. Zhao Z, Sagare AP, Ma Q, Halliday MR, Kong P, Kisler K, Winkler EA, Ramanathan A, Kanekiyo T, Bu G, Owens NC, Rege SV, Si G, Ahuja A, Zhu D, Miller CA, Schneider JA, Maeda M, Maeda T, Sugawara T, et al. Central role for PICALM in amyloid-β blood-brain barrier transcytosis and clearance. *Nat Neurosci*. 2015;18:978-987.
81. Donahue JE< Flaherty SL, Johanson CE, Duncan JA, Silverberg GD, Miller MC, Tavares R, Yang W, Wu Q, Sabo E, Hovanesian V, Stopa EG. *Acta Neuropathol (Berl)* 2006;112:405-415.
82. Austin SA, Katusic ZS. Partial loss of endothelial nitric oxide leads to increased cerebrovascular beta amyloid. *J Cereb Blood Flow Metab.* 2020;40:392-403
83. Tan X-L, Xue Y-Q, Ma T, et al. Partial eNOS deficiency causes spontaneous thrombotic cerebral infarction, amyloid angiopathy, and cognitive impairment. *Mol Neurodegener.* 2015;10:24.
84. Austin SA, Santhanam AV, Katusic ZS. Endothelial nitric oxide modulates expression and processing of amyloid precursor protein. *Cir Res*. 2010;107:1498-1502.
85. Mendel TA, Wierzba-Bobrowicz T, Lewandowska E, Stepień T, & Szpak GM. The development of cerebral amyloid angiopathy in cerebral vessels. A review with illustrations based upon own investigated post mortem cases. *Polish Journal of Pathology.* 2013; 64(4): 260-267. doi: 10.5114/pjp.2013.39334
86. Kalaria RN, Ballard C. Overlap between pathology of Alzheimer disease and vascular dementia. *Alzheimer Dis Assoc Discord*. 1999; 13 (Suppl 3): S115-23.
87. Jellinger KA. Alzheimer disease and cerebrovascular pathology: an update. *J Neuro Transm*. 2002; 109: 813-36.
88. Pantelakis S. A particular type of senile angiopathy of the central nervous system: congophilic angiopathy, topography and frequency [in French]. *Monatsschr Psychiatr Neurol*. 1954; 128: 219-56.
89. Charidimou A, Boulouis G, Gurol ME, Ayata C, Bacskai BJ, Frosch MP, Viswanathan A, Greenberg SM. Emerging concepts in sporadic cerebral amyloid angiopathy. *Brain*. 2017; 140(7): 1829-1850. doi: 10.1093/brain/awx047.
90. Greenberg SM, Salman RA, Biessels GJ, van Buchem M, Cordonnier C, Lee JM et al. Outcome markers for clinical trials in cerebral amyloid angiopathy. *Lancet Neurol*. 2014;13: 419-28.
91. Carare RO, Hawkes CA, Jeffrey M, Kalaria RN, Weller RO. Review: cerebral amyloid angiopathy, prion angiopathy, CADASIL and the spectrum of protein elimination failure angiopathies (PEFA) in neurodegenerative disease with a focus on therapy. *Neuropathol Appl Neurobiol*. 2013; 39:593-611.
92. Keable A, Fenna K, Yuen HM, Johnston DA, Symth NR, Smith C et al. Deposition of amyloid beta in the walls of human leptomeningeal arteries in relation to perivascular drainage pathways in cerebral amyloid angiopathy. *Biochem Biophys Acta*. 2016; 1862: 1037-46.
93. Cordonnier C, van der Flier WM. Brain microbleeds and Alzheimer's disease: innocent observation or key player? *Brain*. 2011; 134(Pt 2): 335-44.
94. Matthews KA, Xu W, Gaglioti AH, et al. Racial and ethnic estimates of Alzheimer's disease and related dementias in the United States (2015-2060) in adults aged ≥65 years. *Alzheimers Dement.* 2019; 15:17-24.
95. Sweeney MD, Sagare AP, Zlokovic BV. Blood-brain barrier breakdown in Alzheimer's disease and other neurodegenerative disorders. *Nat Rev Neurol*. Mar 2018; 14(3): 133-150. doi: 10.1038/nrneurol.2017.188
96. Rodrigues SF & Granger DN. Blood cells and endothelial barrier function. *Tissue Barriers*. 2015; 3:e978720. doi: 10.4161/21688370.2014.978720.

97. Nitta T et al. Size-selective loosening of the blood-brain barrier in claudin-5 deficient mice. *The Journal of Cell Biology*. 2003; 161: 653-660. doi: 10.1083/jcb.200302070.
98. Hagan N & Ben-Zvi A. The molecular, cellular, and morphological components of blood-brain barrier developing during embryogenesis. *Seminars in cell & developmental biology*. 2015; 38:7-15. doi: 10.1016/j.semcdb.2014.12.006.
99. Daneman R, Zhou L, Kebede AA, Barres BA. Pericytes are required for blood-brain barrier integrity during embryogenesis. *Nature*. 2010; 468(7323): 562-566. doi: 10.1038/nature09513.
100. Kröll S et al. Control of the blood-brain barrier by glucocorticoids and the cells of the neurovascular unit. *Ann N Y Acad Sci*. 2009; 1165: 228-239. doi: 10.1111/j.1749-6632.2009.04040.x.
101. Carrano A, Hoozemans JJM, van der Vies S, Rozemuller AJM, van Horssen J, & de Vries HE. Amyloid Beta induces oxidative stress-mediated blood-brain barrier changes in capillary amyloid angiopathy. *Antioxid Redox Signal*. 1 Sep 2011; 15(5): 1167-78. doi: 10.1089/ars.2011.3895.
102. Frost GR, & Li YM. The role of astrocytes in amyloid production and Alzheimer's disease. *Open biology*. 2017;7. doi: 10.1098/rsob.170228.
103. Johnstone M, Gearing AJ, & Miller KM. A central role for astrocytes in the inflammatory response to beta-amyloid; chemokines, cytokines and reactive oxygen species are produced. *J Neuroimmunol*. 1999; 93: 182-193.
104. Abbas N et al. Up-regulation of the inflammatory cytokines IFN-gamma and IL-12 and down-regulation of IL-4 in cerebral cortex regions of APP(SWE) transgenic mice. *J Neuroimmunol*. 2002; 126: 50-57.
105. Chen A, Akinyemi RO, Hase Y, Firbank MJ, Ndung'u MN, Foster V, Craggs LJ, Washida K, Okamoto Y, Thomas AJ, Polvikoski TM, Allan LM, Oakley AE, O'Brien JT, Horsburgh K, Ihara M, Kalaria RN. Frontal white matter hyperintensities, clasmatodendrosis and gliovascular abnormalities in aging and post-stroke dementia. *Brain*. 2016; 139(Pt 1): 242-258. doi: 10.1093/brain/awv328
106. Kaanan NM, Kordower JH, & Collier TJ. Age-related changes in glial cells of dopamine midbrain subregions in rhesus monkeys. *Neurobiol. Aging.* 2010;31:937-952. doi: 10.1016/j.neurobiolaging.2008.07.006
107. Cerbai F, Lana D, Nosi D, Petkova-Kirova P, Zecchi S, Brothers HM, et al. The neuron-astrocyte-microglia triad in normal brain aging and in a model of neuroinflammation in the rat hippocampus. PLoS One. 2012;7:e45250. doi: 10.1371/journal.pone.0045250
108. Jyothi HJ, Vidyadhara DJ, Mahadevan A, Philip M, Parmar SK, Manohari SG, et al. Aging causes morphological alterations in astrocytes and microglia in human substantia nigra pars compacta. *Neurobiol. Aging*. 2015;36: 3321-3333. doi: 10.1016/j.neurobiolaging.2015.08.024
109. Castiglioni AJ, Legare ME, Busbee DL, & Tiffany-Castiglioni E. Morphological changes in astrocytes of aging mice fed normal or caloric restricted diets. Age. 1991; 14: 102-106. doi: 10.1007/bf02435015
110. Amenta F, Bronzetti E, Sabbatini M, & Vega JA. Astrocyte changes in aging cerebral cortex and hippocampus: a quantitative immunohistochemical study. *Microsc. Res. Tech.* 1998; 43: 29-33. doi: 10.1002/(SICI) 1097-0029(19981001)43:1<29::AID-JEMT5>3.0.CO;2-H
111. Robillard KN, Lee KM, Chiu KB, & MacLean AG. Glial cell morphological and density changes through the lifespan of rhesus macaques. *Brain Behav. Immun.* 2016; 55: 60-69. doi: 10.1016/j.bbi.2016.01.006
112. Puschmann TB, Zandén C, Lebkuechner I, et al. HB-EGF affects astrocyte morphology, proliferation, differentiation, and the expression of intermediate filament proteins. *J Neurochem*. 2014;128(6):878-889. doi:10.1111/jnc.12519
113. Hudgins SN, Levison SW. Ciliary neurotrophic factor stimulates astroglial hypertrophy in vivo and in vitro. *Exp Neurol*. 1998;150(2):171-182. doi:10.1006/exnr.1997.6735
114. Cohen J, & Fields R. Activity-dependent neuron-glial signaling by ATP and leukemia-inhibitory factor promotes hippocampus glial cell development. *Neuron Glia Biology.* 2008; 4(1): 43-55. doi: 10.1017/S1740925X09000076
115. Baghdassarian D, Toru-Delbauffe D, Gavaret JM, & Pierre M. Effects of transforming growth factor-β1 on the extracellular matrix and cytoskeleton of cultured astrocytes. *Glia*. 1993; 7(3): 193-202. doi: 10.1002/glia.440070302

116. Herrera F, Chen Q, & Schubert D. Synergistic Effect of Retinoic Acid and Cytokines on the Regulation of Glial Fibrillary Acidic Protein Expression. *The Journal of Biological Chemistry*. 2010; 285(50): 38915-38922. doi: 10.1074/jbc.M110.170274

Chapter 2

Literature Review

The Gliovascular Unit and Astrocytic Regulation of Cerebrovascular Physiology

Astrocytes and The Gliovascular Unit

The Gliovascular Unit (**Figure 1**) (GVU) refers to a conglomerate of cells along with the various physiological activities they implement by synchronously working together (1). Consisting of endothelial cells, the basal lamina, vascular mural cells, microglial cells, and astrocytes-the GVU entities work in concert to execute vital functions aimed at maintaining the internal CNS milieu. The following sections discuss each individual component of the GVU, its anatomical makeup and physiological properties, and emphasize astrocytes as a pivotal and centralized cellular component underlying execution of GVU functionality.

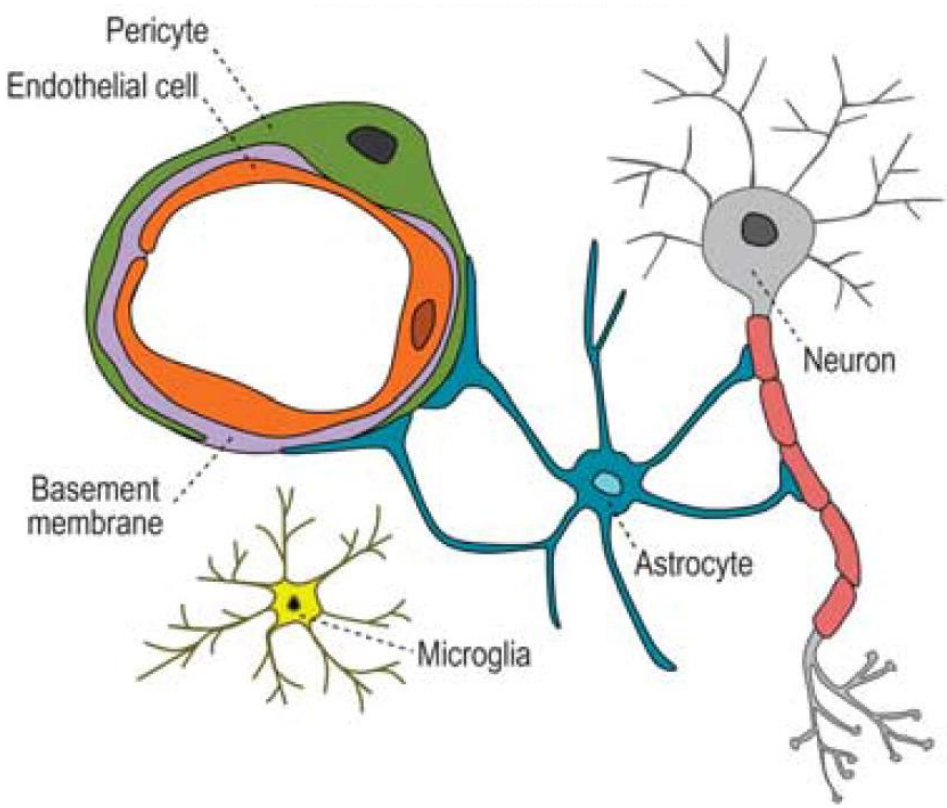

Figure 1- The Gliovascular Unit- The gliovascular unit is composed of multiple cell types including (from left to right), endothelial cells (orange), the vascular/parenchymal basement membrane (magenta), vascular mural cells- including pericytes (green) at capillaries and smooth muscle cells at arterioles and venules (not shown)- microglia (yellow), astrocytes (teal), and neurons (gray). The astrocyte is centrally positioned between the vasculature and neurons, and as such, is an instrumental figure underlying gliovascular physiology. Reproduced from Sweeney et al. (259) with permission

Astrocytes

Astrocytes comprise the most abundant cellular population in the brain (2). Existing in a nexus between synaptic contacts and blood vessels, they are well poised to both indirectly support and actively exert control over neuronal activity. The mechanisms that enable this include physiological functions such as potassium buffering (3-7), modulation of brain pH through regulation of extracellular hydrogen concentration (8-9), the uptake and recycling of neurotransmitters glutamate and GABA (10-14), the regulation of cerebral blood flow (14-19), maintenance and repair of the blood-brain barrier (20-23), water transport through the aquaporin-4 water channel (24), and the release of gliotransmitters such as D-serine (25). The expression of highly specialized transporters and receptors localized to perisynaptic processes abutting synapses along with endfeet ensheathing blood vessels allow for the execution of these physiological responses.

Astrocyte-endothelial cell interactions through endfeet

As mentioned above, astrocytes extend long, flattened processes called endfeet that surround and intimately interact with endothelial cells (**Figure 2**), separated only by the basal lamina. Endfeet cover up to 99% of the cerebrovascular surface (26) where, on average, each astrocyte possesses 3.5 endfeet, though some can have as few as one or as many as seven (27). Depending on the vessel type, both the degree and morphological appearance of astrocyte coverage varies. Endfeet along the capillary bed are in direct contact with the vasculature while larger vessels are separated from endfeet by cerebrospinal fluid-filled spaces (28-29). In addition to endfeet, about one-third of astrocyte somata also contact the vasculature, typically at larger diameter vessels (30).

Endfoot length and thickness also vary along different blood vessel types. Endfoot processes around arteries and veins are thicker and have higher glial fibrillary acidic protein (GFAP) expression levels, whereas the reverse is seen in endfeet around capillaries (31-33). Finally, endfeet also cluster together as a dense meshwork around larger meningeal vessels as well as penetrating arteries and veins to form the glia limitans. Covered by the basal lamina, this process-rich structure forms a barrier distinct from the BBB (34), which is capable of forming tight junction proteins under inflammatory conditions, thereby preventing the entry of blood-borne cells into the parenchymal space (35).

The retraction of endfeet has been documented in various disease states such as ischemia (36-38), major depression (39-41), experimental autoimmune encephalitis (42), and multiple sclerosis (43). These conditions typically present with blood-brain barrier breakdown. Other conditions such as glioma (44) and cerebral amyloid angiopathy (1) result in perturbed endfoot-vascular contact due to intercalation of another entity, and both conditions result in altered blood flow and blood-brain barrier breakdown, as reviewed in Chapter 1.

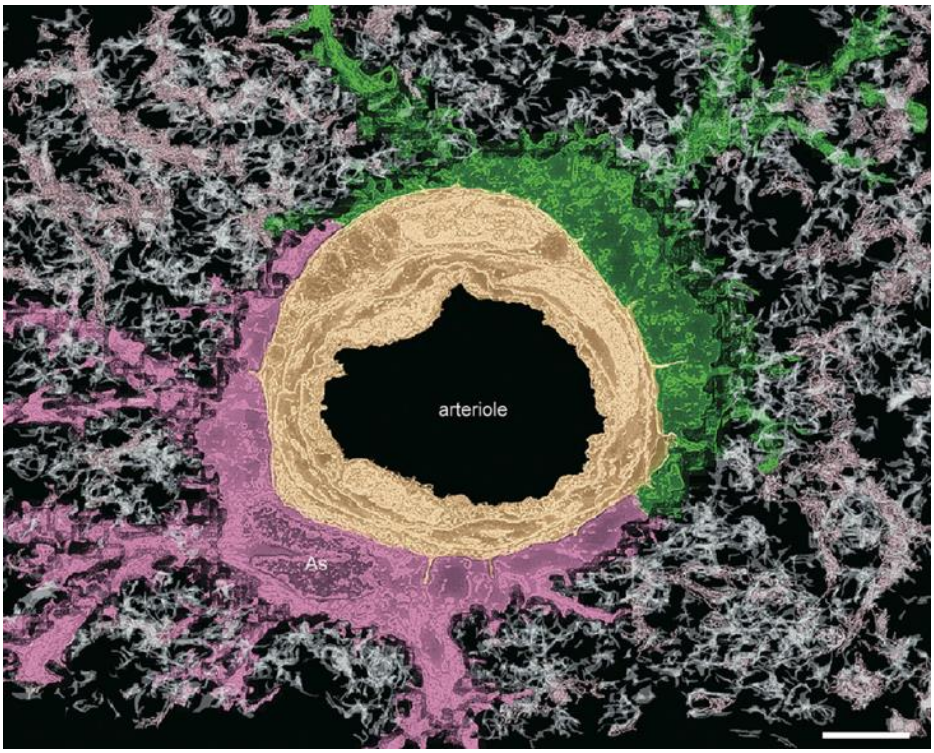

Figure 2- Astrocyte endfeet extensively and intimately cover the cerebrovasculature- An electron micrograph depicting the intimate association between astrocyte endfeet and endothelial cells. Two endfeet are present, one being pseudo-colored in magenta and the other in green. The yellow arteriole endothelial cell is positioned between the two endfeet. Scale bar: 5µms. Reproduced with permission. Image originally published in: Watanabe K, Takeishi H, Hayakawa T, Sasaki H. Three-dimensional organization of the perivascular glial limiting membrane and its relationship with the vasculature: a scanning electron microscope study. Okajimas folia anatomica Japonica. 2010; 87: 109-121 (26). URL: https://www.jstage.jst.go.jp/article/ofaj/87/3/87_3_109/_article/-char/en

Endothelial Cells

Though it exists as one continuous structure throughout the brain, six distinct segments of the cerebrovasculature have been categorized. These include pial arteries, penetrating arteries, arterioles, capillaries, postcapillary venules, and veins (45). Endothelial cells (ECs) form the vasculature but possess transcriptomic

profiles specific to the zone of vascular tree they occupy (arteriole, capillary, or venous) (46). Genes such as *Bmx*, *Vegfc*, *Efnb2*, *Gkn3*, and *Sema3g* identify the arterial zone of the vasculature whereas *Nr2f2* and *Slc38a5* identify the venous zone (46). The capillary zone can be identified by genes such as *Mfsd2a* and *Tfrc*, and in general, transcription factors are the dominant feature of arterial endothelium whereas transporters predominate at capillary and venous endothelium (46).

The Blood-Brain Barrier (BBB)

The Blood-Brain Barrier (BBB) refers to a continuous structure that exists at the plasma membranes of adjacent endothelial cells in penetrating arterioles, capillaries, and ascending venules (47). Paul Ehrlich first described the BBB over a century ago when he observed the exclusion of water-soluble dyes from brain and spinal cord following systemic injection (48-49). His student, Edwin Goldmann, conducted further observational studies and determined that trypan blue is retained within the CSF but not the periphery when injected directly into the CSF (50). The term 'blood-brain barrier' was not coined, however, until Max Lewandowsky determined that the detrimental effects of neurotoxic substances occurred only when injected directly into the brain (51). Since that time, it has been firmly established that the selectivity of the BBB is due to both physical and chemical barriers, as well as a lack of fenestrations and low transcytotic expression- all features that separate the CNS vasculature from the peripheral vasculature. (47). Only molecules that are lipid-soluble, <400Da, and contain fewer than 8 hydrogen bonds can pass freely via lipid-mediated diffusion (52).

In light of this high exclusivity, numerous membrane-bound transport systems which are also localized at the endothelium enable the passage of various molecules essential for cellular metabolism (53). Other transport systems exist that function as efflux transporters, whereby they clear or prevent entry of foreign substances into brain (53). These two transport functions characterize the two major transporter superfamilies- the ATP-binding cassette (ABC) superfamily and solute carrier superfamily (SLC) (54). As suggested in the name, ABC transporters are efflux transporters that utilize energy generated from ATP hydrolysis to restrict passage and entry to drugs, drug conjugates, and xenobiotics (54). SLC transporters are involved in the uptake of carbohydrates,

vitamins, hormones, nucleotides, organic anions/cations, monocarboxylic acids, fatty acids, and amino acids into the brain (53-54).

52 families containing 395 members of membrane-bound SLC transporters have been identified in humans (54). As mentioned above, there is a large array of substrates that SLC transporters can interact with, and different transporters possess varying levels of selectivity. The majority of SLC transporters are either facilitative- that is, they transport substrates across membranes on-the-basis of electrochemical gradients- or secondary-active, whereby ion gradients produced by ATP-dependent pumps allow for molecules to be transported against concentration gradients. A minority of SLC transporters are tertiary-active, where substances are transported against concentration gradients by utilizing energy generated from gradients produced by secondary-active transporters (54). The abluminal sodium pump (Na^+, K^+ ATPase), luminal sodium-hydrogen exchanger, chloride-bicarbonate exchanger, luminal sodium-potassium-chloride cotransporter, and sodium-calcium exchanger all modulate ion concentrations (53, 55).

One prominent SLC transporter is *SLC2A1*, also known as glucose transporter 1 (GLUT1). This transporter is responsible for transporting glucose (47, 56), the main energy substrate of the brain (57-58), across the BBB. GLUT1 is expressed by endothelial cells in early BBB development (59-61), and its reductions in Alzheimer's disease (AD) underlie diminished glucose transport observed early in disease pathogenesis (62-65). This reduction has further been shown to act as a main driver of cerebrovascular degeneration, neuropathology, and cognitive function (66). One other vital transporter executing carrier-mediated transport, but not classified as a member of the SLC family, is the major facilitator superfamily domain-containing protein 2 (MFSD2A). This transporter is responsible for mediating omega-3 fatty acid passage into brain (53), and it is necessary for proper BBB formation as its conditional deletion in endothelial cells resulted in a leaky BBB (67).

48 total ABC transporter genes have been identified in humans. These are classified into seven subfamilies, ATP subfamily A to G (68-69), all of which possess a stereotypical four-domain structure. Two transmembrane domains identify and transport substrates, and two nucleotide-binding cytoplasmic domains provide the energy for transport through the binding and hydrolysis of ATP (70). The diversity of substrate

recognition is endowed by the diversity in transmembrane-domain structure found amongst the seven classes of ATP transporters (71). P-glycoprotein is one prominent ATP transporter highly expressed at endothelial cells that has been shown to transport amyloid-β (Aβ) (72-74). Its function can be studied in human patients using (R)-[^{11}C]verapamil and positron emission tomography, and one study utilizing these methods demonstrated that P-glycoprotein function is diminished in patients with AD, ultimately suggesting that it contributes to amyloid accumulation and thereby AD pathogenesis (75).

Beyond transporters, receptors also facilitate the passage of molecules into the brain or mediate their clearance. Peptides and proteins depend on receptor-mediated transcytosis to enter the brain (53), and examples include the insulin and transferrin receptors (76). One other prominent example is the apolipoprotein E fat-binding proteins (APOE), of which there are three isoforms, APOε2, 3, and 4. APOε4 is considered one of the strongest risk factors for AD and BBB breakdown is most evident in patients with this isoform (53)- a finding corroborated by studies from APOε4 transgenic mice (77-79). In contrast, patients with the APOε3 isoform have a reduced risk for AD and develop a diminished degree of BBB breakdown (80-83). Other receptors such as low-density lipoprotein receptor-related protein 1 (LRP1) mediate transport of Aβ across the BBB and out of the brain (72-74) whereas the receptor for advanced glycation end products (RAGE) transports Aβ into brain (84-87).

In addition to the chemical component of the BBB, there are also constituents forming a physical barrier. Broadly speaking, this physical barrier is composed of adherens and tight junctions (88). Proteins such as the junctional adhesion molecules A-C (JAM A-C), platelet endothelial cell adhesion molecule (PECAM-1), and vascular endothelial cadherin (VE-cadherin) contribute to the formation of adherens junction, which are located at the parenchymal facing, apical side of the endothelial cell (70). Linking these proteins to the actin/vinculin-based cytoskeleton are the α-, β-, and γ-catenin proteins (89).

In the CNS, tight junction proteins consist of Claudins 1 (90), 3, 5, and 12 (91-92), as well as Occludin (70). Each Claudin differentially regulates the BBB's exclusivity to different molecular sizes (70). For example, Claudin-5 deletion results in BBB permeability to molecules less than 800 Da, leading to neonatal death (91). In contrast, BBB formation is not altered when Occludin is deleted entirely (93), yet TJ strand formation itself is

perturbed when its N-terminal domain is deleted (94). Linking Claudins and Occludin to the actin-based cytoskeleton are members of the peripheral membrane-associated guanylate kinase protein (MAGUK) family, zonula occludens 1-3 (ZO1-ZO3) (88). In addition to providing cytoskeletal anchorage, the zonula occludens protein possess a PDZ-binding domain that regulates the spatial distribution of Claudins (70). **Figure 3** highlights the molecular entities comprising the physical and chemical components of the BBB.

Development of the BBB

Blood-brain barrier development commences with the onset of angiogenesis when endothelial progenitor cells invade the embryonic neuroectoderm around embryonic day 9.75 (E9.75) (95). Neural progenitor cells express multiple molecular cues that guide capillary formation to the neuroectoderm along a concentration gradient, the most well characterized being vascular endothelial growth factor A (VEGFA) and Wnt/β-catenin (96). Mice completely deficient in VEGF receptor 2 completely die around E9 due to failure in blood vessel formation (97), and mice deficient for the ligand also die early in embryogenesis, with vessel formation severely compromised (98).

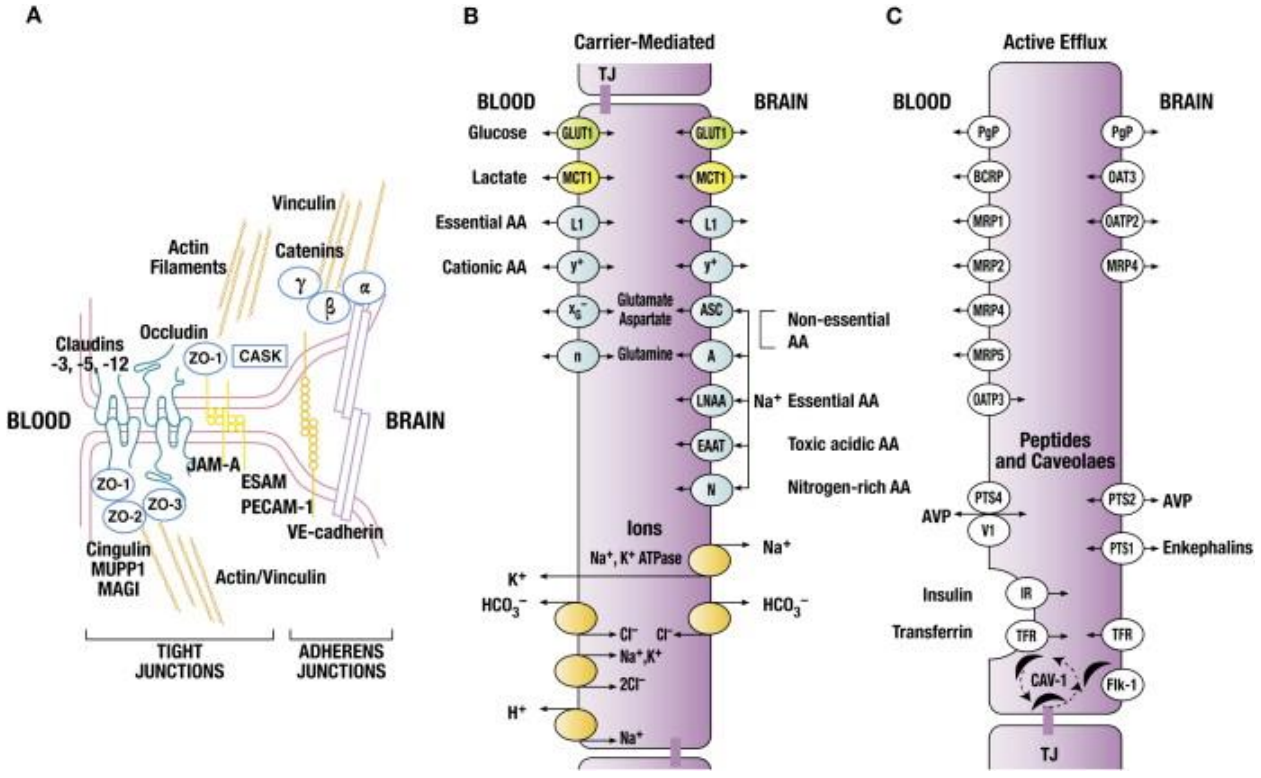

Figure 3- The physical and chemical components of the blood-brain barrier- A) Cartoon depicting the molecular entities comprising the physical component of the blood-brain barrier. This includes the protein that tight and adherens junctions along with the adaptor molecules linking them to the cytoskeleton. B) Cartoon depicting the molecular entities comprising the chemical of the blood-brain barrier, specifically carrier mediated transport systems. C) Cartoon depicting the active efflux transport systems comprising the chemical component of the blood-brain barrier. Reproduced with permission from Zlokovic 2008 (47).

Development of the BBB continued

Wnt/β-catenin signaling is a CNS specific angiogenic program (59). The classical pathway involves Wnt ligands binding to endothelial expressed Frizzled receptors. Upon binding, β-catenin accumulates in the cytoplasm due to inhibition of proteasome-mediated degradation. Following cytoplasmic accumulation, β-catenin translocates to the nucleus and induces expression of target genes through interactions with lymphoid enhancer binding factor 1/T-cell specific transcription factor DNA-binding proteins (99). In addition to its contributions to angiogenesis, Wnt also induces the expression of BBB genes such as the aforementioned glucose transporter, GLUT1 (Slc2a1) (59, 100). Neural progenitor cells express Wnt7a and Wnt7b in forebrain and ventral regions of the neural tube, and deficiency in these ligands results in embryonic lethality at E11.5-E12.5 due to abnormal vessel formation and subsequent hemorrhage (59, 61).

At the time of angiogenesis, endothelial cells express tight junction proteins, leukocyte adhesion molecules, and transcytotic vesicles (96). The acquisition of mature BBB properties involves elaboration of tight junction protein structures, decreased expression of transcytotic vesicles and leukocyte adhesion molecules, as well as increased expression of transporters (96). Interactions with pericytes, a type of vascular mural cell, are necessary for the formation of these properties, and relative vascular permeability is determined by absolute pericyte coverage. Specifically, pericytes inhibit the expression of molecules that increase permeability and leukocyte infiltration rather that inducing BBB specific genes (101).

Until recently, it was thought that angiogenesis peaked until the time of birth and then gradually

declined until postnatal day 25 (P25) (102). Typically, mRNA transcripts encoding angiogenic tip markers, signaling factors controlling CNS angiogenesis, and cell proliferation, as well as cell cycle markers all decline around E15.5-E18.5, which is right when radial glial cells undergo a potency switch and differentiate into astrocytes (103). Recent RNA-sequencing studies, however, have revealed a potential second wave of angiogenesis to occur, where the aforementioned categories of mRNA transcripts peak around postnatal days 5-9 (P5-P9) (104-105). This analysis is supported by observations from *in vivo* multiphoton studies revealing endothelial cell sprouts in the postnatal cerebrovasculature, further backed by BrdU incorporation studies revealing a continuation and increase in endothelial cell proliferation from P5-P10, which gradually diminishes until P25 when angiogenesis is completely abolished (106). Hence, there appears to be an embryonic and postnatal stage of angiogenesis.

As mentioned above, early morphological and physiological studies indicated endothelial cells inherently express tight junction proteins, and recent bulk RNA sequencing studies have confirmed that most BBB transcripts are expressed in the initial embryonic stage of angiogenesis around E10-E11.5 (105). These studies further revealed, however, that marked heterogeneity regarding the timeline of BBB transcript expression exists even within vascular beds of the same brain region. Interestingly, some BBB transcripts that encode for transporters including ABC, amino acid, and organic ion transporters are highly upregulated during postnatal stages of development when astrocytes would have extended endfeet to capillaries, which typically occurs at birth (107). This suggests that even though astrocytes are not necessary for the formation of molecular entities forming the physical component of the BBB, they may regulate the expression of BBB-associated transporters contributing to the chemical component of the BBB (**Figure 4**). These findings add further clarity to a long history of astrocytes and their role in regulating the BBB, which is highlighted next.

Astrocytes and the BBB

The seminal BBB study by Stewart and Wiley demonstrated how pivotal the neural microenvironment is to inducing CNS intrinsic BBB properties (108). Adding to this notion was a study demonstrating that isolated BBB

endothelial cells cultured in conditions differing from the CNS micro-environment lose their physiological barrier capacity as measured by

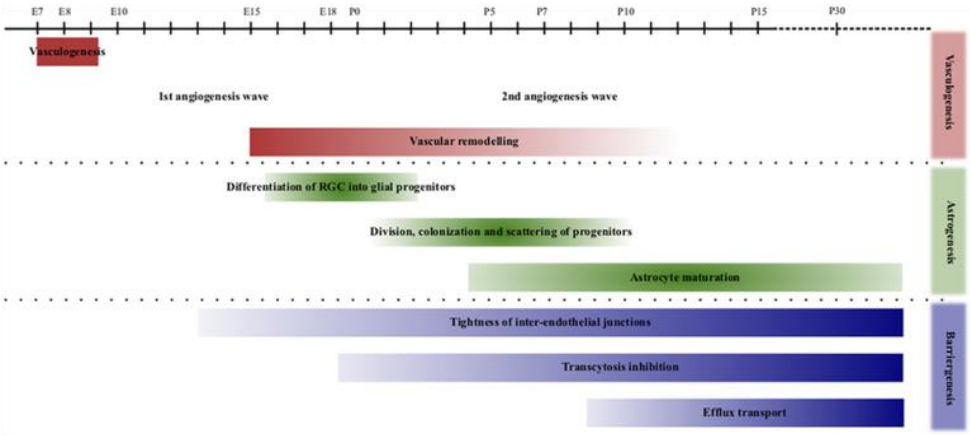

Figure 4-Timeline of angiogenesis and gliogenesis- Cartoon documenting the temporal relationship between vasculogenesis, angiogenesis, barriergenesis, and astrocyte maturation. Recent evidence indicates that angiogenesis may occur in two waves, where the second wave occurs at the time of astrocyte maturation. Hence, astrocytes may regulate the development of some BBB components. Reproduced with permission from Cohen-Salmon et al (45)

Astrocytes and the BBB continued

transendothelial electrical resistance (TEER) recordings and permeability (109).These findings ushered in many studies aimed at determining the necessity of astrocytes in the induction of BBB properties.

Early studies demonstrated that endothelial cells produced more complex tight junctions (110) and TEER recordings (109, 111), a physiological measurement of barrier tightness, when cultured in the presence of astrocytes or astrocyte-conditioned media. One particular study implanted endothelial cells into the anterior chamber of the eye and found that Evans blue dye failed to extravasate from newly formed blood vessels interfacing with astrocytes. This was in contrast to results from experiments that implanted fibroblasts into anterior chambers of the eye (112). However, another study followed up on this citing that the original study did not include electron microscopy (EM)-based evidence to support tight junction formation. Upon acquiring EM data from repeated anterior chamber implantation experiments, the authors demonstrated that endothelial cell implants were actually poorly vascularized, and of the few vessels that successfully formed, none possessed characteristics matching those of brain capillaries. In contrast, fibroblast implants were decidedly vascularized with highly fenestrated vessels, and the authors therefore concluded that this difference in vascularization

accounted for the difference in dye extravasation seen in the previous study (113). Other studies demonstrated that astrocyte-conditioned media (ACM) can reinduce electrical resistance and permeability to large and small molecular tracers in BBB-ECs (114-116). Conversely, a series of BBB-specific properties such as P-glycoprotein and TJ expression can be induced in non-CNS ECs when cultured in the presence of astrocytes or astrocyte-secreted factors (116-118). Furthermore, direct contact with astrocytes induces the establishment of mature BBB properties (119). Taken together, all but one aforementioned *in vitro* study supported the notion that astrocytes were necessary for inducing and maintaining BBB properties.

As mentioned above, by 2010 it was accepted that pericytes are responsible for formation of BBB properties (101), and that this development is completed by the time astrogliogenesis occurs in the brain, which is typically begins around E18.5 (103). The prevailing view therefore became that astrocytes are necessary for BBB maintenance. With the exception of one 2003 study demonstrating *in vivo* the necessity of the Src-suppressed C Kinase substrate in regulating the expression of zonula-occludens 1 expression (120), *in vivo* support for astrocyte-dependent BBB maintenance was lacking. This was critical in light of the original Stewart and Wiley study mentioned above (108). If the neural microenvironment is necessary for inducing BBB properties, then the best evidence supporting the necessity of astrocyte in maintaining the BBB would be from *in vivo* studies. In light of this, several studies in recent years have determined the impact on BBB integrity upon either genetically ablating astrocytes entirely (23) or knocking-out proteins exclusively in astrocytes. Interestingly, one study knocking out connexin 40 and 43 expression in astrocytes revealed BBB disruption, but observed this mostly in deeper brain regions such as striatum, and not in cortical regions (22). This same regional pattern of BBB breakdown was demonstrated when astrocyte specific laminin was ablated as well (21). In addition to the lack of BBB breakdown in cortex, one study employing diphtheria toxin mediated astrocyte ablation revealed no BBB breakdown in spinal cord (121). Interestingly, however, one study recently employed that same strategy and revealed extravasation of the ~1kDa dye Cadaverine in cortex, which is a dye smaller than that previously used in the aforementioned studies (20). Taken together, these experimental results point to the astrocyte being necessary for BBB maintenance, but largely in deeper brain regions rather than cortex.

The BBB in aging

Changes in the BBB throughout the lifespan accompany the changing needs of a maturing brain (122). Amino acid transport, for example, differs between neonates and adults (123). These changes support the theory that a healthy aging brain is accompanied by alterations in BBB functions, and the idea of adaptive senectitude supports this notion (124). However, oftentimes it is unclear if BBB alterations in aging are a causative factor in the etiology of aging-related CNS disorders.

Two examples of transport systems changing with age are LRP1 and those passaging glucose. As mentioned above, LRP1 is responsible for the transport of Aβ from brain to blood. LRP-1 function is inhibited in aging, and studies mimicking this find that Aβ peptide accumulates due to decreased efflux, ultimately resulting in cognitive impairment (125). In yet another example, glucose transport and metabolism along with cerebral blood flow- which are all tightly coupled with each other- decrease in aging. Cerebral blood flow, however, becomes temporally and regionally uncoupled from glucose transport in aging (126-128). Decreases in glucose transport also becomes irrelevant when accounting for brain atrophy (129), and taken together, these findings raise the question if decreases in glucose transport occur because of decreases in demand from aging tissue, or if decreases in transport dysregulate an organ with high metabolic demands. In general, few transport systems have been investigated in the aging brain, and of those that have, most reveal no difference in transport number (122).

With regard to transporters, the same ambiguity applies to studies in BBB disruption and endothelial cell morphology. In terms of morphology, data reveals no change in brain microvessel composition (130), and there are mixed results regarding capillary density and diameter (131-132). Regarding BBB disruption, which means the free passage of plasma solutes across the BBB, the clearest studies documenting breakdown in aging comes from those employing dynamic contrast-enhanced magnetic resonance imaging, where findings revealed BBB disruption in hippocampus (133) as well as gray and white matter of elderly patients (134). Interestingly, this leakage correlated with measures of cognitive decline, including white matter leakage correlating with delayed recall (135). In the gray matter study (134), however, a single patient over the age of 90 possessed white matter

that was less leaky than two individuals under the age of 50. Taken together, this suggests that the BBB does breakdown with aging, though breakdown is small and seems to be highly variable from patient-to-patient.

Vascular Mural Cells

Covering endothelial cells are vascular mural cells (VMCs) (**Figure 5**). VMCs are *broadly* categorized into two cell types, and their anatomical position varies according to the zone of vascular tree in question. Vascular smooth muscle cells (VSMCs) are one type of mural cell and occupy the larger arteries and veins, though their morphological appearance differs between the two vessel types (136). At arteries, VSMCs appear as ring-like structures encasing the vasculature, and the high expression of α-smooth muscle actin (α-SMA) underlies the high amplitude contractions observed in these cells. VSMCs at venules have much lower expression of α-SMA and appear as a meshwork encasing the vessel (136).

Pericytes are the second mural cell type and are present along the surface of capillaries and post-capillary venules. They occupy distinct segments of vasculature and can be placed along either continuous stretches of capillaries or at their branch points (137-138). They can be uniquely identified by the dual expression of platelet-derived growth factor receptor-β (PDGFRβ), a growth factor receptor, and NG2 (neural-glial antigen 2), a proteoglycan that serves as a co-receptor to PDGF (138). Morphologically speaking, they possess a bump-on-a-log appearance, containing an ovoid cell body and long linear processes occupying vast stretches of capillary bed (137-138).

The capillary bed accounts for approximately 85% of total cerebral vessel length (47). Given that pericytes are the most abundant mural cell present, their necessity in the formation and maintenance of BBB integrity was long speculated and subsequently shown to be the case (101). Likewise, many studies suggested the major site of cerebral blood flow (CBF) regulation to reside at capillaries (140-142)- more specifically, the terminal capillary level (141). As was true with the BBB, since pericytes are the predominant mural cell present at this vascular location- they became the presumed cell type regulating capillary responses to neuronal activity- and studies in retina (142-143), cerebellum (141), and cerebral cortex (141) all supported this notion. Furthermore, *in vivo* studies in cortex revealed a nearly equal number of capillaries dilate in response to neuronal activity as did

penetrating arterioles, and importantly, capillary dilation occurred prior to arteriole dilation (141). This temporal profile suggested that active relaxation in pericytes regulates CBF rather than changes in blood pressure caused by VSMC constriction inducing passive changes in pericytes. Finally, studies in ischemia had characterized a 'no-reflow' phenomena (141, 144-145). Here, reperfusion of brain tissue is prevented by the persistence in pericyte constriction long after pericyte cell death. Taken together, these studies posited CBF regulation to occur at the level of capillaries largely under the control of capillary pericytes.

One puzzling aspect remained regarding the contractile ability of pericytes. A significant number of mid-capillary pericytes had indeed been shown to express α-SMA, with the majority of expression occurring in pericytes at the first-order capillary, defined as the first capillary branch segment from a penetrating arteriole (136). Furthermore, many of the aforementioned studies examined pericyte contractility at this vessel type. Seeking to clarify if capillary pericytes at higher branch orders, a recent study by Hill et al (136) demonstrated that capillaries do not have active vasomotor responses in response to multiple stimulation paradigms, including direct pericyte optogenetic stimulation, physiological neural activation, and spreading depolarization. Pericytes at these higher branch-order capillary locations indeed lacked expression of α-SMA, whereas it was abundantly expressed in mural cells at vascular locations exemplifying active vasomotor responses. Interestingly, the morphological appearance of α-SMA+ pericytes at primary capillaries had more of a band-like morphology as that observed in VSMCs, but the diameter of the vasculature they occupied was indistinguishable from that of the higher branch-order pericyte-covered capillaries. Given these findings, the authors defined this first-order capillary segment as a precapillary arteriole, and the mural cells covering them were classified as VSMCs. They further determined that the 'no-flow' phenomena mentioned above actually occurs because of constrictions in VSMCs at precapillary arterioles and not pericytes at capillaries. Taken together, this data supported CBF regulation to lie at the levels of arterioles under the control of VSMC constrictions.

Given that the aforementioned study was performed due to purported issues in distinguishing VSMCs and pericytes at this precapillary arteriole region, several authors responded to these findings by claiming that the conclusions were drawn based off changing the classical definition of pericytes originally given by Zimmerman

(146). First described in the 1870s by Eberth and Rouget (137-138), pericytes were classified as having a bump-on-a-log morphology and being present on the abluminal side of capillaries, both at branch points and on contiguous segments. Zimmerman was the first to name these cells pericytes and decided to include the various morphologies of these cells under this one umbrella term, 'including their transitional forms to smooth muscle fibres.' Given that the Hill paper also found αSMA expression in 30% of pericytes at higher branch order capillaries (136), the question of what constitutes a pericyte comes down to how the morphology of a mural cell at the primary capillary is categorized. Does its resemblance to a smooth muscle cell mean that it should be a smooth muscle cell, or should it remain a pericyte as originally encompassed in the Zimmerman definition? Does the size of the vessel this mural cell occupies, which is consistent with the definition of a capillary, automatically categorize it as an ensheathing pericyte as some recent studies have classified it (147)?

Regardless of the position one takes on this matter, it is clear that this segment of vasculature is critical for CBF regulation and that the mural cell at this location exerts control over the vasculature with a kinetic profile that differs from pericytes at downstream capillaries. Specifically, a very recent study demonstrated that pericytes on higher branch orders do exert control over the vascular diameter but at much slower kinetics than arterioles and precapillary arterioles (147). Hence, studies such as the one conducted by Hill et al may have arrived at a false conclusion regarding the lack of a role higher branch order pericytes have in CBF regulation simply because they didn't acquire or analyze data for long enough time periods post-stimulation. One other study corroborates this notion as they used a similar stimulation paradigm and reported the same kinetic profile of pericyte constriction at higher-order capillaries (148).

As highlighted in Chapter 2, vascular abnormalities can contribute to AD pathogenesis, and onset of AD can further exacerbate vascular deficits present in patients. While arguments over the classification of mural cells at various vascular zones may seem trivial, understanding their contributions to CBF is not. By parsing out the various details of how mural cells contribute to CBF, we can begin to classify how these same mechanisms change in pathologies such as AD and then develop therapeutics accordingly. To that end, an elegant study (150) recently demonstrated that capillaries in human AD tissue are constricted but not arterioles, and that this constriction

occurs due to Endothelin-1 (ET1) binding to the endothelin A receptor on pericytes. ROS production via Aβ oligomer activity was identified as the source inducing ET1 production. By blocking the effects of ET1 with GKT137831 or C-type natriuretic peptide (CNP), the Aβ-induced constriction was reversed. Taken together, vascular mural cells at various locations along the vascular tree exert vasoregulatory control, albeit at varying kinetics. Disease states can alter how these cells regulate vessel diameter, and by understanding how they exert control of vessel diameter under normal physiological conditions, we can target identified perturbations in disease and shed light on potential therapeutic opportunities.

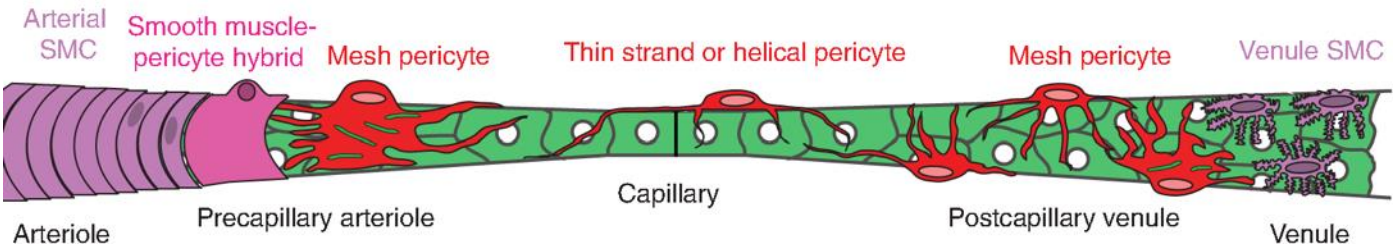

Figure 5-Vascular mural cell composition at different levels of the vascular tree- Cartoon depicting the transition from vascular smooth muscle cells at arterioles to various pericyte forms at precapillary arterioles, capillaries, and postcapillary venules. Smooth muscle cells are present at venules but appear as a meshwork rather than the ring-like structures seen at arterioles. Reproduced with permission from Andy Shih, senior author of the publication this cartoon originally appeared in: Hartmann DA, Underly RG, Grant RI, Watson AN, Lindner V, Shih AY. Pericyte structure and distribution in the cerebral cortex revealed by high-resolution imaging of transgenic mice. Neurophotonics. 2015 2(4): 041402. doi: 10.1117/1.NPh.2.4.041402 (260)

Astrocytes and Neurovascular Coupling (Functional Hyperemia)

One function of blood flow is the delivery of essential nutrients to sustain neuronal metabolic activity. The process of pairing regional alterations in blood flow to match regional changes in neuronal energy demand is known as neurovascular coupling (NVC) (150). This process is pivotal as the brain, though only comprising 2% of total body weıgnt, actually consumes 20% of the body's oxygen (56). The canonical view of NVC is centered on regulation occurring at the arteriole level (14, 17-18). Specifically, neuronal glutamate release would activate astrocytic metabotropic glutamate receptor 5 (mGluR5), subsequently inducing the release of vasoactive substances onto vessels (15). This release was due to inositol triphosphate-3 receptor (IP3R) dependent increases

in intracellular calcium concentrations ($[Ca^{2+}]_i$), which would consequently produce vasodilations or constrictions. These vasoactive substances, arachidonic acid (AA) metabolites produced by phospholipase A2 (14, 17-19), led to both vasodilations, produced by phospholipase A2 conversion to prostaglandin E2 via cyclooxygenase 1, and vasoconstrictions, by the production of 20-hydroxyeicosatetraemoic acid (20-HETE) from AA (15).

Several studies raised concerns with this proposed mechanism. It was shown that astrocyte calcium signals were too slow (151), did not display sufficient magnitude (151), and were too infrequent (152) to be necessary for neurovascular coupling. Subsequent studies, however, demonstrated that physiological stimulation-induced calcium signals in astrocyte endfeet specifically do occur on a time-scale compatible with neurovascular coupling (153-154), and so many of these original studies were dismissed on the basis of their measurements remaining confined to the astrocyte cell soma. A second controversy revolved around how $[Ca^{2+}]_i$ was generated via mGluR5 activation leading to downstream IP_3-dependent release of Ca^{2+} from internal stores (14, 17-18). However, adult astrocytes were shown to lack the mGluR5 receptor (155) and knockout of IP_3R_2 from astrocytes did not modulate neurovascular coupling in any particular way (156).

In light of these controversies, a very pivotal study (16) demonstrated that $[Ca^{2+}]_i$ was generated via postsynaptic ATP release, thereby activating the P2X1 purinergic ATP receptor on astrocytes. This subsequently led to AA production, which was then converted to prostaglandin E2 via diacylglycerol kinase and phospholipase D2 (rather than A2). Interestingly, neurovascular coupling at the level of arterioles was independent of astrocytes and relied instead of activation of neuronal NMDA receptors inducing the release of nitric oxide- hence, signaling occurs directly from neuron to vessel, as had been shown previously (157). Regardless of the controversies surrounding mural cell classification at precapillary arterioles/first order capillaries, findings reveal this segment of vasculature to be largely responsible for initiating conducted vascular responses following neuronal activity and astrocytes to be the cell type responsible for regulating this response. Thus, studies of astrocytes in blood flow regulation should primarily focus here.

The Vascular and Parenchymal Basement Membrane

The vascular basement membrane (VBM) is a complex three-dimensional network consisting of proteins from four glycoprotein families (158-159). These include nidogens, collagen IV isoforms, heparin sulfate proteoglycans (HSPGs), and laminins. Depending on the physiological state or developmental stage (160), expression of other molecules such as fibulin type 1 and 2, collagen XVIII, insoluble fibronectin, thrombospondins 1, and others rich in cysteine (such as SPARC), can be present as well (161-165).

Collagen IV is a trimeric molecule consisting of intertwined polypeptide chains, each being one of six possible α chains (166). The most common isoform expressed in brain is composed of two α1 and one α2 chain (167-170). The initial assembly and intertwining of these α chains occur intracellularly where they form structures called protomers, which subsequently oligomerize extracellularly to form a supramolecular network (171). Nidogen exists in brain as two isoforms, nidogen 1 and 2. Consisting of three globes (G1-G3), G1 and G2 are expressed within the N-terminus and G3 at the C-terminus in both isoforms (172-173).

Three different HSPGs are found within the VBM: agrin, collagen XVII, and perlecan, with agrin and perlecan having the highest expression (174). z+ and z0 are spliced isoforms of agrin, with z0 being the isotype found within the VBM (175-176). Perlecan has a multi-domain protein core possessing a N-terminus with three glycosaminoglycan chains (166). One function of HSPGs is to bind and amass growth factors so as to protect them from degradation, thereby allowing modulation of paracrine signaling of nearby cells (177-178).

Laminins are heterotrimeric transmembrane proteins consisting of α-, β-, and γ-subunits (166). Development of the vascular basement membrane (VBM) begins with this cross-shaped structure self-assembling into a sheet-like structure, followed by binding to nidogen and HSPGs. The linking of HSPGs and nidogen to collagen IV completes VBM development (166). 16 different laminin isoforms exist, the composition of which derives from a combination of one of five possible α-subunits, one of four possible β-subunits, and one of three possible γ-subunits (179-180). Along all zones of the vascular tree, laminin composition contains either α1, α2, α4, or α5 combined with β1 and γ1 chains, giving trimeric isoforms of 111, 211, 411, and 511 (160). Laminin 421 is also found along the cerebrovasculature (164, 181-182).

Different cells of the GVU secrete different isoforms of laminin. Furthermore, the anatomical appearance and laminin composition of the VBM varies according to the vascular zone (166). At the larger arteries and arterioles, the vascular basement membrane consists of contributions from pial cells and astrocytes, which constitute the parenchymal basement membrane (183-184). There is also the contribution from the underlying endothelial cells, constituting the endothelial basement membrane, whose laminin composition consists of isoforms 411 and 511 (179, 185). In contrast, the parenchymal basement membrane contains laminin isoforms 111 and 211, where astrocytes express both isoforms (21). Laminin 411 is expressed at all levels of the vascular tree, whereas laminin 511 correlates with both vessel type and maturation (179, 181).

Descending further down the vascular tree to the level of capillaries, smooth muscle cells transition to pericytes, which are embedded within the endothelial basement membrane. Given the loss of a pial sheet at this level of vasculature (184), the VBM now appears as one unified entity rather than two (166). The laminin composition, just as with larger arterioles, contain isoforms 411 and 511 from endothelial cells, and 211 from astrocytes (160, 184-185). Pericytes also make a critical contribution the VBM at capillaries given their anatomical position within the endothelial basement membrane and the fact that they express all laminin isoforms (21, 186).

Finally, upon examination of the VBM at postcapillary venules, one will find a virtual perivascular space can be found separating the vascular, parenchymal, and basement membranes. This is particularly conspicuous in inflammatory conditions where leukocytes accumulate in this space prior to infiltrating the brain parenchyma (183, 187). Just as with other vessel types, the endothelial basement membrane possesses laminins 411 and 511, although 511 expression is patchy (166, 185).

Linking astrocytes and endothelial cells to the VBM are two molecular entities: dystroglycans and integrins (158, 188). Dystroglycans are heterodimeric proteins consisting of a highly glycosylated extracellular α-subunit, which is responsible for linking cells to the VBM substrate, and an intracellular β-subunit, which is responsible for linking the dystroglycan complex to the actin-based cytoskeleton (189). Integrins are also heterodimeric proteins consisting of α- and β-subunits, both of which are transmembrane glycoproteins (190).

The various cell types at the VBM all express different integrin isoforms. Specifically, endothelial cells express α1β1, α3β1, α6β1, and αvβ1 (188, 191-193). Pericytes express α4β1 (194) and astrocytes express α1β1, α5β1, and α6β1 (192). **Table 1** summarizes the laminin and integrin molecules expressed by pericytes, astrocytes, and endothelial cells.

Cell type	**Laminin expression**	**Integrin expression**
Pericyte	All laminin isoforms	α4β1
Astrocyte	α2β1γ1 and α1β1γ1	α1β1, α5β1, and α6β1
Endothelial	α4β1γ1 and α5β1γ1	α1β1, α3β1, α6β1, and αvβ1

Table 1- Laminin and integrin expression specified by cell type

Microglial Cells

As members of the innate immune system (195-197), microglial cells are mononuclear phagocytes of the CNS that derive from yolk sac macrophage progenitors (196-200). These cells primarily engage in immune defense and maintenance of CNS homeostasis (201), and as such, exhibit high dynamism though the extension of their processes (195-197). By contacting surrounding cellular structures, they are able to continually assess their local microenvironment. Upon detection of injury, microglial responses involve resolving tissue injury, mitigating the effects of inflammation on the CNS, and supporting tissue repair and remodeling (202-203). Microglial cells also engage in phagocytic clearance of cellular debris (204), which can be modeled with experimental methods. One such method is the targeted two-photon chemical apoptotic ablation (2Phatal) single-cell apoptosis induction method where microglia have been shown to engulf apoptotic cells (205).

Dynamic Interactions of Astrocytes with the Vasculature

Cajal first characterized the intimate spatial proximity between astrocytes and blood vessel many years ago (206). Upon consideration of what physiological implications this spatial arrangement may have, he hypothesized that astrocytes controlled changes in vessel diameter through extensions and retractions of their endfeet, and that this was primarily how blood-flow was regulated in the brain (207). While modern studies have

precluded that possibility, other studies have clearly demonstrated that astrocytes dynamically interact with synapses, and that this can vary by neuronal activity (208-210) or by physiological state (211-216). However, it was only recently demonstrated for the first time that astrocytes can exert plasticity at the vascular interface (217), but how this occurs and if these endfeet physiologically exert control over the vasculature remained unknown.

Astrocytes in Aging

Zamanian et al. 2012 (218) demonstrated through transcriptional profiling that astrocytes become reactive following systemic lipopolysaccharide injection, taking on more of an inflammatory state. These astrocytes have become known as A1 reactive astrocytes, and some of the genetic changes that occur in astrocytes classified as A1 have been found to increase with age (219-220). Rather than having gene expression increase or decrease, the astrocyte transcriptomic profile shifts towards a more inflammatory state, with the magnitude in change differing for each brain region (219-220). The A1 nomenclature, however, is not without controversy.

Further studies in humans (221-223), rodents (224-225), and primates (221, 226) indicate that astrocyte morphology in aging differs markedly from young astrocytes, with older astrocytes' processes becoming short and stubby relative to the long and slender processes of young astrocytes. One other study even found that astrocyte endfeet retract later in life (227). Taken together, these changes are suggestive that astrocytes become more reactive with age.

Given known astrocyte reactivity with age, a recent study (228) documented the time course of maximal GFAP expression following traumatic brain injury in young versus aged mice. This study determined that young mice have a maximal response at three days post-injury which subsequently attenuates whereas this response is prolonged to seven days in old mice. Given further data from electron microscopy studies revealing no change in astrocyte cell numbers with aging (229-230), these findings seem to suggest that the extent of reactivity with age does not change, but that the kinetics of an astrogliosis response does.

Astrogliosis

Astrogliosis is a process whereby astrocytes take on a multitude of phenotypes in response to CNS insults and disorders (231) (**Figure 6**). Also called astrocyte reactivity, this is an evolutionary primitive response long considered to be homogenous and physiologically inconsequential (232-235). Studies from the past two decades, however, have utilized gene-editing technologies to enable precise hypothesis testing, the findings from which have uncovered a diverse group of potential alterations in astrocyte morphology, molecular expression, and physiology.

The discovery of the striking diversity exemplified by astrocytes in disease has given rise to the idea that astrocytes may adopt different subtypes, each with different functions. RNA sequencing and proteomics has allowed for a delineation in precise molecular expression profiles of various reactive astrocyte subtypes, but what this means for physiological outcomes in disease states cannot be determined solely from this data alone. The field, therefore, is currently pushing for a more comprehensive approach, including data on cellular morphology, physiology, cellular interactions, proliferation, and tissue architecture to which reactive astrocytes contribute (231). To this end, astrocyte 'subtypes' are distinguished from 'states' based upon whether or not alterations encompass all the aforementioned categories and are more permanent in nature (231). Combining data from decades of studies broadly suggests two subtypes exist, which are based upon whether or not astrocytes are proliferative, form borders around regions of CNS inflammation and/or conspicuous damage thereby resulting in permanent changes to underlying tissue architecture- and retain basic cellular morphology and physiology as observed in healthy tissue. Though these categories successfully combine data from many studies on astrocyte reactivity, they are by no means exhaustive in nature (231).

One feature that is consistent across all reactive astrocytes is the upregulation of the intermediate filament protein GFAP mentioned above. (232). The extent of upregulation varies with the degree of astrogliosis, and the degree of astrogliosis varies with severity of CNS insult. In instances of mild astrogliosis, such as that observed in areas distal to focal CNS lesions, GFAP upregulation is minimal, and if triggering mechanisms are simply acute in nature and resolve over time, then this form of gliosis has the potential to be a form of 'resolving reactivity' gliosis, where GFAP levels return to baseline values. In contrast, GFAP upregulation is substantial in

severe diffuse reactive gliosis which sometimes also results in glial 'scar' formation, where the 'scar' is thought of as a neuroprotective barrier. Such phenotypes are found in more detrimental CNS insults such as penetrating trauma and chronic neurodegeneration, and GFAP levels remain elevated long after the initiating insult may have resolved (232).

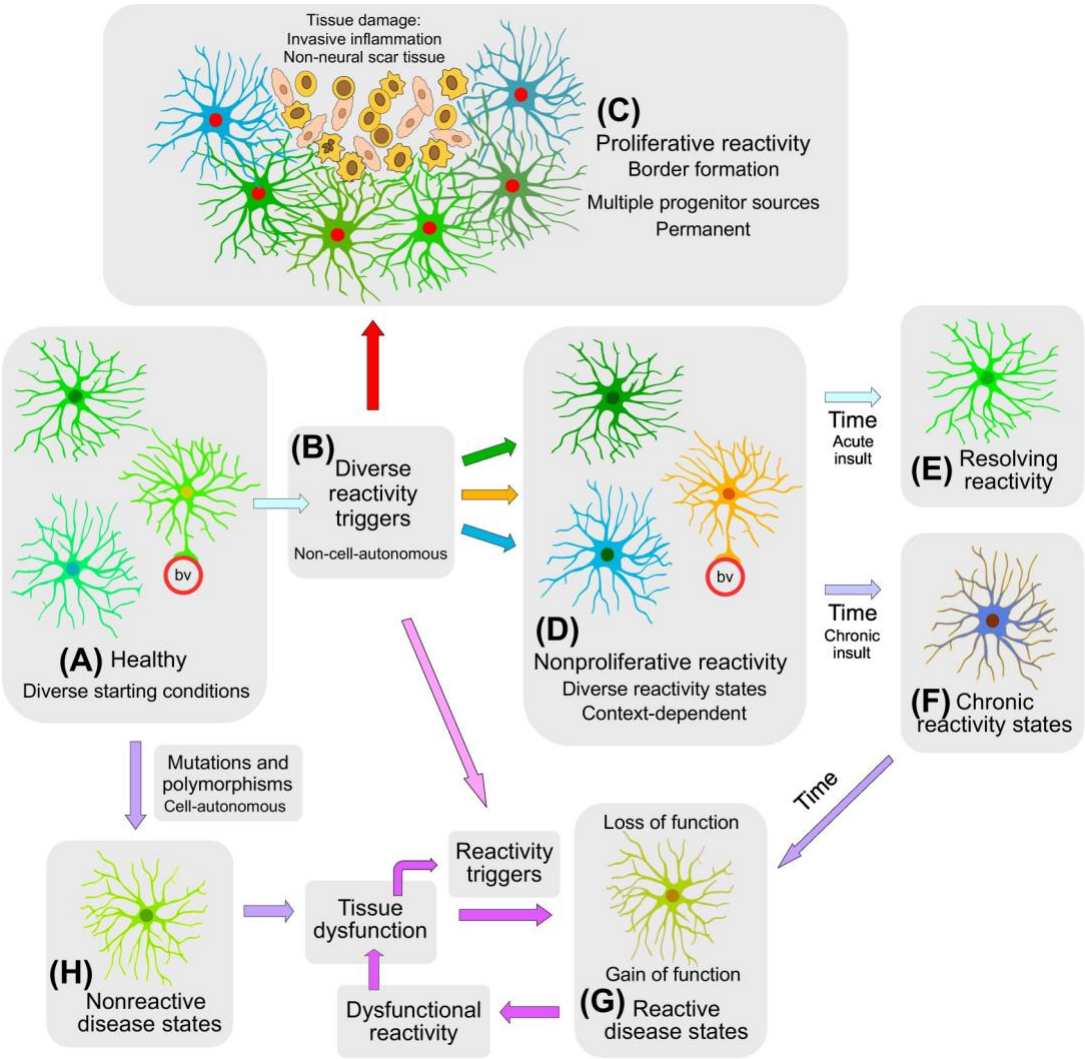

Figure 6- The astrocyte response to CNS disorders is very diverse- A) At baseline, astrocytes are a non-homogenous cell population with diversity in gene expression and function. B) Each CNS insult activates various non-cell-autonomous signaling cascades that in turn triggers various forms of astrocyte reactivity. C) Injury types such as ischemia or traumatic brain injury induce proliferative astrocyte reactivity. Newly proliferated astrocytes (red nuclei) can form limitans borders that separate damaged, inflamed, and non-neural scar tissue from viable, healthy tissue. D) Nonproliferative astrocyte reactivity exhibits context-specific gene expression and functional alterations as determined by baseline conditions and encountered reactivity triggers. E) Nonproliferative astrocyte reactivity can either resolve over time if the triggering insult ceases, or F) become

chronic if the triggering insult persists. G) Chronic astrocyte reactivity can result in loss or gain of function capable of engendering dysfunctional reactivity that aggravates tissue pathology in disease state and exacerbates disorder outcomes. H) Genetic mutations and polymorphisms can induce cell-autonomous perturbations in astrocyte physiology that leads to nonreactive disease states. This scenario commences an iterative cycle whereby astrocytes, though not reacting to a trigger, can induce a CNS trigger because of gained and/or lost functions present within them. Triggered reactivity in turn leads to further gain or loss of function capable of exacerbating tissue pathology and disease outcomes. Reproduced with permission from Sofroniew MV 2020 (231).

Mechanisms of Astrogliosis

A plethora of cytokines and growth factors released from a variety of cellular sources are capable of inducing GFAP upregulation. These ligands bind to their receptors and initiate downstream signaling, ultimately converging onto transcription factors that facilitate the astrogliosis response. Two particular transcriptional factors (TFs), nuclear factor κ-light-chain-enhancer of activated B cells (NF- κB) (236) and the *Janus* kinase-2(JAK2)/signal transducer and activator of transcription 3 (STAT3) cascade (237), are the best-characterized regulators of astrogliosis. In particular, the phosphorylation of STAT3 by JAK2 has been the most extensively studied; as such, the majority of this review will focus there.

The Interleukin-6 (IL-6) family of cytokines, including IL-6, leukemia inhibitory factor (LIF), ciliary neurotrophic factor (CNTF), Interleukin-11, cardiotrophin 1, and Oncostatin M (OSM) are all activators of the glycoprotein 130 (gp130) receptor (238-239), which is the defining feature of this cytokine family. Upon gp130 activation, the phosphorylation and activation of JAK2/STAT3 ensues, and STAT3 then forms a transcriptional complex with p300/CBP. This transcriptional complex then binds to the GFAP promoter subsequently increasing GFAP levels. Phosphatidylinositol-3-kinase (PI3K) activity lies upstream of STAT3 phosphorylation (240). Accordingly, mice overexpressing IL-6 under control of the GFAP promoter exhibited spontaneous reactive astrogliosis as well as seizures and ataxia (241). A separate study employing a cryolesion model demonstrated wound closure occurred with increased velocity and that GFAP levels were elevated for a longer duration of time (242).

The tumor growth factor- β (TGF-β) family of cytokines are capable of potentiating IL-6 induced astrogliogenesis. Upon binding to the TGF-β receptor, signal transducers and transcriptional modulators (SMAD) proteins undergo phosphorylation, activation, and heterodimerization, and subsequently bind to the p300/CBP-STAT3 transcriptional complex, which leads to increased GFAP expression (240). Smad3 is one particular protein that has been implicated in this cascade, as Smad3 knockout mice possessed fewer GFAP+ astrocytes around a stab wound lesion site (243). One other molecule converging onto p300/CBP regulation of GFAP expression involves the binding of retinoic acid to retinoic acid receptor α (RARα), where RARα expression at this complex is induced by the aforementioned cytokines binding to their respective receptors (240). Comprehensively speaking, the combined IL-6/TGF-β pathway represents the canonical pathway regulating GFAP expression levels (240) (**Figure 7**).

Activation of the Epidermal Growth Factor Receptor (EGFR) also leads to downstream JAK2/STAT3 activation, where its associated ligands- such as transforming growth factor-α (TGF-α)- have been implicated in the induction of astrogliosis (244). Four members comprise this receptor tyrosine kinase family: EGFR (ErbB1, HER1), ErbB2 (HER2), ErbB3 (HER3), and ErbB4 (HER4). These receptors share structural similarity as single-transmembrane glycoproteins, with each possessing an extracellular domain, transmembrane domain, a short juxtamembrane section, and tyrosine kinase domain with tyrosine-containing C-terminal tail. Upon ligand binding to the extracellular domain, receptors form homo- or heterodimers, upon which the intracellular tyrosine kinase domain is activated, thus leading to phosphorylation of the C-terminal tail (245-246). These phosphotyrosine residues then directly or indirectly activate downstream signaling pathways (246-247).

The transcription activator BRG1, also known as ATP-dependent chromatin remodeler SMARCA4, has recently been identified as a reactive astrocyte transcriptional regulator. Upon recruitment to STAT3 recognition regions, it potentiates GFAP aggregation and expression prior to the initiation and upregulation of GFAP transcription. Accordingly, inhibition of the JAK2/STAT3 pathway diminishes BRG1 recruitment and subsequent GFAP upregulation. This same phenotype is also observed upon knockdown of BRG1 (248). One final transcription factor whose expression and secretion increases in concert with activation of the JAK2/STAT3

pathway is lipocalin 2. A member of the lipocalin family, lipocalin 2 is an autocrine mediator of reactive astrogliosis, and it has been particularly implicated in GFAP regulation following inflammatory stimulation (249).

Many of the previously mentioned ligands have been linked to the activation of JAK2/STAT3 in various disease states- for example, IL-6 activates the GFAP gene in C6 malignant glioma cells (237), and epidermal growth factor in human glioblastoma (250). Furthermore, many of these ligands are implicated in astrocyte morphological maturation, with molecules such as heparin-binding epidermal growth factor having been linked to astrocyte endfoot formation (251). In adulthood, many of these inflammatory mediators are expressed at the mRNA level by cell types such as microglial and endothelial cells (252-253), suggestive that these cell types may be responsible for guiding endfeet to their appositional vascular location in development.

As mentioned above, NF-κB signaling is another prominent transcription factor linked to the regulation of GFAP expression (236, 254), as conditional deletion of NF-κB signaling in astrocytes ameliorates gliosis and astrocyte loss (255). Ligands upstream of NF-κB signaling, such as fibroblast growth factor 2 (FGF-2), have been linked to inducing astrogliosis. FGF2 knockout mice have reduced hippocampal and cortical GFAP expression levels, and mice deficient for both FGF2 and FGF5 have altered astrocyte endfoot polarity associated with blood-brain barrier abnormalities (244).

One final transcription factor associated with GFAP regulation is the c-Jun-AP-1 cascade (256). Scratch-induced injury in primary cortical astrocyte cultures induced waves of Ca^{2+} influx through gap junction, which subsequently activated c-Jun N-terminal kinase. C-Jun phosphorylation ensued, which facilitated the binding of AP-1 to the GFAP gene promoter and thereby upregulated expression (257). Interleukin-1β (IL-1β) is one particular ligand upstream of the c-Jun-AP-1 cascade implicated in gliosis (244). Specifically, IL-1β knockout mice (258) presented with delayed upregulation of GFAP mRNA and protein relative to controls following focal injury, and further presented with defects in repair of the BBB. Interestingly, a delayed upregulation of GFAP was not affected in IL-1β knockout mice, which is not surprising given the multitude of signals regulating GFAP expression as discussed above. Figure 6 illustrates the canonical JAK2/pSTAT3 signaling pathway.

Conclusion

The gliovascular unit is a conglomerate of cells that work in unison to maintain the CNS internal milieu. Through the extension of their perisynaptic processes and endfeet, astrocytes are well poised to dynamically interact with neurons and blood vessels, respectively. This morphological arrangement along with their high abundance in CNS position astrocytes as a central figure in the GVU. Astrocyte endfeet in particular have been shown to be responsible for maintaining the BBB at all levels of the vascular tree and regulating neurovascular coupling at primary capillaries. The up-regulation of GFAP following CNS injury has long been recognized as a central hallmark of astrogliosis, and the mechanisms regulating GFAP expression has been well characterized. Depending on injury type and duration, astrocytes can take on various reactive subtypes. Though the overall extent of reactivity does not dampen with aging, the kinetics of a maximal response does. Typically, reactivity is

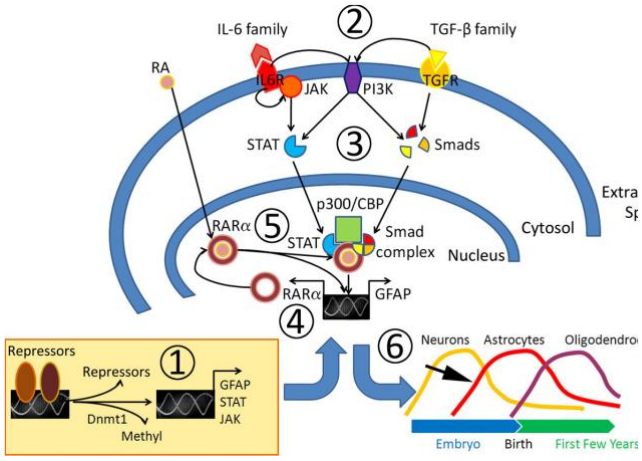

Figure 7-The canonical JAK2/pSTAT3 pathway- Step 1) transcription factors gain access to promoters of the genes for GFAP and other glial markers, as well as key components of the canonical astrogliogenic pathway, and these proteins are expressed. Steps 2 and 3) Cytokines such as Interleukin-6 bind to their receptors thereby triggering the canonical pathway. JAK, STAT, and Smad proteins undergo phosphorylation, activation, and translocation to the nucleus, where they combine with p300/CBP to form a potent transcriptional complex. Steps 4 and 5) cytokines induce the expression of RARα, its binding to the Stat3-p300/CBP-Smad complex, and to DNA. Retinoic acid activation of retinoic acid receptor α (RARα) may make this transcriptional complex more active and thus further potentiate the expression of GFAP. Step 6) The robust increase in GFAP expression during the perinatal period may be explained by the synergism between retinoic acid and cytokines. Reproduced with permission from Herrera et al. (240)

Conclusion continued

Typically, reactivity is characterized by morphological alterations such as the retraction of astrocytic endfeet- a phenotype also accompanied by breakdown of the blood-brain barrier. Understanding how endfeet arrive at their appositional vascular location, remain stable, and retract in disease could prove vital for mitigating cerebrovascular abnormalities that arise throughout the lifespan. Additionally, determining if astrocyte endfoot plasticity bears functional relevance to vascular physiology would further bolster this outcome.

References

1.) Kimbrough IF, Robel S, Roberson ED, Sontheimer H. Vascular amyloidosis impairs the gliovascular unit in a mouse model of Alzheimer's disease. Brain, 138(12). doi: 10.1093/brain/awv327.

2.) Herculano-Houzel, S. The human brain in numbers: a linearly scaled-up primate brain. *Frontiers in Human Neuroscience.* 2009. doi: 10.13389/neuro.09.031.2009

3.) Orkand RK, Nicholls JG, Kuffler SW. Effect of nerve impulses on the membrane potential of glial cells in the central nervous system of amphibia. J Neurophysiol 1966;29:788–806.

4.) Lothman EW, Somjen GG. Extracellular potassium activity, intracellular and extracellular potential responses in the spinal cord. J Physiol 1975;252:115–136.

5.) Dietzel I, Heinemann U, Hofmeier G, Lux HD. Transient changes in the size of the extracellular space in the sensorimotor cortex of cats in relation to stimulus-induced changes in potassium concentrations. Exp Brain Res 1980;40:432–439.

6.) Kimelberg HK. Anisotonic media and glutamate-induced ion transport and volume responses in primary astrocyte cultures. J Physiol (Paris) 1987;82:294–303.

7.) McGrail KM, Sweadner KJ. Immunofluorescent localization of two different Na, K-ATPases in the rat retina and in identified dissociated retinal cells. J Neurosci 1986;6:1272–1283.

8.) Tschirgi RD. The blood–brain barrier. In: Windle WF, editor. Biology of neuroglia. Springfield, IL: Charles C. Thomas, 1958: 130 –138.

9.) Kimelberg HK, Biddlecome S, Bourke RS. SITS-inhibitable Cl^- transport and Na^{2+}-dependent H^+ production in primary astroglial cultures. Brain Res 1979;173:111–124.

10.) Berl S, Lajtha A, Waelsch H. Amino acid and protein metabolism. VI: Cerebral compartments of glutamic acid metabolism. J Neurochem 1961;7:186 –197.

11.) Martinez-Hernandez A, Bell K, Norenberg MD. Glutamine synthetase: glial localization in brain. Science 1977;195:1356 –1358.

12.) Schousboe A, Hertz L, Svenneby G. Uptake and metabolism of GABA in astrocytes cultured from dissociated mouse brain hemispheres. Neurochem Res 1977;2:217–229.

13.) Levi G, Wilkin GP, Ciotti MT, Johnstone S. Enrichment of differentiated, stellate astrocytes in cerebellar interneuron cultures as studied by GFAP immunofluorescence and autoradiographic uptake patterns with [^{3}H]aspartate and [^{3}H]GABA. Brain Res 1983; 312:227–241.

14.) Zonta M, Angulo MC, Gobbo S, et al. Neuron-to-astrocyte signaling is central to the dynamic control of brain microcirculation. Nat Neurosci 2003;6:43–50.

15.) Attwell, D. et al. Glial and neuronal control of brain blood flow. Nature468,232-243 (2010).

16.) Mishra, A., Reynolds, J., Chen, Y. et al. Astrocytes mediate neurovascular signaling to capillary pericytes but not to arterioles.Nat Neurosci19,1619–1627 (2016). https://doi.org/10.1038/nn.44289.

17.) Mulligan SJ, Macvicar BA. Calcium transients in astrocyte endfeet cause cerebrovascular constrictions.Nature.2004;431:195–199.11.

18.) Takano T, et al. Astrocyte-mediated control of cerebral blood flow.Nat Neurosci.2006;9:260–267.8.12.

19.) Mishra A, Hamid A, Newman EA. Oxygen modulation of neurovascular coupling in the retina.Proc Natl Acad Sci USA.2011;108:17827–17831.

20.) Heithoff B, George KK, Phares AN, Zuidhoek IA, Munoz-Ballester C, & Robel S. Astrocytes are necessary for blood-brain barrier maintenance in the adult mouse brain. Glia 2020; https://doi.org/10.1002/glia.23908

21.) Yao Y, Chen ZL, Norris E H & Strickland S. Astrocytic laminin regulates pericyte differentiation and maintains blood brain barrier integrity. Nature communications. 2014; 5:3413. doi:10.1038/ncomms4413

22.) Ezan P, André P, Cisternino S, Sabaméa B, Boulay AC, Doutremer S, Thomas MA, Quenech'Du N, Giaume C, Cohen-Salmon M. Deletion of astroglial connexins weakens the blood-brain barrier. Journal of Cerebral Blood Flow and Metabolism : Official Journal of the International Society of Cerebral Blood Flow and Metabolism. 2012 Aug;32(8):1457-1467. DOI: 10.1038/jcbfm.2012.45.

23.) Faulkner JR, Herrmann JE, Woo MJ, Tansey KE, Doan NB, & Sofroniew MV. Reactive astrocytes protect tissue and preserve function after spinal cord injury. Journal of Neuroscience. 2004; 24(9), 2143-2155. https://doi.org/10.1523/JNEUROSCI.3547-03.2004

24.) Nielsen S, Nagelhus EA, Amiry-Moghaddam M, Bourque C, Agre P, Ottersen OP. Specialized membrane domains for water transport in glial cells: high-resolution immunogold cytochemistry of aquaporin-4 in rat brain. J Neurosci 1997;17:171–180.

25.) Martineau M, Shi T, Puyai J, Knolhoff AM, Dulong J, Gasnier B, Klingauf J, Sweedler JV, Jahn R, Mothet JP. Storage and Uptake of D-Serine into Astrocytic Synaptic-Like Vesicles Specify Gliotransmission. Journal of Neuroscience. 2013; 33(8): 3413-3423. doi: 10.1523/JNEUROSCI.3497-12.2013

26.) Watanabe K, Takeishi H, Hayakawa T, Sasaki H. Three-dimensional organization of the perivascular glial limiting membrane and its relationship with the vasculature: a scanning electron microscope study. Okajimas folia anatomica Japonica. 2010; 87: 109-121

27.) Bindocci E, Savtchouk I, Liaudet N, Becker D, Carriero G, & Volterra A. Three-dimensional Ca2+imaging advances understanding of astrocyte biology. Science. 19 May 2017; 356(6339). doi: 10.1126/science.aai8185

28.) Abnet K, Fawcett J W, & Dunnett SB. Interactions between meningeal cells and astrocytes in vivo and in vitro. Brain Research. Developmental Brain Research. 1991; **59**(2): 187– 196.

29.) Brochner, C. B., Holst, C. B., & Mollgard, K. Outer brain barriers in rat and human development. Frontiers in Neuroscience. 2015; 9(75). https://doi.org/10.3389/fnins.2015.00075

30.) Bardehle S, Kruger M, Buggenthin F, Schwausch J, Ninkovic J, Clevers H, Snippert HJ, Theis FJ, Meyer-Luehmann M, Bechmann I, Dimou L, Gotz M. Live imaging of astrocyte responses to acute injury reveals selective juxtavascular proliferation. Nature Neuroscience. 2013;16(5):580– 586. https://doi.org/10.1038/nn.3371

31.) Cali C, Agus M, Kare K, Boges D J, Lehvaslaiho H, Hadwiger M, & Magistretti PJ. 3D cellular reconstruction of cortical glia and parenchymal morphometric analysis from serial block-face Electron microscopy of juvenile rat. Progress in Neurobiology. 2019;183, 101696.

32.) McCaslin A F, Chen BR, Radosevich AJ, Cauli B, & Hillman EM. In vivo 3D morphology of astrocyte-vasculature interactions in the somatosensory cortex: Implications for neurovascular coupling. Journal of Cerebral Blood Flow and Metabolism. 2011;31(3):795– 806.

33.) Simard M, Arcuino G, Takano T, Liu QS, & Nedergaard M. Signaling at the gliovascular interface. The Journal of Neuroscience. 2003;23(27):9254– 9262 Retrieved from http://www.ncbi.nlm.nih.gov/entrez/query.fcgi?cmd=Retrieve&db=PubMed&dopt=Citation&list_uids=14534260

34.) Balslev Y, Dziegielewska KM, Mollgard K, & Saunders NR. Intercellular barriers to and transcellular transfer of albumin in the fetal sheep brain. Anatomy and Embryology. 1997;195(3):229– 236. https://doi.org/10.1007/s004290050042

35.) Horng S, Therattil A, Moyon S, Gordon A, Kim K, Argaw AT, Hara Y, Mariani JN, Sawai S, Flodby P, Crandall ED, Borok Z, Sofroniew MV, Chapouly C, John GR. Astrocytic tight junctions control inflammatory CNS lesion pathogenesis. The Journal of Clinical Investigation. 2017;127(8):3136– 3151. https://doi.org/10.1172/JCI91301

36.) Frydenlund D S, Bhardwaj A, Otsuka T, Mylonakou MN, Yasumura T, Davidson KG, et al. Temporary loss of perivascular aquaporin-4 in neocortex after transient middle cerebral artery occlusion in mice. Proc. Natl. Acad. Sci. USA. 2006;103:13532–13536. doi: 10.1073/pnas.060579610314.18.
37.) Steiner E, Enzmann GU, Lin S, Ghavampour S, Hannocks M. J, Zuber B, et al. Loss of astrocyte polarization upon transient focal brain ischemia as a possible mechanism to counteract early edema formation. Glia. 2012;60:1646–1659. doi: 10.1002/glia.2238315.19.
38.) Wang Y. & Parpura V. Central Role of Maladapted Astrocytic Plasticity in Ischemic Brain Edema Formation. Front. Cell. Neurosci. 2016; 10:129. doi: 10.3389/fncel.2016.00129
39.) Rajkowska G, Hughes J, Stockmeier CA, Javier Miguel-Hidalgo J, & Maciag D. Coverage of blood vessels by astrocytic endfeet is reduced in major depressive disorder. Biological psychiatry. 2013;73(7):613–621. https://doi.org/10.1016/j.biopsych.2012.09.02411.15.
40.) Gudmundsson P, Skoog I, Waern M, Blennow K, P·lsson S, Rosengren L, Gustafson D. The relationship between cerebrospinal fluid biomarkers and depression in elderly women. Am J Geriatr Psychiatry. 2007;15:832. doi: 10.1097/JGP.0b013e3180547091.12.16.
41.) Bechter K, Reiber H, Herzog S, Fuchs D, Tumani H, Maxeiner HG. Cerebrospinal fluid analysis in affective and schizophrenic spectrum disorders: identification of subgroups with immune responses and blood-CSF barrier dysfunction. J Psychiatr Res. 2010;44:321–330. doi: 10.1016/j.jpsychires.2009.08.008.
42.) Wolburg-Bucholz K, Mack AF, Steiner E, Pfeiffer F, Engelhardt B, Wolburg H. Loss of astrocyte polarity marks blood-brain barrier impairment during experimental autoimmune encephalomyelitis. Acta Neuropathol. 2009;118(2): 219-233. doi: 10.1007/s00401-009-0558-4.
43.) Niu J, Tsai H, Hoi KK, Huang N, Yu G, Kim K, Baranzini SE, Xiao L, Chan JR, Fancy SPJ. Aberrant oligodendroglial–vascular interactions disrupt the blood–brain barrier, triggering CNS inflammation. Nat Neuroscience. 2019; 22:709-718. https://doi.org/10.1038/s41593-019-0369-4
44.) Watkins S, Robel S, Kimbrough IF, Robert SM, Ellis-Davies G, Sontheimer H. Disruption of astrocyte-vascular coupling and the blood-brain barrier by invading glioma cells. Nature Communications. 2014; 5: 4196. doi: 10.1038/ncomms5196
45.) Cohen-Salmon M, Slaoui L, Mazaré N, Gilbert A, Oudart M, Alvear-Perez R, Elorza-Vidal X, Chever O, Boulay AC. Astrocytes in the regulation of cerebrovascular functions. Glia. 2020;69(4):817-841. doi: 10.1002/glia.23924**.**
46.) Vanlandewijck M, He L, Mäe MA, Andrae J, Ando K, Del Gaudio F, Nahar K, Lebouvier T, Laviña B, Gouveia L, Sun Y, Raschperger E, Räsänen M, Zarb Y, Mochizuki N, Keller A, Lendahl U, Betsholtz C. A molecular atlas of cell types and zonation in the brain vasculature. Nature. 2018; 554: 475-480. doi: 10.1038/nature25739
47.) Zlokovic B. The Blood-Brain Barrier in Health and Chronic Neurodegenerative Disorders. Neuron. 2008; 57(2):178-201. doi:10.1016/j.neuron.2008.01.003.
48.) Ehrlich P. Das sauerstoff-bedürfnis des organisms. in Eine Farbenanalytische Studie, (1885).
49.) Ehrlich P. Ueber die beziehungen von chemischer constitution, vertheilung, und pharmakologischen wirkung. J. Wiley & Sons, 1906).
50.) Goldmann EE. Vitalfärbung am zentralnervensystem. Abhandl Königl Preuss Akad Wiss, 1-60 (1913).
51.) Engelhardt B. Development of the blood-brain barrier. Cell and tissue research. 2003; 314: 119-129. doi:10.1007/s00441-003-0751-z.
52.) Pardridge WM. Blood-brain barrier delivery. Drug Discovery Today. 2007;12: 54-61. doi:10.1016/j.drudis.2006.10.013
53.) Sweeney MD, Sagare AP, & Zlokovic B. Blood-brain barrier breakdown in Alzheimer's disease and other neurodegenerative disorders. Nature Reviews Neurology. 2018; 14(3): 133-150. doi: 10.1038/nrneurol.2017.188
54.) Lin L, Yee SW, Kim RB, Giacomini KM. SLC Transporters as Therapeutic Targets: Emerging Opportunities. Nature Reviews Drug Discovery. 2015;14(8):543-560. doi: 10.1038/nrd4626
55.) Mokgokong R, Wang S, Taylor CJ, Barrand MA, Hladky SB. Ion transporters in brain endothelial cells that contribute to formation of brain interstitial fluid. Pflugers Arch. 2014; 466:887-901.

56.) Zlokovic BV. Neurovascular pathways to neurodegeneration in Alzheimer's disease and other disorders. *Nature Reviews Neuroscience*. 2011; 12(12): 723-738.
57.) Qutub AA, Hunt CA. Glucose transport to the brain: a systems model. Brain Research Reviews. 2005**;** 49: 595-617. doi: 10.1016/j.brainresrev.2005.03.002
58.) Simpson IA, Carruthers A, Vannucci SJ. Supply and demand in cerebral energy metabolisms: the role of nutrient transporters. J. Cereb. Blood Flow Metab. 2007: 27: 1766-1791. doi: 10.1038/sj.jcbfm.9600521
59.) Daneman R, Agalliu D, Zhou L, Kuhnert F, Kuo CJ, Barres BA. Wnt/beta-catenin signaling is required for CNS, but not non-CNS, angiogenesis. Proc. Natl. Acad. Sci. USA. 2009; 106: 641-646. doi: 10.1073/pnas.0805165106
60.) Liebner S, Corada M, Bangsow T, Babbage J, Taddei A, Czupalla CJ, Reis M, Felici A, Wolburg H, Fruttiger M. et al. Wnt/β-catenin signaling controls development of the blood-brain barrier. J. Cell Biol. 2008; 183: 409-417. doi: 10.1083/jcb.200806024.
61.) Stenman JM, Rajagopal J, Carroll TJ, Ishibashi M, McMahon J, McMahon AP. Canonical Wnt signaling regulates organ-specific assembly and differentiation of CNS vasculature. Science. 2008; 322: 1247-1250. doi: 10.1126/science.1164594
62.) Simpson IA, Chundu KR, Davies-Hill T, Honer WG, Davies P. Decreased concentrations of GLUT1 and GLUT3 glucose transporters in the brains of patients with Alzheimer's disease. Annal Neurol. 1994;35:546-551.
63.) Mooradian AD, Chung HC, Shah GN. GLUT-1 expression in the cerebra of patients with Alzheimer's disease. Neurobiol Aging. 1997;18:469-474.
64.) Kalaria RN, Harik SI. Reduced glucose transporter at the blood-brain barrier and in cerebral cortex in Alzheimer disease. J Neurochem. 1989;53:1083-1088.
65.) Horwood N, Davies DC. Immunolabelling of hippocampal microvessel glucose transporter protein is reduced in Alzheimer's disease. Virchows Arch Int J Pathol. 1994; 425:69-72.
66.) Winkler EA, Nishida Y, Sagare AP, Rege SV, Bell RD, Perlmutter D, Sengillo JD, Hillman S, Kong P, Nelson AR, Sullivan JS, Zhao Z, Meiselman HJ, Wendy RB, Soto J, Abel ED, Makshanoff J, Zuniga E, De Vivo CD, Zlokovic B. GLUT1 reductions exacerbate Alzheimer's disease vasculoneuronal dysfunction and degeneration. Nature Neuroscience. 2015; 18(4):521-530. doi: 10.1038/nn.3966
67.) Ben-Zvi A, Lacoste B, Kur E, Andreone BJ, Mayshar Y, Yan H, Gu C. MSFD2A is critical for the formation and function of the blood brain barrier. Nature. 2014; 509(7501): 507-511. doi: 10.1038/nature13324
68.) Szakacs G, Paterson JK, Ludwig JA, Booth-Genthe C, & Gottesman MM. Targeting multidrug resistance in cancer. *Nat. Rev. Drug Discov.* **5**, 219–234 (2006).
69.) Ambudkar SV, Kimchi-Sarfaty C, Sauna ZE, & Gottesman MM. P-Glycoprotein: from genomics to mechanism. *Oncogene* **22**, 7468–7485 (2003).
70.) Robey RW, Pluchino KM, Hall MD, Fojo AT, Bates SE, Gottesman MM. Revisiting the role of ABC transporters in multidrug-resistance cancer. Nature Reviews Cancer. 2018; 18: 452-464. doi: 10.1038/s41568-018-0005-8
71.) Dean M, Hamon Y, Chimini G. The human ATP-binding cassette (ABC) transporter superfamily. Journal of Lipid Research. 2001; 42(7):1007-1017.
72.) Cirrito JR, Deane R, Fagan AM, Spinner ML, Parsadanian M, Finn MB, Jiang H, Prior JL, Sagare A, Bales KR, Paul SM, Zlokovic BV, Piwnica-Worms D, Holtzman D. P-glycoprotein deficiency at the blood-brain barrier increases amyloid-β deposition in an Alzheimer disease mouse model. Journal of Clinical Investigation. 2005; 115(11): 3285-3290. doi: 10.1172/JCI25247
73.) Wang W, Bodles-Brakhop AM, Barger SW. A Role for P-Glycoprotein in Clearance of Alzheimer Amyloid β-Peptide from the Brain. Curr Alzheimer Res. 2016;13:615-620.
74.) McInerney MP, Short JL, Nicolazzo JA. Neurovascular Alterations in Alzheimer's Disease: Transporter Expression Profiles and CNS Drug Access. AAPS J. 2017;19:940-956.
75.) van Assema D ME, Lubberink M, Bauer M, van der Flier WM, Schuit RC, Windhorst AD, Comans E FI, Hoetjes NK, Tolboom N, Langer O, Müller M, Scheltnes P, Lammertsma AA, van Berckel BNM. Blood-

brain barrier P-glycoprotein function in Alzheimer's disease. Brain. 2012; 135(1): 181-189. doi: 10.1093/brain/awr298
76.) Pardridge WM. Targeted delivery of protein and gene medicines through the blood-brain barrier. Clinical Pharmacology & Therapeutics. 2014; (97)4: 347-361. doi: 10.1002/cpt.18
77.) Bell RD, Winkler EA, Singh I, Sagare AP, Deane R, Wu Z, Holtzman DM, Betsholtz C, Armulik A, Sallstrom J, Berk BC, Zlokovic BV. Apolipoprotein E controls cerebrovascular integrity via cyclophilin A. Nature. 2012 16; 485(7399): 512-516.
78.) Alata W, Ye Y, St-Amour I, Vandal M, Calon F. Human apolipoprotein E ε4 expression impairs cerebral vascularization and blood-brain barrier function in mice. J Cereb Blood Flow Metab. 2015; 35(1): 86-94.
79.) Nishitsuji K, Hosono T, Nakamura T, Bu G, Michikawa M. Apolipoprotein E regulates the integrity of tight junctions in an isoform-dependent manner in an in vitro blood-brain barrier model. J Biol Chem. 2011; 286(20): 17536-17542.
80.) Hultman K, Strickland S, Norris EH. The APOE ε4/ε4 genotype potentiates vascular fibrin(ogen) deposition in amyloid-laden vessels in the brains of Alzheimer's disease patients. J Cereb Blood Flow Metab Off J Int Soc Cereb Blood Flow Metab. 2013; 33:1251-1258.
81.) Zipser BD, Johanson CE, Gonzalez L, Berzin TM, Tavares R, Hulette CM, Vitek MP, Hovanesian V, Stopa EG. Microvascular injury and blood-brain barrier leakage in Alzheimer's disease. Neurobiol Aging. 2007; 28(7):977-986. doi:10.1016/j.neurobiolaging.2006.05.016.
82.) Halliday MR, Rege SV, Ma Q, Zhao Z, Miller CA, Winkler EA, Zlokovic B. Accelerated pericyte degeneration and blood-brain barrier breakdown in apolipoprotein E4 carriers with Alzheimer's disease. J Cereb Blood Flow Metab. 2016; 36(1): 216-227. doi: 10.1038/jcbfm.2015.44
83.) Salloway S, Gur T, Berzin T, Zipser B, Correia S, Hovanesian V, Fallon J, Kuo-Leblanc V, Glass D, Hulette C, Rosenberg C, Vitek M, Stopa E. Effect of APOE genotype on microvascular basement membrane in Alzheimer's disease. Journal of the Neurological Sciences. 2002; 203-204: 183-187.
84.) Deane R, Yan SD, Submamaryan RK, LaRue B, Jovanovic S, Hogg E, Welch D, Manness L, Lin C, Yu J, Zhu H, Ghiso J, Frangione B, Stern A, Schmidt AM, Armstrong DL, Arnold B, Liliensiek B, Nawroth P, Hofman F, Kindy M, Stern D, Zlokovic B. RAGE mediates amyloid-beta peptide transport across the blood-brain barrier and accumulation in brain. Nature Medicine. 2003; 9(7): 907-913. doi: 10.1038/nm890
85.) Yan SD, Chen X, Chen M, Zhu H, Roher A, Slattery T, Zhao L, Nagashima M, Morser J, Migheli A, Nawroth P, Stern D, Schmidt AM. RAGE and amyloid-beta peptide neurotoxicity in Alzheimer's disease. Nature. 1996; 382(6593): 685-691. doi: 10.1038/3826850
86.) MacKic JB, Stins M, McComb JG, Calero M, Ghiso J, Kim KS, Yan SD, Stern D, Schmidt AM, Frangione B, Zlokovic BV. Human blood-brain barrier receptors for Alzheimer's amyloid-beta-1-40. Asymmetrical binding, endocytosis, and transcytosis at the apical side of brain microvascular endothelial cell monolayer. J Clin Invest. 1998; 102(4): 734-743. doi: 10.1172/JCI2029.
87.) Deane R, Singh I, Sagare AP, Bell RD, Ross NT, LaRue B, Love R, Perry S, Paquette N, Deane RJ, Thiyagarajan M, Zarcone T, Fritz G, Friedman AE, Miller BL, Zlokovic BV. A multimodela RAGE-specific inhibitor reduces amyloid β-mediated brain disorder in a mouse model of Alzheimer disease. J Clin Invest. 2012; 122(4): 1377-1392. doi: 10.1172/JCI58642
88.) Hawkins BT, Davis TP. The blood-brain barrier neurovascular unit in health and disease. Pharmacol. Rev. 2005; 57: 173-185.
89.) Bazzoni G, Dejana E. Endothelial cell-to-cell junctions: molecular organization and role in vascular homeostasis. Physiol. Rev. 2004; 84: 869-901.
90.) Lee SW, Kim WJ, Choi YK, Song HS, Son MJ, Gelman IH, Kim YJ, Kim KW. SSeCKS regulates angiogenesis and tight junction formation in blood-brain barrier. Nature Medicine. 2003; 9: 900-906.
91.) Nitta T, Hata M, Gotoh S, Seo Y, Sasaki H, Hashimoto N, Furuse M, Tsukita S. Size-selective loosening of the blood-brain barrier in claudin-5-deficient mice. J. Cell Biol. 2003; 161: 653-660.
92.) Wolburg H. (2006). The Endothelial Frontier. In Blood-Brain Interface: From Ontogeny to Artificial Barriers, R. Dermietzel, D.C. Spray, and M. Nedergaard, eds. (Weinheim, Germany: Wiley-VCH), pp. 77-109

93.) Saitou M, Furuse M, Sasaki H, Schulzke JD, Fromm M, Takano H, Noda T, Tsukita S. Complex phenotype of mice lacking occluding, a component of tight junction strands. Mole. Biol. Cell. 2000; 11: 4131-4142.
94.) Bamforth SD, Kniesel U, Wolburg H. Engelhardt B, Risau W. A dominant mutant of occluding disrupts tight junction structure and function. J. Cell Sci. 1999; 112: 1879-1888.
95.) Fantin A, Vieira JM, Plein A, Maden CH, Ruhrberg C. The embryonic mouse hindbrain as a qualitative and quantitative model for studying the molecular and cellular mechanisms of angiogenesis. Nature Protocols. 2013; 8(2): 418-429.
96.) Obermeier B, Daneman R, Ransohoff RM. Development, maintenance and disruption of the blood-brain barrier. Nature Medicine. 2013; 19(12): 1584-1596.
97.) Shalaby F, Rossant J, Yamaguchi TP, Gertsenstein M, Wu XF, Breitman ML, Schuh AC. Failure of blood-island formation and vasculogenesis in Flk-1-deficient mice. Nature. 1995; 376: 62-66.
98.) Carmeliet P, Ferreira. V, Breier G, Pollefeyt S, Kieckens L, Gertsenstein M, Fahrig M, Vandenhoeck A, Harpal K, Eberhardt C, Declercq C, Pawling J, Moons L, Collen D, Risau W, Nagy A. Abnormal blood vessel development and lethality in embryos lacking a single VEGF allele. Nature. 1996; 380(6573): 435-439. doi: 10.1038/380435a0
99.) Logan CY, Nusse R. The Wnt signaling pathway in development and disease. Annu. Rev. Cell Dev. Biol. 2004; 20: 781-810.
100.) Daneman R, Zhou L, Agalliu D, Cahoy JD, Kaushal A, Barres B. The mouse blood-brain barrier transcriptome: a new resource for understanding the development and function of brain endothelial cells. PLoS One. 2010; 5(10):e13741. doi:10.1371/journal.pone.0013741.
101.) Daneman R, Zhou L, Kebede A, Barres B. Pericytes are required for blood-brain barrier integrity during embryogenesis. Nature. 2010; 468(7323): 562-566. doi: 10.1038/nature09513
102.) Engelhardt B, Liebner S. Novel insights into the development and maintenance of the blood-brain barrier. Cell Tissue Res. 2014; 355(3): 687-699: doi:10.1007/s00441-014-1811-2.
103.) Biswas S, Cottarelli A, Agalliu D. Neuronal and glial regulation of CNS angiogenesis and barriergenesis. The Company of Biologists. 2020; 147: dev182279. doi:10.1242/dev.182279.
104.) Corada M, Orsenigo F, Bhat GP, Conze LL, Breviario F, Cunha SI, Claesson-Welsh L, Beznoussenko GV, Mironov AA, Bacigaluppi M, Martino G, Pitulescu ME, Adams RH, Magnusson P, Dejana E. Fine-Tuning of Sox17 and Canonical Wnt Coordinates the Permeability Properties of the Blood-Brain Barrier. Circulation Research. 2019; 124:511-525. doi: 10.1161/CIRCRESAHA.118.313316
105.) Hupe M, Li MX, Kneitz S, Davydova D, Yokota C, Kele J, Hot B, Stenman JM, Gessler M. Gene expression profiles of brain endothelial cells during embryonic development at bulk and single-cell levels. ScienceSignaling. 2017; 10(487): eaag2476. doi: 10.1126/scisignal.aag2476
106.) Harb R, Whiteus C, Freitas C, Grutzendler J. *In Vivo* Imaging of Cerebral Microvascular Plasticity from Birth to Death. Journal of Cerebral Blood Flow & Metabolism. 2012; 33(1): 146-156. doi: 10.1038/jcbfm.2012.152
107.) Martowicz A, Trusohamn M, Jensen N, Wisniewska-Kruk J, Corada M, Ning FC, Jele J, Dejana E, Nyqvist D. Endothelial β-Catenin Signaling Supports Postnatal Brain and Retinal Angiogenesis by Promoting Sprouting, Tip Cell Formation, and VEGFR (Vascular Endothelial Growth Factor Receptor) 2 Expression. Ateriosclerosis Thromb Vasc Biol. 2019; 39(11):2273-2288. doi:10.1161/ATVBAHA. 119.312749.
108.) Stewart PA, Wiley MJ. Developing nervous tissue induces formation of blood-brain barrier characteristics in invading endothelial cells: a study using quail—chick transplantation chimeras. Dev Biol. 1981; 84(1): 183-192. doi: 10.1016/0012-1606(81)90382-1
109.) Rubin LL. The blood-brain barrier in and out of cell culture. Current Opinion in Neurobiology. 1991; 1(3):360-363.
110.) Tao-Cheng JH, Nagy Z, Brightman MW. Tight junctions of brain endothelium in vitro are enhanced by astroglia. Journal of Neuroscience. 1987; 7(10):3293-3299. doi: 10.1523/JNEUROSCI.07-10-03293.1987.

111.) Dehouck MP, Méresse S, Dehouck B, Fruchart JC, Cecchelli R. In vitro reconstituted blood-brain barrier. Journal of Controlled Release. 1992; 21(1-3): 81-91. doi: 10.1016/0168-3659(92)90010-O
112.) Janzer RC, Raff MC. Astrocytes induce blood-brain barrier properties in endothelial cells. Nature. 1987; 325: 253-257.
113.) Holash JA, Noden DM, Stewart PA. Re-Evaluating the Role of Astrocytes in Blood-Brain Barrier Induction. Developmental Dynamics. 1993;197:14-25.
114.) Alvarez JI, Dodelet-Devillers A, Kebir H, Ifergan I, Fabre PJ, Terouz S, Sabbagh M, Wosik K, Bourbonnière L, Bernard M, Van Horssen J, de Vries HE, Charron F, Prat A. The Hedgehog pathway promotes blood-brain barrier integrity and CNS immune quiescence. Science. 2011; 334(6063): 1727-1731. doi: 10.1126/science.1206936.
115.) Neuhaus J, Risau W, Wolburg H. Induction of blood-brain barrier characteristics in bovine brain endothelial cells by rat astroglial cells in transfilter coculture. Ann NY Acad Sci. 1991; 633: 578-580.
116.) Prat A, Biernacki K, Wosik K, Antel JP. Glial cell influence on the human blood-brain barrier. Glia. 2001; 36: 145-155.
117.) Abbott NJ, Ronnback L, Hansson E. Astrocyte-endothelial interactions at the blood-brain barrier. Nature Reviews Neuroscience. 2006;7:41-53.
118.) Wosik K, Cayrol R, Dodelet-Devillers A, Berthelet F, Bernard M, Moumdjian R, Bouthillier A, Reudelhuber TL, Prat A. Angiotensin II controls occludin function and is required for blood brain barrier maintenance: Relevance to multiple sclerosis. Journal of Neuroscience. 2007; 27: 9032-9042.
119.) Kröll S, El-Gindi J, Thanabalasundaram G, Panpumthong P, Schrot S, Hartmann C, Galla HJ. Control of the blood-brain barrier by glucocorticoids and the cells of the neurovascular unit. Ann N Y Acad Sci. 2009;1165:228-239. doi: 10.1111/j.1749-6632.2009.04040.x.
120.) Lee SW, Kim WJ, Choi YK, Song HS, Son MJ, Gelman IH, Kim YJ, Kim KW. SSeCKS regulates angiogenesis and tight junction formation in blood-brain barrier. Nature Medicine. 2003; 9(7): 900-906. doi: 10.1038/nm889
121.) Tsai HH, Li H, Fuentealba LC, Molofsky AV, Taveira-Marques R, Zhuang H, Tenney A, Murnen AT, Fancy S PJ, Merkle F, Kessaris N, Alvarez-Buylla A, Richardson WD, Rowitch DH. Regional astrocyte allocation regulates CNS synaptogenesis and repair. Science. 2012; 337(6092):358-362. doi: 10.1126/science.1222381.
122.) Banks WA, Reed MJ, Logsdon AF, Rhea EM, Erickson MA. Healthy aging and the blood-brain barrier. Nature Aging. 2021; 1: 243-254. doi: 10.1038/s43587-021-00043-5
123.) Conford EM, Braun LD, Oldendorf WH. Developmental modulations of blood-brain barrier permeability as an indicator of changing nutritional requirements in the brain. Pediatric Research. 1982; 16: 324-328.
124.) Le Couteur DG, Simpson SJ. Adaptive senectitude: the prolongevity effects of aging. J. Gerontol. A Biol Sci. Med Sci. 2011; 66: 179-182.
125.) Jaeger LB, Dohgu S, Hwang MC, Farr SA, Murphy MP, Fleegal-Demotta MA, Lynch JL, Robinson SM, Niehoff ML, Johnson SN, Kumar VB, Banks WA. Testing the Neurovascular Hypothesis of Alzheimer's Disease: LRP-1 Antisense Reduces Blood-Brain Barrier Clearance, Increases Brain Levels of Amyloid-β Protein, and Impairs Cognition. J Alzheimers Dis. 2009; 17(3): 553-570. doi:10.3233/JAD-2009-1074.
126.) Mooradian AD, Morin AM, Cipp LJ, Haspel HC. Glucose transport is reduced in the blood-brain barrier of aged rats. Brain Res. 1991; 551: 145-149.
127.) Daniel PM, Love ER, Pratt OE. The effect of age upon the influx of glucose into the brain. J. Physiol. 1978; 274: 141-148.
128.) Ohata M, Sundaram U, Fredericks WR, London ED, Rapoport SI. Regional cerebral blood flow during development and ageing of the rat brain. Brain. 1981; 104: 319-332
129.) Ibáñez V, Pietrinin P, Furey ML, Alexander GE, Milleet P, Bokde A LW, Teichberg D, Schapiro MB, Horwitz B, Rapoport SI. Resting state brain glucose metabolism is not reduced in normosensitive health

men during aging, after correction for brain atrophy. Brain Res Bull. 2004; 63(2): 147-154. doi:10.1016/j.brainresbull.2004.02.003
130.) Mooradian AD, Smith TL. The effect of age on lipid composition and order of rat cerebral microvessels. Neurochem Res. 1992; 17: 233-237.
131.) Kalaria RN. Cerebral vessels in ageing and Alzheimer's disease. Pharmacol. Ther. 1996; 72: 193-214.
132.) Sonntag WE, Eckman DM, Ingraham J, Riddle DR in Brain Aging: Models, Methods, and Mechanisms (Ed. Riddle, D.R.) (CRC Press/Tay & Francis, 2007).
133.) Montagne A, Barnes SR, Sweeney MD, Halliday MR, Sagare AP, Zhao Z, Toga AW, Jacobs RE, Liu CY, Amezcua L, Harrington MG, Chui HC, Law M, Zlokovic BV. Blood-brain barrier breakdown in the aging human hippocampus. Neuron. 2015; 85(2): 296-302. doi: 10.1016/j.neuron.2014.12.032.
134.) Verheggen ICM, de Jong JJA, van Boxtel MPJ, Gronenschild E HBM, Palm WM, Postma AA, Jansen J FA, Verhey R RJ, Backes WH. Increase in blood-brain barrier leakage in healthy, older adults. GeroScience. 2020; 42(4): 1183-1193. doi: 10.1007/s11357-020-00211-2
135.) Verheggen ICM, de Jong J JA, van Boxtel M PJ, Postma AA, Jansen J FA, Verhey F RJ, Backes WH. Imaging the role of blood-brain barrier disruption in normal cognitive ageing. GeroScience. 2020; 42: 1751-1764.
136.) Hill RA, Tong L, Yuan P, Murikinati S, Gupta S, Grutzendler J. Regional blood flow in the normal and ischemic brain is controlled by arteriolar smooth muscle cell contractility and not by capillary pericytes. Neuron. 2015; 87(1): 95-110. doi:10.1016/j.neuron.2015.06.001
137.) Ebert CJ. Hanbuch der Lehre von der Gewegen des Menschen und der Tiere (Vol. 1). Leipzig: Engelmann, 1871.
138.) Rouget C. Mémoire sur le development, la structure et les proprietés physiologieques des capillaries sanguins et lymphatiques. Arch Physiol Norm Path 1873; 5: 603-663.
139.) Attwell D, Mishra A, Hall CN, O'Farrell FM, Dalkara T. What is a pericyte? J Cereb Blood Flow Metab. 2016; 36(2): 451-455. doi: 10.1177/0271678X15610340
140.) Chaigneau E, Oheim M, Audinat E, Charpak S. Two-photon imaging of capillary blood flow in olfactory bulb glomeruli. Proc. Natl. Acad. Sci. USA. 2003; 100: 13081-13086.
141.) Hall CN, Reynell C, Gesslein B, Hamilton NB, Mishra A, Sutherland BA, O'Farrell FM, Buchan AM, Lauritzen M, Attweel D. Capillary pericytes regulate cerebral blood flow in health and disease. Nature. 2014; 508: 55-60.
142.) Peppiatt CM, Howarth C, Mobbs P, Attwell D. Bidirectional control of CNS capillary diameter by pericytes. Nature. 2006; 443: 700-704.
143.) Wu DM, Kawamura H, Sakagami K, Kobayashi M, Puro DG. Choligneric regulation of pericyte-containing retinal microvessels. Am J Physiol Heart Circ Physiol. 2003; 284(6): H2083-2090.
144.) O'Farrell FM, Atwell D. A role for pericytes in coronary no-reflow. Nat. Rev. Cardiol. 2014; 11: 427-432.
145.) Yemisci M, Gursoy-Ozdemir Y, Vural A, Can A, Topalkara K, Dalkara T. Pericyte contraction induced by oxidative-nitrative stress impairs capillary reflow despite successful opening of an occluded cerebral artery. Nature Medicine. 2009; 15: 1031-1037.
146.) Zimmerman KW. Der feinere Bau der Blutkapillaren. Z Anat Entwicklungsgesch. 1923; 68: 29-109.
147.) Hartmann DA, Berthiaume AA, Grant RI, Harill SA, Koski T, Tieu T, McDowell KP, Faino AV, Kelly A, Shih AY. Brain capillary pericytes exert a substantial but slow influence on blood flow. Nature Neuroscience. 2021. doi: 10.1038/s41593-020-00793-2
148.) Nelson AR, Sagare MA, Wang Y, Kisler K, Zhao Z, Zlokovic B. Channelrhodopsin Excitation Contracts Brain Pericytes and Reduces Blood Flow in the Aging Mouse Brain *in vivo*. Front. Aging. Neurosci. 2020; 12:108. doi: 10.3389/fnagi.2020.00108
149.) Nortley R, Korte N, Izquierdo P, Hirunpattarasilp C, Mishra A, Jaunmuktane Z, Kyragyri V, Pfeiffer T, Khennouf L, Madry C, Gong H, Richard-Loendt A, Huang W, Saito T, Saido TC, Brandner S, Sethi H, Attwell D. Amyloid β oligomers constrict human capillaries in Alzheimer's disease via signaling to pericytes. Science. 2019; 365(6450): eaav9518. doi: 10.1126/science.aav9518

150.) Iadecola C. Neurovascular regulation in the normal brain and in Alzheimer's disease. Nature Reviews Neuroscience. 2004; 5(5): 347-360.
151.) Nizar K, Uhlirova H, Tian P, Saisan P, Cheng A, Reznichenko L, Weldy K, Steed T, Sridhar VB, MacDonald CL, Cui J, Gratiy SL, Sakadzic S, Boas DA, Beka TI, Einevoll GT, Chen J, Masliah E, Dale AM, Silva GA, Devor A. In vivo stimulus-induced vasodilation occurs without IP3 receptor activation and may precede astrocytic calcium release. J. Neurosci. 2013; 33: 8411-8422. doi: 10.1523/JNEUROSCI.3285-12.2013
152.) Winship IF, Plaa N, Murphy TH. Rapid astrocyte calcium signals correlate with neuronal activity and onset of the hemodynamic response in vivo. J. Neurosci. 2007; 27: 6268-6272.
153.) Reeves AM, Shigetomi E, Khakh BS. Bulk loading of calcium indicator dyes to study astrocyte physiology: key limitations and improvements using morphological maps. J. Neurosci. 2011; 31: 9353-9358.
154.) Lind BL, Brazhe AR, Jessen SB, Tan FC, Lauritzen MJ. Rapid stimulus-evoked astrocyte Ca^{2+} elevations and hemodynamic responses in mouse somatosensory cortex in vivo. Proc. Natl. Acad. Sci. USA. 2013; 110: E4678-E4687.
155.) Sun W. Glutamate-dependent neuroglial calcium signaling differs between young and adult brain. Science. 2013; 339: 197-200.
156.) Bonder DE, McCarthy KD. Astrocytic Gq-GPCR-linked IP3R-dependent Ca^{2+} signaling does not mediate neurovascular coupling in mouse visual cortex in vivo. J Neurosci. 2014; 34: 13139-13150.
157.) Hamel E. Perivascular nerves and the regulation of cerebrovascular tone. J Appl Physiol. 2006; 100: 1059-1064.
158.) Engelhardt B, Sorokin L. The blood-brain and the blood-cerebrospinal fluid barriers: function and dysfunction. Semin Immunopathol. 2009; 31(4): 497-511.
159.) Timpl R. Structure and biological activity of basemenet membrane proteins. Eur J Biochem. 1989; 180(3): 487-502.
160.) Hallman R, Horn N, Selg M, et al. Expression and function of laminins in the embryonic and mature vasculature. Physiol Rev. 2005; 85: 979-1000
161.) Rauch U, Zhou XH, Roos G. Extracellular matrix alterations in brains lacking four of its components. Biochem Biophys Res Commun 2005; 328: 608-617.
162.) Tilling T, Korte D, Hoheisel D, et al. Basement membrane proteins influence brain capillary endothelial barrier function in vitro. J Neurochem. 1998; 71: 1151-1157.
163.) Yonezawa T, Hattori S, Inagaki J, et al. Type IV collagen induces expression of thrombospondin-1 that is mediated by integrin alpha1beta1 in astrocytes. Glia. 2010; 58: 755-767.
164.) Zhang Y, Sloan SA, Clarke LE, et al. Purification and characterization of progenitor and mature human astrocytes reveals transcriptional and functional differences with mouse. Neuron. 2016; 89: 37-53.
165.) Utriainen A, Sormunen R, Kettunen M, et al. Structurally altered basement membranes and hydrocephalus in a type XVIII collagen deficient mouse line. Hum Mol Genet. 2004; 13: 2089-2099.
166.) Thomsen MS, Routhe LJ, Moos T. The vascular basement membrane in the healthy and pathological brain. J Cereb Blood Flow Metab. 2017; 37(10): 3300-3317.
167.) Paulsson M. Basement membrane proteins: structure, assembly, and cellular interactions. Crit Rev Biochem Mol Biol. 1992; 27(1-2): 93-127.
168.) Yurchenco PD, Schittny JC. Molecular architecture of basement membranes. FASEB J. 1990; 4: 1577-1590.
169.) Rowe RG, Weiss SJ. Breaching the basement membrane: who, when, and how? Trends Cell Biol. 2008; 18: 560-574.
170.) Gould DB, Phalan FC, Breedveld GJ, et al. Mutations in Col4a1 cause perinatal cerebral hemorrhage and porencephaly. Science. 2005; 308: 1167-1171.
171.) Cummings CF, Pedchenko V, Brown KL, et al. Extracellular chloride signals collagen IV network assembly during basement membrane formation. J Cell Biol. 2016; 213: 479-494.

172.) Fox JW, Mayer U, Nischt R, et al. Recombinant nidogen consists of three globular domains and mediates binding of laminin to collagen type IV. EMBO J. 1991; 10: 3137-3146.
173.) Salmivirta K, Talts JF, Olsson M, et al. Binding of mouse nidogen-2 to basement membrane components and cells and its expression in embryonic and adult tissues suggest complementary functions of the two nidogens. Exp Cell Res. 2002; 279: 188-201.
174.) Sarrazin S, Lamanna WC, Esko JD. Heparan sulfate proteoglycans. Cold Spring Harb Perspect Biol. 2011; 3: 1-33.
175.) Kroger S, Schroder JE. Agrin in the developing CNS: new roles for a synapse organizer. News Physiol Sci. 2002; 17: 207-212.
176.) Steiner E, Enzmann GU, Lyck R, et al. The heparan sulfate proteoglycan agrin contributes to barrier properties of mouse brain endothelial cells by stabilizing adherens junctions. Cell Tissue Res. 2014; 358: 465-479.
177.) Yurchenco PD. Basement membranes: cell scaffoldings and signaling platforms. Cold Spring Harb Perspect Biol. 2011; 3: 1-27.
178.) Whitelock JM, Melrose J, Iozzo RV. Diverse cell signaling events modulated by perlecan. Biochemistry. 2008; 47: 11174-11183.
179.) Yousif LF, Di Russo J, Sorokin L. Laminin isoforms in endothelial and perivascular basement membranes. Cell Adh Migr. 2013; 7(1): 101-110.
180.) Hohenester E, Yurchenco PD. Laminins in basement membrane assembly. Cell Adh Migr. 2013; 7(1): 56-63.
181.) Thomsen MS, Birkelund S, Burkhart A, Stensballe A, Moos T. Synthesis and deposition of basement membrane proteins by primary brain capillary endothelial cells in a murine model of the blood-brain barrier. J Neurochem. 2017; 140(5): 741-754.
182.) Ljubimova JY, Fujita M, Khazenzon NM, et al. Changes in laminin isoforms associated with brain tumor invasion and angiogenesis. Front Biosci. 2006; 11: 81-88.
183.) Engelhardt B, Vajkoczy P, Weller RO. The movers and shapers in immune privilege of the CNS. Nat Immunol. 2017; 18: 123-131.
184.) Zhang ET, Inman CB, Weller RO. Interrelationships of the pia mater and the perivascular (Virchow-Robin) spaces in the human cerebrum. J Anat. 1990; 170: 111-123.
185.) Sixt M, Engelhardt B, Pausch F, Hallmann R, Wendler O, Sorokin LM. Endothelial cell laminin isoforms, laminins 8 and 10, play decisive roles in T cell recruitment across the blood-brain barrier in experimental autoimmune encephalomyelitis. J Cell Biol. 2001; 153(5): 933-946.
186.) Stratman AN, Malotte KM, Mahan RD, Davis MJ, Davis GE. Pericyte recruitment during vasculogenic tube assembly stimulates endothelial basement membrane matrix formation. Blood. 2009; 114(24): 5091-5101.
187.) Song J, Wu C, Korpos E, Zhang X, Agrawal SM, Wang Y, Faber C, Schäfers M, Körner H, Opdenakker G, Hallmann R, Sorokin L. Focal MMP-2 and MMP-9 activity at the blood-brain barrier promotes chemokine-induced leukocyte migration. Cell Rep. 2015; 10(7): 1040-1054.
188.) Engelhardt B. β1-integrin/matrix interactions support blood-brain barrier integrity. J Cereb Blood Flow Metab. 2011; 31(10): 1969-1971.
189.) Winder SJ. The complexities of dystroglycan. Trends Biochem Sci. 2001; 26(2): 118-124.
190.) Barcyzk M, Carracedo S, Gullberg D. Integrins. Cell Tissue Res. 2010; 339(1): 269-280.
191.) Paulus W, Baur I, Schuppan D, et al. Characterization of integrin receptors in normal and neoplastic human brain. Am J Pathol. 1993; 143: 154-163.
192.) Milner R, Campbell IL. Increased expression of the beta and alpha5 integrin subunits in cerebral blood vessels of transgenic mice chronically producing the pro-inflammatory cytokines IL-6 or IFN-alpha in the central nervous system. Mol Cell Neurosci 2006; 33: 429-440.
193.) Milner R, Campbell IL. Developmental regulation of beta1 integrins during angiogenesis in the central nervous system. Mol Cell Neurosci. 2002; 20: 616-626.

194.) Grazioli A, Alves CS, Konstantopoulos K, Yang JT. Defective blood vessel development and pericyte/pvSMC distribution in alpha 4 integrin-deficient mouse embryos. Dev Biol. 2006; 293(1): 165-177.
195.) Lehnardt S. Innate immunity and neuroinflammation in the CNS: The role of microglia in Toll-like receptor-mediated neuronal injury. Glia. 2010; 58: 253-263.
196.) Nimmerjahn A, Kirchoff F, Helmchen F. Resting microglial cells are highly dynamic surveillants of brain parenchyma in vivo. Science. 2005; 308: 1314-1318.
197.) Davalos D, Grutzendler J, Yang G, Kim JV, Zuo Y, Jung S, Littman DR, Dustin ML, Gan WB. ATP mediates rapid microglial response to local brain injury in vivo. Nature Neuroscience. 2005; 8: 752-758.
198.) Ginhoux F, Greter M, Leboeuf M, Nandi S, See P, Gokhan s, Mehler MF, Conway SJ, Ng LG, Stanley ER, et al. Fate mapping analysis reveals that adult microglia derive from primitive macrophages. Science. 2010; 330: 841-845.
199.) Kierdorf K, Prinz M. Factors regulating microglia activation. Front Cell Neurosci. 2013; 7: 44.
200.) Kierdorf K, Erny D, Goldmann T, Sander V, Schulz C, Perdiguero EG, Wieghofer P, Heinrich A, Riemke P, Hölscher C. et al. Microglia emerge from erythromyeloid precursors via Pu. 1- and Irf-8-dependent pathways. Nature Neuroscience. 2013a; 16: 273-280.
201.) Ginhoux F, Prinz M. Origin of Microglia: Current Concepts and Past Controversies. Cold Spring Harbor Perspectives in Biology. 2015; 7: a020537
202.) Minghetti L, Levi G. Microglia as effector cells in brain damage and repair: Focus on prostanoids and nitric oxide. Prog Neurobiol. 1998; 54: 99-125.
203.) Goldmann T, Prinz M. Role of microglia in CNS autoimmunity. Clin Dev Imunol. 2013; 208093-208098.
204.) Del Río-Hortega P. Microglia. 1932. In *Cytology and cellular pathology of the nervous system* (ed. Penfield W), Vol. 2, pp. 483-534. P.B. Hoeber, New York.
205.) Hill RA, Damisah EC, Chen F, Kwan AC, Grutzendler J. Targeted two-photon chemical apoptotic ablation of defined cell types in vivo. Nature Communications. 2017; 8, 15837. doi: 10.1016/j.bbrc.2016.08.088.
206.) Ramón y Cajal, S. Sobre un nuevo proceder de impregnación de la neuroglia y sus resultados en los centros nerviosos del hombre y animales. Trab. Lab Invest. Biol. 1913; XI: 103-112.
207.) Ramón y Cajal, S. Algunas conjeturas sobre el mechanism anatómico de la ideación, asociación. Imprenta y Librería de Nicolás Moya. 1895.
208.) Bernardinelli Y, Randall J, Janett E, Nikonenko I, König S, Jones EV, Flores CE, Murai KK, Bochet CG, Holtmaat A, Muller D. Activity-dependent structural plasticity of perisynaptic astrocytic domains promotes excitatory synapse stability. Curr. Biol. 2014; 24: 1679-1688
209.) Genoud C, Quairiaux C, Steiner P, Hirling H, Welker E, Knott GW. Plasticity of astrocytic coverage and glutamate transporter expression in adult mouse cortex. PLoS Biol. 2006; 4: e343.
210.) Xu-Friedman MA, Harris KM, Regehr WG. Three-dimensional comparison of ultrastructural characteristics at depressing and facilitating synapses onto cerebellar Purkinje cells. J. Neurosci. 2001; 21: 6666-6672.
211.) Hirrlinger J, Hülsmann S, Kirchhoff F. Astroglial processes show spontaneous motility at active synaptic terminals in situ. Eur. J. Neurosci. 2004; 20: 2235-2239.
212.) Procko C, Lu Y, Shaham S. Glia delimit shape changes of sensory neuron receptive endings in C. elegans. Development. 2011; 138: 1371-1381.
213.) Theodosis DT, Poulain DA, Oliet SHR. Activity-dependent structural and functional plasticity of astrocyte-neuron interactions. Physiol. Rev. 88; 983-1008.
214.) Theodosis DT. Oxytocin-secreting neurons: a physiological model of morphological neuronal and glial plasticity in the adult hypothalamus. Front. Neuroendocrinol. 2002; 23: 101-135. doi: 10.1006/frne.2001.0226

215.) Tatsumi K, Okuda H, Morita-Takemura S, Tanaka T, Isonishi A, Shinjo T, et al. Voluntary exercise induces astrocytic structural plasticity in the globus pallidus. Font. Cell. Neurosci. 2016; 10: 165. doi: 10.3389/fncel.2016.00165
216.) Bellesi M, de Vivo L, Chini M, Gilli F, Tononi G, Cirelli C. Sleep loss promotes astrocytic phagocytosis and microglial activation in mouse cerebral cortex. J Neurosci. 2017; 37: 5263-5273. doi: 10.1523/JNEUROSCI.3981-16.2017
217.) Kubotera H, Ikeshima-Kataoka H, Hatashit Y, Mascaro ALA, Pavone FS, Inoue T. Astrocytic endfeet recover blood vessels after removal by laser ablation. Scientific Reports. 2019; 9(1): 1263. doi: 10.1038/s41598-018-37419-4
218.) Zamanian JL, Xu L, Foo LC, Nouri N, Zhou L, Giffard RG, Barres BA. Genomic analysis of reactive astrogliosis. Journal of Neuroscience. 2012; 32(18): 6391-6410. doi: 10.1523/jneurosci.6221-11.2012
219.) Boisvert MM, Erikson GA, Shokhirev MN, Allen NJ. The aging astrocyte transcriptome from multiple regions of the mouse brain. Cell Reports. 2018;22: 269-285. doi: 10.1016/j.celrep.2017.12.039
220.) Clarke LE, Liddelow SA, Chakraborty C, Munch AE, Heiman M, Barres BA. Normal aging induces A1-like astrocyte reactivity. Proc. Natl. Acad. Sci. USA. 2018; 115: E1896-1905. doi: 10.1073/pnas.1800165115
221.) Kanaan NM, Kordower JH, Collier TJ. Age-related changes in glial cells of dopamine midbrain subregions in rhesus monkeys. Neurobiol. Aging. 2010; 31: 937-952. doi: 10.1016/j.neurobiolaging.2008.07.006
222.) Cerbai F, Lana D, Nosi D, Petkova-Kirova P, Zecchi S, Brothers HM, et al. The neuron-astrocyte-microglia triad in normal brain aging and in a model of neuroinflammation in the rat hippocampus. PLoS One. 2012;7:e45250. doi:10.1371/journal.pone.0045250
223.) Jyothi HJ, Vidyadhara DJ, Mahadevan A, Philip M, Parmar SK, Manohari SG, et al. Aging causes morphological alterations in astrocytes and microglia in human substantia nigra pars compacta. Neurobiol. Aging. 2015; 36: 3321-3333. doi: 10.1016/j.neurobiolaging.2015.08.024
224.) Castiglioni AJ, Legare ME, Busbee DL, Tiffany-Castiglioni E. Morphological changes in astrocytes of aging mice fed normal or caloric restricted diets. Age. 1991; 14: 102-106. doi: 10.1007/bf02435015
225.) Amenta F, Bronzetti E, Sabbatini M, Vega JA. Astrocyte changes in aging cerebral cortex and hippocampus: a quantitative immunohistochemical study. Microsc. Res. Tech. 1998; 43: 29-33. doi: 10.1002/(SICI)1097-0029(19981001)43:1<29::AID-JEMT5>3.0.CO;2-H
226.) Robillard KN, Lee KM, Chiu KB, and MacLean AG. Glial cell morphological and density changes through the lifespan of rhesus macaques. Brain Behav. Immun. 2016: 55; 60-69. doi: 10.1016/j.bbi.2016.01.006
227.) Chen A, Akinyemi RO, Hase Y, Firbank MJ, Ndung'u MN, Foster V, Craggs LJ, Washida K, Okamoto Y, Thomas AJ, Polvikoski TM, Allan LM, Oakley AE, O'Brien JT, Horsburgh K, Ihara M, Kalaria RN. Frontal white matter hyperintensities, clasmatodendrosis and gliovascular abnormalities in aging and post-stroke dementia. *Brain*. 2016; 139(Pt 1): 242-258. doi: 10.1093/brain/awv328
228.) Early AN, Gorman AA, Van Eldik LJ, Bachstetter AD, Morganti JM. Effects of advanced age upon astrocyte-specific responses to acute traumatic brain injury in mice. J Neuroinflammation. 2020; 17: 115. doi: 10.1186/s12974-020-01800-w
229.) Fabricius K, Jacobsen JS, Pakkenberg B. Effect of age on neocortical brain cells in 90+ year old human females-a cell counting study. Neurobiol. Aging. 2013; 34: 91-99. doi: 10.1016/j.neurobiolaging.2007.07.015
230.) Pelvig DP, Pakkenberg H, Stark AK, Pakkenberg B. Neocortical glial cell numbers in human brains. Neurobiol. Aging. 2008; 29: 1754-1762. doi: 10.1016/j.neurobiolaging.2007.04.013
231.) Sofroniew MV. Astrocyte Reactivity: Subtypes, States, and Functions in CNS Innate Immunity. Trends in Immunology. 2020; 41(9):758-770. doi: 10.1016/j.it.2020.07.004
232.) Sofroniew MV, Vinters HV. Astrocytes: biology and pathology. Acta Neuropathol. 2010; 119:7-35.
233.) Burda JE, Sofroniew MV. Reactive gliosis and the multicellular response to CNS damage and disease. Neuron. 2014; 81: 229-248.

234.) Pekny M, Pekna M. Astrocyte reactivity and reactive astrogliosis: costs and benefits. Physiol Rev. 2014; 94: 1077-1098.
235.) Lu TY, et al. Axon degeneration induces glial responses through Draper-TRAF4-JNK signaling. Nature Communications. 2017; 8:14355.
236.) Hlavac N, VandeVord PJ. Astrocyte mechano-activation by high-rate overpressure involves alterations in structural and junctional proteins. Frontiers in Neurology. 2019; 10: 99.
237.) Shu M, Zhou Y, Zhu W, Wu S, Zheng X, Yan G. Activation of a pro-survival pathway IL-6/JAK2/STAT3 contributes to glial fibrillary acidic protein induction during the cholera toxin-induced differentiation of C6 malignant glioma cells. Molecular Oncology. 2011; 5: 265-272
238.) Bonni A, Sun Y, Nadal-Vicens M, Bhatt A, Frank DA, Rozovsky I, Stahl N, Yancopoulos GD, Greenberg ME. Regulation of gliogenesis in the central nervous system by the JAK-STAT signaling pathway. Science. 1997; 278:477-483.
239.) Ruprecht K, Kuhlmann T, Seif F, Hummel V, Kruse N, Bruck W, Rieckmann P. Effects of oncostatin M on human cerebral endothelial cells and expression in inflammatory brain lesions. Journal of Neuropathology and Experimental Neurology. 2001; 60: 1087-1098.
240.) Herrera F, Chen Q, & Schubert D. Synergistic Effect of Retinoic Acid and Cytokines on the Regulation of Glial Fibrillary Acidic Protein Expression. *The Journal of Biological Chemistry*. 2010; 285(50): 38915-38922. doi: 10.1074/jbc.M110.170274
241.) Campbell IL, Abraham CR, Masliah E, et al. Neurologic disease induced in transgenic mice by cerebral overexpression of interleukin 6. Proc Natl Acad Sci USA. 1993; 90: 10061-65.
242.) Penkowa M, Giralt M, Lago N, et al. Astrocyte-targeted expression of IL-6 protects the CNS against a focal brain injury. Exp Neurol. 2003; 181: 130-148.
243.) Wang Y, Moges H, Bharucha Y, Symes A. Smad3 null mice display more rapid wound closure and reduced scar formation after a stab wound to the cerebral cortex. Exp Neurol. 2007; 203: 168-184.
244.) Correa-Cerro LS, Mandell JW. Molecular Mechanisms of Astrogliosis: New Approaches With Mouse Genetics. Neuropathol Exp Neurol. 2007; 66(3): 169-176.
245.) Linggi B, Carpenter G. ErbB receptors: new insights on mechanisms and biology. Trends Cell Biol. 2006; 16(12): 649-656.
246.) Wieduwilt MJ, Moasser MM. The epidermal growth factor receptor family: Biology driving targeted therapeutics. Cell Mol Life Sci. 2008; 65(10): 1566-1584.
247.) Scaltriti M, Baselga J. The epidermal growth factor receptor pathway: a model for targeted therapy. Clin Cancer Res. 2006; 12(18): 5268-5272.
248.) Ito K, Noguchi A, Uosaki Y, Taga T, Arakawa H, Takizawa T. Gfap and Osmr regulation by BRG1 and STAT3 via interchromosomal gene clustering in astrocytes. Molecular Biology of the Cell. 2018; 29: 209-219.
249.) Shiratori-Hayashi M, Koga K, Tozaki-Saitoh H, Kohro Y, Toyonaga H, Yamaguchi C, et al. STAT3-dependent reactive astrogliosis in the spinal dorsal horn underlies chronic itch. Nature Medicine. 2015; 21: 927-931.
250.) He K, Qi Q, Chan CB, Xiao G, Liu X, Tucker-Burden C, et al. Blockage of glioma proliferation through allosteric inhibition of JAK2. Science Signaling. 2013; 6: ra55.
251.) Foo LC, Allen NJ, Bushong EA, Ventura PB, Chung W, Zhou L, Cahoy JD, Daneman R, Zong H, Ellisman MH, Barres BA. Development of a Novel Method for the Purification and Culture of Rodent Astrocytes. Neuron. 2011; 71(5): 799-811. doi: 10.1016/j.neuron.2011.07.022
252.) Zhang Y, Chen K, Sloan SA, Bennett ML, Scholze AR, O'Keeffe S, Phatnani HP, Guarnieri P, Caneda C, Ruderisch N, Deng S, Liddelow SA, Zhang C, Daneman R, Maniatis T, Barres BA, Wu JQ. An RNA-Sequencing Transcriptome and Splicing Database of Glia, Neurons, and Vascular Cells of the Cerebral Cortex. Journal of Neuroscience. 2014; 34(36): 11929-11947. doi: 10.1523/JNEUROSCI.1860-14.2014
253.) Zhang Y, Sloan SA, Clarke LE, Caneda C, Plaza CA, Blumenthal PD, Vogel H, Steinberg GK, Edwards M SB, Li G, Duncan III JA, Cheshier SH, Shuer LM, Chang EF, Grant GA, Hayden Gephart MG,

Barres BA. Purification and Characterization of Progenitor and Mature Human Astrocytes Reveals Transcriptional and Functional Differences with Mouse. Neuron. 2016; 89(1): 37-53. doi: 10.1016/j.neuron.2015.11.013

254.) Yeo S, Bandyopadhyay S, Messing A, Brenner M. Transgenic analysis of GFAP promoter elements. Glia. 2013; 61: 1488-1499.

255.) Saggu R, Schumacher T, Gerich F, Rakers C, Tai K, Delekate A, Petzold GC. Astroglial NF-κB contributes to white matter damage and cognitive impairment in a mouse model of vascular dementia. Acta Neuropathologica Communications. 2016; 4: 76.

256.) Li D, Liu X, Liu T, Liu H, Tong L, Jia S, Wang YF. Neurochemical regulation of the expression and function of glial fibrillary acidic protein in astrocytes. Glia. 2019; 68: 878-897.

257.) Gao K, Wang CR, Jiang F, Wong AY, Su N, Jiang JH, et al. Traumatic scratch injury in astrocytes triggers calcium influx to activate the JNK/c-Jun/AP-1 pathway and switch on GFAP expression. Glia. 2013; 61: 2063-2077.

258.) Herx LM, Yong VW. Interleukin-1β is required for the early evolution of reactive astrogliosis following CNS lesion. J Neuropathol Exp Neurol. 2001; 60: 961-971.

259.) Sweeney MD, Sagare AP, Zlokovic BV. Cerebrospinal fluid biomarkers of neurovascular dysfunction in mild dementia and Alzheimer's disease. *J Cereb Blood Flow Metab.* 2015;35:1055-1068.

260.) Hartmann DA, Underly RG, Grant RI, Watson AN, Lindner V, Shih AY. Pericyte structure and distribution in the cerebral cortex revealed by high-resolution imaging of transgenic mice. Neurophotonics. 2015 2(4): 041402. doi: 10.1117/1.NPh.2.4.041402

Chapter 3

Astrocyte plasticity ensures continued endfoot coverage of cerebral blood vessels and integrity of the blood brain barrier, with plasticity declining with normal aging.

Abstract

Astrocytes extend endfeet that enwrap the vasculature. Disruptions to this association in disease coincide with breaches in blood-brain barrier (BBB) integrity, so we asked if the focal ablation of an astrocyte is sufficient to disrupt the BBB. 2Phatal ablation of astrocytes induced a plasticity response whereby surrounding astrocytes extended processes to cover vascular vacancies. This occurred prior to endfoot retraction in young mice yet occurred with significant delay in aged animals. Laser-stimulating replacement astrocytes showed them to induce constrictions in pre-capillary arterioles indicating that replacement astrocytes are functional. Inhibition of EGFR and pSTAT3 significantly reduced astrocyte replacement post-ablation yet without perturbations to BBB integrity. Identical endfoot replacement following astrocyte cell death due to reperfusion post-stroke supports the conclusion that astrocyte plasticity ensures continual vascular coverage so as to retain the BBB. Together, these studies uncover the ability of astrocytes to maintain cerebrovascular coverage via substitution from nearby cells and may represent a novel therapeutic target for vessel recovery post-stroke.

Introduction

Astrocytes serve essential roles in supporting normal brain physiology (1). This is made possible, in part, by the extension of large, flattened processes, called endfeet, that wrap around blood vessels. Thought to cover up to ~99% of the cerebrovascular surface (2), astrocytic endfeet, in conjunction with pericytes (3), help to maintain expression of molecules that form the blood-brain barrier (BBB)- including endothelial tight junction, enzymatic, and transporter proteins (4-6). Astrocytic endfeet also mediate neurovascular coupling, also known as functional hyperemia, whereby local blood flow adjusts to local energy demand. Astrocytes sense changes in neuronal activity via purinergic receptors that cause increases in $[Ca^{2+}]_i$, leading to the release of vasoactive molecules onto pericytes at capillaries (7-8), or directly release vasoactive signals onto arterioles (9-12), leading to change in vessel diameter.

Interestingly, a number of CNS diseases are marked by retraction or separation of astrocytic endfeet from blood vessels- a phenotype often simultaneously presenting with vascular deficits such as altered blood-brain barrier permeability or elevated CSF-to-serum albumin ratio, which is indicative of blood-brain barrier breakdown. Examples include multiple sclerosis (13), major depressive disorder (14-16) ischemia (17-19), and even normal biological aging (20-22). We previously demonstrated separation of endfeet from the vasculature due to invading glioma cells (23) as well as due to amyloid accumulation on vessels (24). Both conditions resulted in disruption to neurovascular coupling and, in the case of glioma, BBB breakdown. This raises the question of whether astrocyte endfeet are required to maintain an intact BBB, or whether lost endfeet can be replaced by other astrocytes as has been shown for pericytes (25). Moreover, since changes in astrocyte morphology and function are known to occur with physiological changes of the organism- i.e. parturition, lactation, chronic dehydration, starvation, voluntary exercise or sleep deprivation (26-29) – it is possible that astrocyte association with blood vessels is equally dependent on the physiological context .

Given the multitude of conditions marked by regions of abnormal vasculature lacking endfoot coverage, we were interested in determining whether replacement endfeet have functional relevance in maintaining blood-

brain barrier integrity and astrocyte-vascular coupling. Using multiphoton imaging through a cranial window, we were able to induce single-cell apoptosis using the 2Phatal method (30) to question whether loss of endfeet on blood vessels would be compensated for by neighboring cell(s). We find remarkable plasticity, discovering that the ablation of single astrocytes reliably causes innervation by neighboring cells. In young animals, this happens before the ablated cell completely retrieves its process; yet in 12-month-old animals, replacement occurs with a significant 1-2h delay after the ablated cell has vacated the vessel. Endfoot replacement engages the EGFR/STAT3 signaling pathway as pharmacological inhibition via AG490 injection impairs replacement. Once in place, the replacement endfeet have the ability to vasoconstrict precapillary arterioles like normal astrocytes. Despite recent evidence that global astrocyte loss results in impairments of the blood-brain barrier (31), we did not find this to be the case even when replacement endfoot coverage was impaired by inhibition of EGFR and/or STAT3 phosphorylation. Finally, we demonstrate using focal photothrombosis that astrocyte apoptosis following reperfusion triggers a focal gliovascular plasticity response wherein astrocyte-vascular coverage is maintained. Together, these results reveal a novel process in which astrocytes cover for neighboring cells to maintain vascular coverage in an EGFR/pSTAT3-dependent manner.

Materials & Methods

In vivo multiphoton imaging through a cranial window

All surgeries were performed as described previously (19-20) with slight modifications. Following induction of surgical plane anesthesia with 2-5% isofluorane, pre-operative analgesics and antibiotics were administered intraperitoneally. Following this, the hair and skin of the skull was removed, and a 3x3 mm craniectomy anterior to lambda and posterior to bregma was subsequently performed on one hemisphere. A durotomy was performed next, followed by placement of a 3x3mm #1 cover glass that was then affixed and sealed with dental cement. All mice were allowed to recover for 5-7 days before experiments commenced. For imaging, animals were placed on a Kopf stereotax with heating pad. While imaging, animals were lightly anaesthetized (~100 beats per minute), and their vitals constantly monitored. Cerebral vessels were visualized by retro-orbital injection of 70kDa TRITC, 3kDa TRITC, and/or 967 Da Cadaverine Alexa Fluor 555. A Chameleon Vision II(Coherent) laser tuned

to 870nm was used to excite all dyes. Optical sections were acquired using a four-channel Olympus FV1000MPE multiphoton laser scanning fluorescence microscope equipped with a XLPLN25X/1.05 NA water-immersion objective (Olympus). Z projections were created using FIJI(NIH) and NIS-Elements(Nikon).

2Phatal Ablation

To induce single-cell apoptosis in astrocytes, Hoechst 33342 (ThermoFisher catalogue number H5370) was applied topically (0.04 mg ml^{-1} diluted in PBS) to the durotomized cortex of Aldh1l1-eGFP mice for 10 minutes and washed thoroughly with cold 1XPBS.-To ablate, an 8x8 µm square ROI was placed over dual eGFP Hoechst positive astrocyte nuclei whose soma was either on the vessel or that had endfeet contacting the vasculature. Pixel dwell time was set to 100 µs/pixel, laser wavelength was set to 775 nm and photobleaching was achieved by scanning for a duration of 20 s. A Newport Model 1919-R power meter with a silicone based OD3 photodetector attached was used to determine power at the objective for all ablation experiments, and a range of 2.33 mW to 53.4 mW was used for all experiments, where power increased with increasing depth and/or decreasing Hoechst intensity measured in the activation ROI. eGFP was visualized by setting laser wavelength to 870 nm.

Quantification of astrocyte morphometrics

To determine the number of astrocytes extending processes to innervate vascular vacancies, NIS elements was used to compare the baseline z-stack to z-stacks from time points following complete removal of ablated astrocytes. Specifically, ablated astrocytes and the optical section(s) their soma occupied was denoted in the baseline image. The surrounding vascular landmarks and astrocytes that weren't ablated could therefore serve as fiduciary landmarks when evaluating that same field post-ablation. Any astrocyte at post-ablation timepoints that appeared to extend processes and innervate a vascular vacancy was identified in the baseline image, again using 1) the surrounding vascular profile, 2) astrocytes that were not ablated, and 3) z location of the astrocyte in question relative to the ablated astrocyte. If, at baseline, the replacement astrocyte in question did not appear to have processes interacting with the vasculature, even upon dramatically increasing the look up table, it was considered a replacement astrocyte. The total numbers of cells fulfilling these criteria were reported as the total number of replacement cells.

For analysis of replacement kinetics, only astrocytes extending clear processes to the vascular interface were chosen for ablation. Longitudinal imaging was performed following astrocyte ablation. Specifically, images were acquired twice per day to determine if the abated astrocyte's soma has begun to swell, indicative that it would undergo phagocytosis within the next 24 hours. Once identified, z stacks were captured every 5 minutes until the time point of first seeing a process from a replacement astrocyte occupy the vacant vascular territory or identifying the time of fluorescence fading in the process of the ablated astrocyte. To quantify the number of minutes to endfoot replacement in 4-month and 12-month-old mice, the time of fluorescence fading in the process of the ablated astrocyte was considered time point zero. From there, the number of minutes until observing a process from a replacement astrocyte occupy the vascular territory of the ablated was then determined from the captured z-stacks. If the replacement process made contact with the vessel prior to time point zero, this was reported as negative minutes. If the replacement process made contact with the vessel after time point zero, this was reported as positive minutes.

For eGFP volumetric analysis in AG490 studies, images were opened in NIS elements volume viewer and underwent background subtraction using the rolling ball radius feature. A median filter and binary threshold were subsequently applied and eGFP volume recorded. The same number of optical sections were used for time points being directly compared. To ensure that the region of astrocyte ablation was compared pre- and post-ablation, the rotating rectangle feature was used. This allows for area selection in an image without changing the underlying metadata. An ROI of the same size was applied to images of time points being compared. so that it could be used as size reference for the rotating rectangle.

Quantification of BBB leakage- Prior to astrocyte ablation (time point 1), a 30-µL bolus of 100mg/ml 3kDa TRITC (D3307 Invitrogen) was retro-orbitally injected, and a timer started at the moment of injection. The mouse was moved immediately to the stereotax under the microscope, and a z stack was captured. The times at the start of image capture and end of image capture were recorded to enable proper comparison at all subsequent time points. This process was repeated at the moment of fluorescence fading in the process at the vascular interface (time point 2) and the same imaging parameters used as that of the baseline image. FIJI (ImageJ) was

used to create sum intensity projections and the same number of optical sections was used for all time points, where optical sections in which the ablated astrocyte was covering the vasculature were selected. Background subtraction was performed using the rolling ball radius feature, and an average fluorescent value was measured at the location of endfoot coverage at both time points. For the induction of vessel injury as a positive control, 870nm line scans at a laser power of 50 to 85mW were applied across the vessel wall for 90 to 120 seconds. As in prior BBB measurements, a z stack was captured at the same time after retro-orbital injection of 3kDa TRITC, and the average intensity just beside the damaged vessel was compared at both time points, pre- to post-vessel injury.

***In vivo* replacement astrocyte induced-precapillary arteriole constriction-** To determine if replacement astrocytes can vasoregulate precapillary arterioles, Aldh1l1cre x GCaMP5G mice received a cranial window following the methodology described above. The first branching capillary segment from Alexa 633 hydrazide positive penetrating arterioles was selected for imaging if the soma of astrocytes making contact with the precapillary arterioles were on a focal plane similar to the vessel. Using a four-channel Olympus FV1000MPE multiphoton laser scanning fluorescence microscope equipped with a XLPLN25X/1.05 NA water-immersion objective (Olympus), single-plane images of 1024x800 pixels were obtained every 3 seconds. Astrocytes were targeted for laser irradiation by selecting a focal plane where the soma and associated precapillary arteriole were visible. Astrocyte stimulation was achieved using a 4μm^2 circular region of interest centered within the astrocyte soma for 800 milliseconds at 7-10x imaging power levels. A two-minute measurement was recorded before and after astrocyte activation. Vessel diameter was measured as the cross-section of the vessel using FIJI (ImageJ) software. Motion correction in videos was performed using the Intravital Microscopy Toolbox ImageJ macro developed by Soulet et al (32).

Rose Bengal Photothrombosis- To focally and transiently induce Rose Bengal intravascular clot formation, Aldh1l1-eGFP mice were retro-orbitally injected with Alexa 633 hydrazide and penetrating arterioles identified prior to the beginning of the experiment. Rose Bengal was then retro-orbitally injected, and all mice <20g received a 25µL injection whereas mice >20g received a 50µL injection. Mice were then transferred to the multiphoton as

soon as possible and a square ROI was placed over a penetrating arteriole. The dimensions of the ROI were based upon the dimensions of the penetrating vessel, and imaging was conducted 90µms from the surface of the brain. Imaging duration was set to two minutes and wavelength set to 870nm. Laser power was set between 50-90 mW, with power determined on the average intensity of Rose Bengal at the beginning of the experiment. If only part of the vessel was occluded at the end of two minutes, the vessel would be imaged in laser scanning mode for until dye nucleation was complete. In all instances, this was not longer than two minutes. Upon successful intravascular clot formation, a z-stack was captured to visualize the clot, and then the animal was placed back in its home cage. The animal was then subsequently imaged one hour later to confirm that the clot had cleared. All instances of reported endfoot replacement come from depths below the plane of dye nucleation.

Drug Treatment-AG490 at 10mg/kg in 40%DMSO/PBS was subcutaneously injected daily for initial studies comparing percent increase in eGFP volume at day post ablation 5 relative to baseline (Figure 6). This dosage was increased to 3x/day for studies aiming to prolong the time a vessel region remained vacant post-ablation (Supplementary Figure 4).

Statistics- GraphPad Prism software was used to perform all statistical analyses. Details for every statistical test are reported in the figure legends. Every parametric test used was validated by first performing tests of normality on the dataset once outliers were removed. Parametric tests were further selected based on datasets having equivalent or different standard deviations, where a difference of <1.5 was counted as being equal.

Results

Focal ablation of single astrocytes does not breach the blood-brain barrier but induces an astrocyte endfoot replacement response

Given our previous finding of compromised blood-brain barrier (BBB) integrity in regions of focal endfoot separation due to invading glioma cells, we questioned if the focal ablation of a single astrocyte is sufficient to induce breaches in blood-brain barrier integrity. To do so, we implanted cranial windows in mice and adopted the 2Phatal ablation method developed by Hill et al (30). This technique employs the focal

illumination properties of a femtosecond-pulsed laser to activate the nucleic-acid binding Hoechst dye **(Figure 1a)**, triggering apoptosis. Given the ability to induce single-cell apoptosis, we were able to image astrocytes in Aldh1l1-eGFP mice up to and beyond removal of their corpse, which included the retraction of their endfeet **(Figure 1b**). We also employed Alexa Fluor 633 hydrazide (**Supplementary figure 1a-b)** to selectively label arterioles (33) so as to avoid perturbations to pericyte physiology, which are known to play a role in BBB integrity and vasodilation of capillaries. Comparing the extravasation of retro-orbitally injected 3kDa TRITC at the time of endfoot retraction to baseline revealed no apparent difference in BBB permeability **(Figure 1c-e**). 3kDa TRITC was chosen because initial attempts to use the ~1kDa Cadaverine revealed that at baseline, this dye extravasates and is taken up by astrocytes **(Supplementary Figure 2a)**. Positive control experiments utilizing direct laser irradiation of the vasculature demonstrated that we were able to detect leakage of 3kDa TRITC from the vasculature **(Supplementary Figure 2c-g)**. At the initial stages of astrocyte endfoot retraction, we observed nearby neighboring astrocytes extended processes to the soon-to-be vacancy left by the ablated astrocyte **(Figure 1e)**.

Given that astrocyte endfeet have been reported to cover up to 99% of the entire cerebrovascular surface (34), we then asked if this process occurred at all levels of the vascular tree. To answer this, Alexa Fluor 633 hydrazide was again employed to specifically label arterioles, and Alexa 633 negative vessels larger than 10µm were identified as venules. All vessels smaller than 10µm were identified as capillaries **(Supplementary Figure 1)**. 2Phatal ablation of astrocytes revealed that the replacement of endfeet also occurred at capillaries **(Figure 1g-i)** and venules **(Figure 1k-n)**. **(Figure 1)**. Taken together, these data suggest that focal loss of single astrocytes is sufficient to induce an endfoot replacement response from nearby surrounding astrocytes, regardless of vessel type.

Replacement endfeet can vasoconstrict precapillary arterioles

Astrocytes have been reported to mediate neurovascular coupling at precapillary arterioles (8). Furthermore, laser-activation of astrocytes has been shown to be a convenient way to probe their contribution to

vascular physiology, as it induces a focal rise in intracellular calcium which subsequently leads to the release of vasoactive molecules (35). In order to determine if replacement endfeet have the machinery to perform neurovascular coupling, and thus cause changes in blood vessel diameter, we ablated astrocytes in Aldh1l1-cre x GCaMP5G mice occupying vascular territories on precapillary arterioles. We then laser-activated astrocytes that extended processes to the vacant vascular locations. We consistently observed the laser stimulation triggering an increase in intracellular calcium, immediately followed by a decrease in vessel diameter (**Fig. 2e, i, j and Supplementary video 1**). Compared to original astrocytes, the induced constriction by replacement astrocytes occurred with a similar kinetic profile (**Fig 2m-n**). A higher change in laser-induced original astrocyte intracellular calcium correlated with a higher magnitude of vessel constriction (**Fig. 2k, m and Supplementary video 2**). These data suggest that replacement astrocytes are capable of assuming the original astrocyte's role in glio-vascular coupling, or at a minimum have the ability to release vasoactive molecules, regardless of their existing relationship with a blood vessel.

Endfoot replacement slows with aging

Studies in humans (36), rodents (37-39), and primates (40) indicate that astrocytic morphology in aged astrocytes differs markedly from young astrocytes, and other reports have shown that endfeet actually retract later in life (20). We therefore asked how aging would impact focal endfoot replacement. First, we wanted to confirm that this process remained intact at all levels of the vascular tree, consistent with the observations in young mice. 2Phatal ablation of astrocytes at arterioles, venules, and capillaries revealed that this was indeed the case **(Figure 3a-f).** To determine if aging impacted the fidelity of replacement, we quantified the number of cells extending or growing new processes to the vacant vascular region at each vessel type and found no difference between age groups (**Figure 3g-i**).

A recent study documented a not only enhanced, but more importantly, prolonged astrogliosis response in aged mice following TBI (41). This ultimately suggest that aging would impact the velocity of an astrocyte response, rather than the extent of it. We therefore next sought to determine if the kinetics of replacement

significantly slowed with aging. Engaging in long-term repetitive *in-vivo* imaging revealed that this was indeed the case. 2–4-month-old mice on average had an endfoot replacement event 17 minutes prior to endfoot retraction of the ablated cell **(Figure 4a-b**).In contrast, however, this process was significantly slowed in aged mice to an average replacement time of 112 minutes after endfoot retraction of the ablated cell (**Figure 4c-d, analysis in Figure 4f**). Finally, given that aged animals had vascular vacancies unoccupied for roughly two hours following endfoot retraction of the previously ablated astrocyte, we again aimed to determine if 3kDa TRITC would extravasate at this location. Results revealed this to not be the case **(Supplementary Figure 3)**, which suggests that vascular vacancies unoccupied by astrocytes for this duration of time are not sufficient to disrupt BBB integrity.

Pharmacological inhibition of STAT3 phosphorylation via subcutaneous injection of AG490 significantly impairs the endfoot plasticity response

When first questioning which signaling pathways might underlie gliovascular structural plasticity, we noted that the phenotype observed in Figure 1 at venules and capillaries appeared markedly like reactive astrogliosis. This suggested that molecules previously shown to be mediators of gliosis would be valid candidates to explore. The phosphorylation of the signal transducer and activator of transcription 3 (pSTAT3) molecule by janus kinase 2 (JAK2) has long been known to underlie astrogliosis, as its pharmacological and/or genetic inhibition results in a significantly dampened gliotic response. This is evidenced by a significant reduction in glial fibrillary acidic protein (GFAP), which is considered to be a marker of reactive astrogliosis (42-43). To test the hypothesis that pSTAT3 is necessary for focal endfoot replacement, we subcutaneously injected the JAK2 inhibitor AG490 over a seven-day period **(Figure 5A)**. Comparing the volume of eGFP signal in astrocyte processes post-ablation in AG490 to vehicle-injected control animals revealed a significantly attenuated response (**Figure 5b-f),** suggesting that pSTAT3 is indeed a necessary arbiter of the focal endfoot replacement response. We further wanted to assess if any perturbations in BBB integrity ensued at a penetrating arteriole after an attenuated plasticity response , and as our previous results would suggest, this was not the case (**Figure 5g-h**).

Given that we only attenuated an overall increase in astrocyte volume following one dosage per day of AG490, we wanted to determine how BBB integrity might be impacted if we significantly reduced overall astrocyte volume at arterioles post-ablation when increasing AG490 dosage to three times per day. Results revealed that, though we were able to significantly reduce the gliovascular structural plasticity response, we were not able to completely abolish it. Furthermore, even in locations along penetrating arterioles that were severely stripped of endfoot coverage, the BBB remained intact (**Supplementary Figure 4b-e**). Taken together, these results suggest that a significant loss of endfoot coverage is not sufficient to disrupt BBB integrity.

2Phatal as a model of focal endfoot replacement following astrocyte loss post- transient photothrombotic stroke

We initially turned to 2Phatal to model a loss of endfoot coverage on the underlying vasculature based off what had we had previously characterized in two disease conditions (23-24). 2Phatal, however, results in complete loss of an astrocyte cell body and associated processes rather than just an endfoot; we therefore wanted to determine if 2Phatal might more closely model other disease conditions. Given that 2Phatal presumably triggers apoptosis through ROS-induced DNA damage (30), we searched for reports on any disease conditions marked by astrocyte cell death at the vascular interface due to ROS-induced DNA damage. Ischemia-reperfusion is a condition whereby blood-flow is restored to a vessel following an ischemic insult due to vessel occlusion, and astrocytes have been reported to be just as sensitive as neurons to reperfusion-induced apoptosis following restoration of blood flow (44).

We therefore set out to model this condition *in vivo* by utilizing the Rose Bengal photothrombosis stroke model. Rose Bengal is a light-sensitive dye that, upon encountering a green laser, undergoes nucleation and forms a clot. Successful clot formation can be visualized by a dark area forming in the vessel, indicative of red blood cell accumulation, and intense fluorescence due to dye accumulation above that dark mass (**Figure 6d-f**) (45). Critically, this method allowed us to focally occlude penetrating arterioles and thereby examine if a structural plasticity response would occur following focal loss of astrocyte-vascular coverage. In all instances of successful

vessel occlusion, reperfusion occurred within 1 hour (data not shown), making this more akin to a transient ischemic attack rather than a stroke. We subsequently looked in regions below the plane of dye nucleation for signs of astrocyte cell death at the vascular interface. Cell death was indeed observed, and in the days following, surrounding astrocytes reached out to that vacant vascular location **(Figure 6g-I, compare to baseline images in Figure 6a-c)**. This data suggests that the 2Phatal ablation of astrocytes at vascular interfaces could potentially be thought of as a model for focal loss of endfoot coverage due to reperfusion-induced apoptosis. Given that stroke does lead to neural injury and subsequent astrogliosis, these data further support the notion that gliovascular plasticity is a focal gliosis response aimed at ensuring continual vascular coverage by astrocytes.

Discussion

Previous studies suggest that a number of nervous system insults and diseases present with impaired gliovascular interactions and even BBB disruption. Here we set out to determine if focal ablation of single astrocytes is sufficient to compromise BBB integrity focally. We had previously shown that focal endfoot separation due to invading glioma cells resulted in extravasation of various molecular weight dextran dyes and significant losses in tight junction proteins zonula-occludens-1 and Claudin 5 (23). By employing the 2Phatal ablation technique to induce single-cell apoptosis, we found that focal loss of an astrocyte did not compromise blood-brain barrier integrity **(Figure 1e-f)**, but instead reliably induced a plastic response whereby surrounding astrocytes reach out their processes to fill the vascular vacancy left by the ablated astrocyte **(Figure 1e)**. Moreover, the BBB remained intact in conditions where the vasculature was vacant for prolonged periods of time **(Supplementary Figure 3c)** or was almost entirely stripped of endfoot coverage **(Supplementary Figure 4).**

These results are interesting given a recent study (31) demonstrating the necessity of astrocytes in maintaining BBB integrity. These prior findings were obtained using a sparser and more permanent astrocyte ablation and relied on extravasation of ~1kDa Cadaverine as a marker for BBB disruption. Unfortunately, in our studies we found this dye flawed in its ability to discriminate between normal and abnormal BBB function, since we observed baseline leakage in control mice. **(Supplementary Figure 2a)**. Another recent study (46) that used

albumin, a reliable extravasation marker, showed that an astrocyte-specific connexin-30 and -43 double knockout resulted in both swollen astrocytic endfeet and impaired BBB integrity. However, this was most prevalent in deep brain structures such as the striatum and basal ganglia rather than cortical regions, which is very similar to what was demonstrated upon deletion of astrocyte-specific laminins (47). Note that care must be taken to account for changes in pericyte support, given that pericyte-deficient mouse models have been shown to alter astrocyte properties (48); therefore, loss of astrocytes may have affected pericyte coverage and thus indirectly altered BBB integrity. To avoid a confounding contribution of pericyte dysfunction to BBB integrity, we exclusively studied penetrating arterioles where pericytes are absent.

While it is conceivable that the role of astrocytes in maintaining BBB integrity may be region-specific, which aligns with evidence supporting astrocyte functional heterogeneity in the brain (49), we believe that our data points to the rapid plasticity or repair response by neighboring astrocytes as the primary reason that vessel function and BBB integrity are unaffected by the loss of a single or few astrocytes. This is in excellent agreement with a recent study that focally ablated pericytes, which similarly did not damage BBB integrity- but did result in a comparable plasticity response (25). Yet, global pericyte-deficient mouse models have been clearly shown to perturb the BBB (48). Unlike focal pericyte ablation, which resulted in an absence of pericyte-capillary coverage for days, focal ablation of astrocytes in our hands only results in a lapse of endfoot coverage for minutes to hours. Indeed, we were surprised to find that the reinnervation of the blood vessel by replacement astrocytes typically preceded complete retraction of the lesioned cell by a few minutes. Given that the half-life for the tight junction protein ZO-1 is 5.2 hours in MDCK cells (50), and 90 minutes for claudin-5 (51), it is likely that we were unable to strip a vessel of endfoot contact long enough to breach the barrier, assuming focal ablation is sufficient to do so. It is further possible that the pharmacological inhibition of STAT3 prevented BBB breakdown following astrocyte ablation, as other studies have documented restoration of BBB integrity following prevention of STAT3 activation via inhibition of JAK (52). Future studies focally ablating astrocytes should aim to do so in conditions where the replacement of endfeet is either stalled for longer periods or completely abolished. Alternatively, such

studies may find- as was the case in focal pericyte ablation studies- that a more permanent focal ablation of astrocytes is not sufficient to perturb BBB integrity.

Beyond the BBB, we also built off a previous study that documented endfoot plasticity (53) and further determined that it occurs at all levels of the vascular tree **(Figure 1g-n)**. Furthermore, this process begins even prior to the ablated astrocyte having its corpse entirely removed in young mice, whereas aging significantly slows down the swift kinetics of replacement **(Figure 4c-f)**. These results are interesting given our observations of endfoot plasticity following transient ischemic attack (TIA) **(Figure 6).** It is known that the probability of stroke occurrence following TIA increases with aging (54), and presumably any reduction of or lapse in endfoot coverage could affect vessel recovery following ischemic onset- potentially contributing to this increased stroke probability.

Finally, inhibiting the phosphorylation of STAT3 by JAK2 via AG490 injection revealed pSTAT3 to be an essential regulator of the focal endfoot plasticity response. Though many studies have documented AG490 inhibition of JAK2-mediated phosphorylation of STAT3 (42, 55-56), AG490 also inhibits the epidermal growth factor receptor (EGFR). Given that pharmacological inhibition of EGFR with the specific inhibitor PD168393 also attenuated reactive astrogliosis following spinal cord injury (57), these results point to focal endfoot replacement response as being dependent on genes classically associated with astrogliosis (58).

Taken together, this is the first study to characterize gliovascular structural plasticity at all levels of the vascular tree, its physiological relevance to blood flow and the BBB, and its alterations in aging. These findings add to the burgeoning literature regarding the complexities of basic astrocyte biology and the role of the astrocytes in supporting the cerebrovasculature.

\

References

1. Kimelberg, H.K. & Nedergaard, M. Functions of astrocytes and their potential as therapeutic targets. *Neurotherapeutics* **7**, 338-353 (2010).
2. Mathiisen, T.M., Lehre, K.P., Danbolt, N.C. & Ottersen, O.P. The perivascular astroglial sheath provides a complete covering of the brain microvessels: an electron microscopic 3D reconstruction. *Glia* **58,** 1094-1103 (2010).
3. Winkler, E. A., Bell, R.D. & Zlokovic, B.V. Central nervous system pericytes in health and disease. *Nat Neurosci*. **14,** 1398-1405 (2011).
4. Abbott, N.J., Patabendige, A. A., Dolman, D.E., Yusof, S.R. & Begley, D.J. Structure and function of the blood-brain barrier. *Neurobiol. Dis.* **37,** 13-25 (2010).
5. Abbott, N.J., Ronnback, L. & Hansson, E. Astrocyte-endothelial interactions at the blood-brain barrier. *Nat. Rev. Neurosci.* **7,** 41-53 (2006).
6. Wolburg, H., Noell, S., Mack, A., Wolburg-Buchholz, K. & Fallier-Becker, P. Brain endothelial cells and the glio-vascular complex. *Cell. Tissue Res.* **335,** 75-96 (2009).
7. Attwell, D. *et al*. Glial and neuronal control of brain blood flow. *Nature* **468,** 232-243 (2010).
8. Mishra, A., Reynolds, J., Chen, Y. *et al.* Astrocytes mediate neurovascular signaling to capillary pericytes but not to arterioles.*Nat Neurosci* **19,** 1619–1627 (2016). https://doi.org/10.1038/nn.4428
9. Zonta M, et al. Neuron-to-astrocyte signaling is central to the dynamic control of brain microcirculation. *Nat Neurosci.* 2003;6:43–50.
10. Mulligan SJ, Macvicar BA. Calcium transients in astrocyte endfeet cause cerebrovascular constrictions. *Nature.* 2004;431:195–199.
11. Takano T, et al. Astrocyte-mediated control of cerebral blood flow. *Nat Neurosci.* 2006;9:260–267.
12. Mishra A, Hamid A, Newman EA. Oxygen modulation of neurovascular coupling in the retina. *Proc Natl Acad Sci USA.* 2011;108:17827–17831.
13. Niu, J., Tsai, H., Hoi, K.K. *et al.* Aberrant oligodendroglial–vascular interactions disrupt the blood–brain barrier, triggering CNS inflammation. *Nat Neurosci* 22, 709–718 (2019). https://doi.org/10.1038/s41593-019-0369-4
14. Rajkowska, G., Hughes, J., Stockmeier, C. A., Javier Miguel-Hidalgo, J., & Maciag, D. (2013). Coverage of blood vessels by astrocytic endfeet is reduced in major depressive disorder. *Biological psychiatry*, *73*(7), 613–621. https://doi.org/10.1016/j.biopsych.2012.09.024
15. Gudmundsson P, Skoog I, Waern M, Blennow K, P·lsson S, Rosengren L, Gustafson D. The relationship between cerebrospinal fluid biomarkers and depression in elderly women. Am J Geriatr Psychiatry. 2007;15:832. doi: 10.1097/JGP.0b013e3180547091.
16. Bechter K, Reiber H, Herzog S, Fuchs D, Tumani H, Maxeiner HG. Cerebrospinal fluid analysis in affective and schizophrenic spectrum disorders: identification of subgroups with immune responses and blood-CSF barrier dysfunction. J Psychiatr Res. 2010;44:321–330. doi: 10.1016/j.jpsychires.2009.08.008.
17. Frydenlund, D. S., Bhardwaj, A., Otsuka, T., Mylonakou, M. N., Yasumura, T., Davidson, K. G., et al. (2006). Temporary loss of perivascular aquaporin-4 in neocortex after transient middle cerebral artery occlusion in mice. *Proc. Natl. Acad. Sci. U S A* 103, 13532–13536. doi: 10.1073/pnas.0605796103
18. Steiner, E., Enzmann, G. U., Lin, S., Ghavampour, S., Hannocks, M. J., Zuber, B., et al. (2012). Loss of astrocyte polarization upon transient focal brain ischemia as a possible mechanism to counteract early edema formation. *Glia* 60, 1646–1659. doi: 10.1002/glia.22383
19. Wang, Y. & Parpura, V. Central Role of Maladapted Astrocytic Plasticity in Ischemic Brain Edema Formation. *Front. Cell. Neurosci* **10,** 129 (129).
20. Chen A, Akinyemi RO, Hase Y, Firbank MJ, Ndung'u MN, Foster V, Craggs LJ, Washida K, Okamoto Y, Thomas AJ, Polvikoski TM, Allan LM, Oakley AE, O'Brien JT, Horsburgh K, Ihara M, Kalaria RN.

Frontal white matter hyperintensities, clasmatodendrosis and gliovascular abnormalities in ageing and poststroke dementia. Brain. 2016; 139(Pt 1): 242-258. doi: 10.1093/brain/awv328

21. Montagne A, Barnes SR, Sweeney MD, Halliday MR, Sagare AP, Zhao Z, Toga AW, Jacobs RE, Liu CY, Amezcua L, Harrington MG, Chui HC, Law M, Zlokovic BV. Blood-Brain Barrier Breakdown in the Aging Human Hippocampus. Neuron; 85(2): 296-302.
22. Elahy M, Jackaman C, Mamo JCL, Lam V, Dhaliwal SS, Giles C, Nelson D, Takechi R. Blood-brain barrier dysfunction developing during normal aging is associated with inflammation and loss of tight junctions but not with leukocyte recruitment. Immun Ageing. 2015; 12:2. doi: 10.1186/s11979-015-0029-9.
23. Watkins, S., Robel, S., Kimbrough, I. *et al.* Disruption of astrocyte–vascular coupling and the blood–brain barrier by invading glioma cells. *Nat Commun* **5,** 4196 (2014). https://doi.org/10.1038/ncomms5196
24. Kimbrough, I. F., Robel, S., Roberson, E. D., & Sontheimer, H. (2015). Vascular amyloidosis impairs the gliovascular unit in a mouse model of Alzheimer's disease. *Brain : a journal of neurology*, *138*(Pt 12), 3716–3733. https://doi.org/10.1093/brain/awv327
25. Berthiaume AA, Grant RI, McDowell KP, Levy M, Bhat NR, Shih AY. Dynamic Remodeling of Pericytes In Vivo Maintains Capillary Coverage in the Adult Mouse Brain. 2018; 22(1): 8-16. doi: 10.1016/j.celrep.2017.12.016
26. Theodosis, D. T. (2002). Oxytocin-secreting neurons: a physiological model of morphological neuronal and glial plasticity in the adult hypothalamus. *Front. Neuroendocrinol.* 23, 101–135. doi: 10.1006/frne.2001.0226
27. Procko, C., Lu, Y., and Shaham, S. (2011). Glia delimit shape changes of sensory neuron receptive endings in *C. elegans*. *Development* 138, 1371–1381. doi:10.1242/dev.058305
28. Tatsumi, K., Okuda, H., Morita-Takemura, S., Tanaka, T., Isonishi, A., Shinjo, T., et al. (2016). Voluntary exercise induces astrocytic structural plasticity in the globus pallidus. *Front. Cell. Neurosci.* 10:165. doi: 10.3389/fncel.2016.00165
29. Bellesi, M., de Vivo, L., Chini, M., Gilli, F., Tononi, G., and Cirelli, C. (2017). Sleep loss promotes astrocytic phagocytosis and microglial activation in mouse cerebral cortex. *J. Neurosci.* 37, 5263–5273. doi: 10.1523/JNEUROSCI.3981-16.2017
30. Hill RA, Damisah EC, Chen F, Kwan AC, Grutzendler, J. Targeted two-photon chemical apoptotic ablation of defined cell types in vivo. Nature communications. 2017; 8, 15837. doi: 10.1016/j.bbrc.2016.08.088
31. Heithoff, B., George, K.K., Phares, A.N., Zuidhoek, I.A., Munoz-Ballester, C., & Robel, S. Astrocytes are necessary for blood-brain barrier maintenance in the adult mouse brain. Glia 2020; https://doi.org/10.1002/glia.23908
32. Soulet D, Paré A, Coste J, Lacroix S. Automated Filtering of Intrinsic Movement Artifacts during Two-Photon Intravital Microscopy. PLoS ONE 8(1): e53942. https://doi.org/10.1371/journal.pone.0053942.
33. Shen Z, Lu Z, Chhatbar P. O'Herron P, Kara P. An artery-specific fluorescent dye for studying neurovascular coupling. Nature Methods. 2012; 9(3): 273-276. doi: 10.1038/nmeth.1857
34. Watanabe K, Takeishi H, Hayakawa T, Sasaki H. Three-dimensional organization of the perivascular glial limiting membrane and its relationship with the vasculature: a scanning electron microscope study. Okajimas folia anatomica Japonica. 2010; 87: 109-121
35. Myunghwan Choi, Taeyun Ku M.D., Kyungsun Choi, Chulhee Choi, Jonghee Yoon, "Label-free optical activation of astrocyte *in vivo*," J. Biomed. Opt. 16(7) 075003 (1 July 2011) https://doi.org/10.1117/1.3600774Jyothi, H. J., Vidyadhara, D. J., Mahadevan, A., Philip, M., Parmar, S. K., Manohari, S. G., et al. Aging causes morphological alterations in astrocytes and microglia in human

substantia nigra pars compacta. Neurobiol. Aging. 2015;36: 3321–3333. doi: 10.1016/j.neurobiolaging.2015.08.024

36. Castiglioni, A. J., Legare, M. E., Busbee, D. L., and Tiffany-Castiglioni, E. Morphological changes in astrocytes of aging mice fed normal or caloric restricted diets. Age. 1991; 14: 102–106. doi:10.1007/bf02435015
37. Amenta, F., Bronzetti, E., Sabbatini, M., and Vega, J. A. Astrocyte changes in aging cerebral cortex and hippocampus: a quantitative immunohistochemical study. Microsc. Res. Tech. 1998; 43: 29–33. doi:10.1002/(SICI)1097-0029(19981001)43:1<29::AID-JEMT5>3.0.CO;2-H
38. Cerbai, F., Lana, D., Nosi, D., Petkova-Kirova, P., Zecchi, S., Brothers, H. M., et al. The neuron astrocyte-microglia triad in normal brain ageing and in a model of neuroinflammation in the rat hippocampus. PLoS One. 2012;7:e45250. doi: 10.1371/journal.pone.0045250
39. Kanaan, N. M., Kordower, J. H., and Collier, T. J. Age-related changes in glial cells of dopamine midbrain subregions in rhesus monkeys. Neurobiol. Aging. 2010;31: 937–952. doi: 10.1016/j.neurobiolaging.2008.07.006
40. Robillard, K. N., Lee, K. M., Chiu, K. B., and MacLean, A. G. Glial cell morphological and density changes through the lifespan of rhesus macaques. Brain Behav. Immun. 2016: 55; 60–69. doi:10.1016/j.bbi.2016.01.006
41. Early, A.N., Gorman, A.A., Van Eldik L.J., Bachstetter, A.D., Morganti, J.M. Effects of advanced age upon astrocyte-specific responses to acute traumatic brain injury in mice. *J Neuroinflammation* **17,** 115 (2020). https://doi.org/10.1186/
42. Sriram, K., Benkovic, S.A., Hebert, M.A., Miller, D.B., & O'Callaghan J.P. Induction of gp130-related Cytokines and Activation of JAK2/STAT3 Pathway in Astrocytes Precedes Up-regulation of Glial Fibrillary Acidic Protein in the 1-Methyl-4-phenyl-1,2,3,6-tetrahydropyridine Model of Neurodegeneration. The Journal of Biological Chemistry. 2004; 279(19): 19936-19947. doi: 10.1074/jbc.M309304200
43. Herrmann, J.E., Imura, T. Song, B., Qi, J., Ao, Y., Nguyen, T.K., Korsak, R.A., Takeda, K., Akira, S., Sofroniew, M.V. STAT3 is a Critical Regulator of Astrogliosis and Scar Formation after Spinal Cord Injury. The Journal of Neuroscience. 2008; 28(28):7231-7243. doi: 10.1523/JNEUROSCI.1709-08.2008
44. Giffard, R. G., & Swanson, R. A. (2005). Ischemia-induced programmed cell death in astrocytes. *Glia*, *50*(4), 299–306. https://doi.org/10.1002/glia.20167
45. Talley Watts L, Zheng W, Garling RJ, Frohlich VC, Lechleiter JD. Rose Bengal Photothrombosis by Confocal Optical Imaging In Vivo: A Model of Single Vessel Stroke. J Vis Exp. 2015 Jun 23;(100):e52794. doi: 10.3791/52794. PMID: 26131664; PMCID: PMC4652424.
46. Ezan P., André P., Cisternino S., Sabaméa, B., Boulay. A.C., Doutremer, S., Thomas, M.A., Quenech'Du, N., Giaume, C., Cohen-Salmon, M. Deletion of astroglial connexins weakens the blood-brain barrier. Journal of Cerebral Blood Flow and Metabolism : Official Journal of the International Society of Cerebral Blood Flow and Metabolism. 2012 Aug;32(8):1457-1467. DOI: 10.1038/jcbfm.2012.45.
47. Yao, Y., Chen, Z. L., Norris, E. H. & Strickland, S. Astrocytic laminin regulates pericyte differentiation and maintains blood brain barrier integrity. Nature communications. 2014; 5:3413. doi:10.1038/ncomms4413
48. Armulik, A., Genové, G., Mäe, M., Nisancioglu, M.H., Wallgard, E., Niaudet, C., He, L., Norlin, J., Lindblom, P., Strittmatter, K., Johansson, B.R., Betsholtz, C. Pericytes regulate the blood-brain barrier. Nature. 2010 Nov 25;468(7323):557-61. doi: 10.1038/nature09522. Epub 2010 Oct 13. PMID: 20944627.
49. Haim, L., Rowitch, D. Functional diversity of astrocytes in neural circuit regulation. *Nat Rev Neurosci* 18, 31–41 (2017). https://doi.org/10.1038/nrn.2016.159

50. Chen, Y. h., Lu, Q., Schneeberger, E. E., & Goodenough, D. A. (2000). Restoration of tight junction structure and barrier function by down-regulation of the mitogen-activated protein kinase pathway in ras-transformed Madin-Darby canine kidney cells. *Molecular biology of the cell*, *11*(3), 849–862. https://doi.org/10.1091/mbc.11.3.849
51. Mandel, I, et al. The ubiquitin-proteasome pathway regulates claudin 5 degradation. J Cell Biochem. 2012;113(7):2415–23.
52. Takata F, Dohgu S, Matsumoto J, Machida T, Sakaguchi S, Kimura I, Yamauchi A, Kataoka Y. Oncostatin M-induced blood-brain barrier impairment is due to prolonged activation of STAT3 signaling in vitro. *J Cell Biochem.* 2018; 119: 9055-9063. https://doi.org/10.1002/jcb.27162
53. Kubotera, H., Ikeshima-Kataoka, H., Hatashita, Y. *et al.* Astrocytic endfeet re-cover blood vessels after removal by laser ablation. *Sci Rep* **9,** 1263 (2019). https://doi.org/10.1038/s41598-018-37419-4
54. Johnston, S.C., Gress, D.R., Browner, W.S., Sidney, S. Short-term prognosis after emergency department diagnosis of TIA. JAMA 2000;284:2901-6.
55. An, J., Pang, H.G., Huang, T., Song, J., Li, D., Zhao, Y., Ma, X. AG490 ameliorates early brain injury via inhibition of JAK2/STAT3-mediated regulation of HMGB1 in subarachnoid hemorrhage. Ex Ther Med. 2018 Feb; 15(2): 1330-1338. doi: 10.3892/etm.2017.5539
56. Ignarro, R.S., Vieira, A.S., Sartori, C.R., Langone, F., Rogério, F., Parada, C.A. JAK2 inhibition is neuroprotective and reduces astrogliosis after quinolinic acid striatal lesion in adult mice. Journal of Chemical Neuroanatomy. 2013 Mar; 48: 14-22. doi: 10.1016/j.jchemneu.2013.02.005
57. Li, ZW., Li, JJ., Wang, L. *et al.* Epidermal growth factor receptor inhibitor ameliorates excessive astrogliosis and improves the regeneration microenvironment and functional recovery in adult rats following spinal cord injury. *J Neuroinflammation* 11, 71 (2014). https://doi.org/10.1186/1742-2094-11-71
58. Sofroniew, M. V. (2020). Astrocyte Reactivity: Subtypes, States, and Functions in CNS Innate Immunity. *Trends in Immunology*, *41*(9), 758–770. https://doi.org/10.1016/j.it.2020.07.004

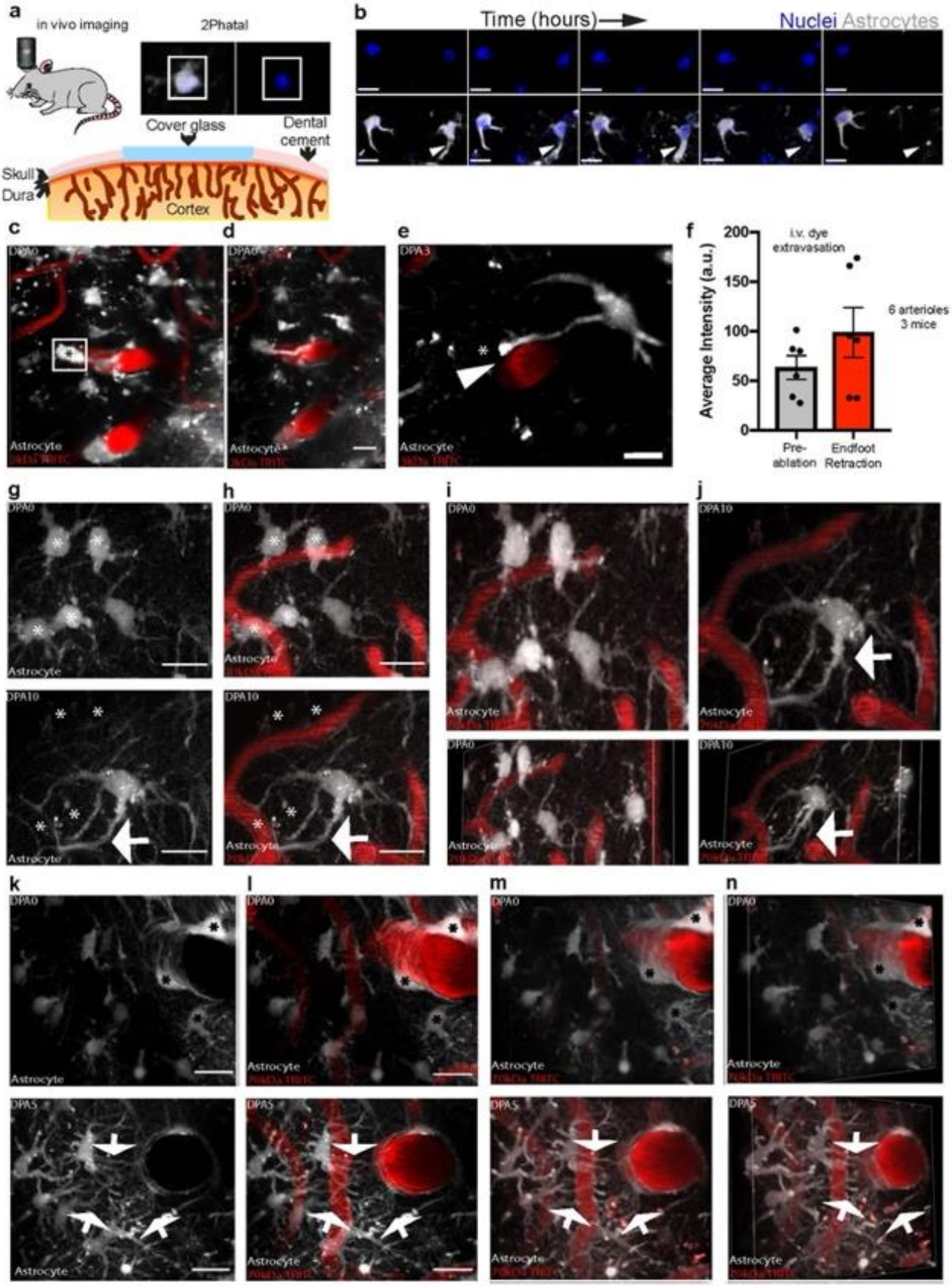
a
in vivo imaging
2Phatal
Cover glass
Dental cement
Skull
Dura
Cortex
b
Time (hours)
Nuclei Astrocytes
c
d
e
f
i.v. dye extravasation
Average Intensity (a.u.)
200
150
100
50
0
6 arterioles
3 mice
Pre-ablation
Endfoot Retraction
g
h
i
j
k
l
m
n
Astrocyte
DPA0
DPA3
DPA10
DPA5

Figure 1-The focal ablation of an astrocyte induces a gliovascular structural plasticity response at all levels of the vascular tree- To determine if the focal ablation of an astrocyte is sufficient to induce breaches in blood-brain barrier integrity, we utilized the *in vivo* single-cell 2Phatal cellular ablation method. In all images, asterisks indicate the ablated astrocyte(s) and arrows demarcate replacement processes. **a)** Cartoon diagram depicting the experimental approach, including the bath application of Hoechst at the time of surgery and prior to cranial window implantation. By using low laser-power to activate Hoechst, we could **b)** visualize astrocytes in Aldh1l1-eGFP mice up to and beyond removal of their cell body and associated processes, scale bar = 15 µm. **c)** Volumetric reconstruction of an astrocyte at a penetrating arteriole on day post-ablation 0 (dpa0), with **d)** maximum intensity projection of the same field, scale bar = 10 µm, and **e)** maximum intensity projection at dpa5 showing no apparent disruption to blood-brain barrier integrity. Instead, an astrocyte polarizing a process to the vacant vascular location can be seen, scale bar = 10 µm. **f)** Average intensity quantification of 3kDa TRITC extravasation at baseline relative to the moment of endfoot retraction. n = 6 vessels across 3 mice, two-tailed paired end t-test, $p < 0.1100$. **g)** and **h)** Maximum intensity projection of astrocytes surrounding capillaries at dpa0 (top) and dpa10 (bottom), scale bar = 15 µm. **i)** Volumetric reconstruction at dpa0 of capillary field showing both dorsal (top) and dorsolateral (bottom) views compared to **j)** at dpa10. The arrow indicates replacement processes from neighboring astrocytes. Representative image for n=40 astrocytes/4 mice **k)** and **l)** Maximum intensity projection of an ascending venule at dpa0 (top) and dpa5 (bottom). Arrows represent replacement processes from neighboring astrocytes, scale bar = 20 µm. **m)** Volumetric reconstruction showing dorsal view at dpa0 (top) and dpa5 (bottom). **n)** Same image from the dorsolateral view at dpa0 (top) and dpa5 (bottom). Representative image for n=40 astrocytes/7 mice.

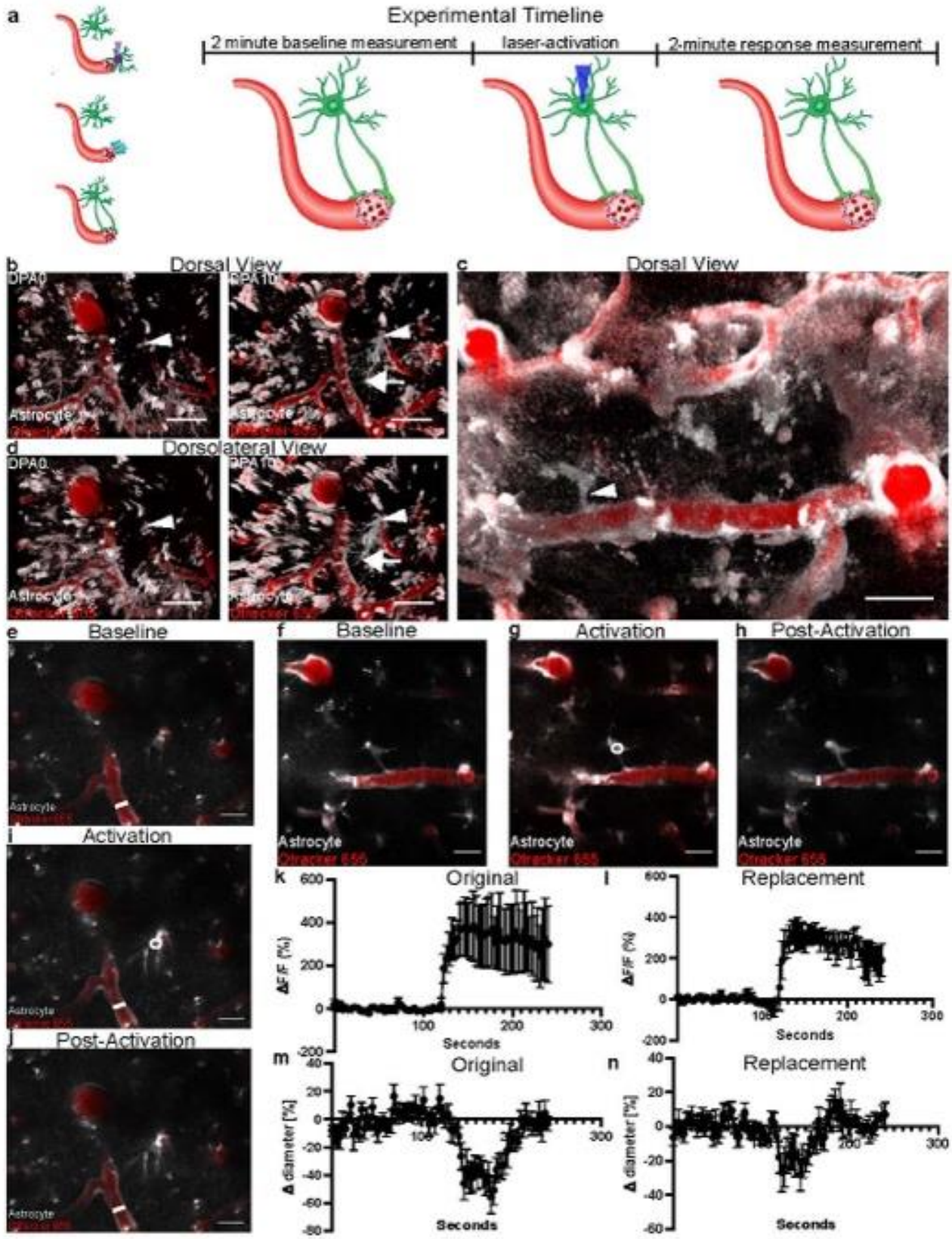
a
Experimental Timeline
2 minute baseline measurement
laser-activation
2-minute response measurement
b
Dorsal View
DPA0
DPA10
Astrocyte
c
Dorsal View
d
Dorsolateral View
DPA0
DPA10
Astrocyte
e
Baseline
f
Baseline
g
Activation
h
Post-Activation
Astrocyte
i
Activation
j
Post-Activation
k
Original
l
Replacement
ΔF/F (%)
Seconds
m
Original
n
Replacement
Δ diameter [%]
Seconds

Figure 2-Replacement endfeet vasoconstrict precapillary arterioles- To determine if replacement endfeet can vasoconstrict precapillary arterioles, we 2Phatal ablated astrocytes in Aldh1l1cre x GCaMP5G mice, targeting astrocytes contacting the first branching capillary segment from an Alexa-633 hydrazide positive penetrating arteriole. **a)** Cartoon depicting experimental paradigm. Upon 2Phatal ablation, astrocytes undergo microglial engulfment, and a new astrocyte subsequently extends processes to reinnervate the vascular vacancy. Replacement astrocytes underwent two minutes of imaging to assess baseline vessel diameter and calcium levels, were then laser-activated, and another two minutes of imaging ensued. **b)** Left-side image is a volumetric reconstruction showing a dorsal view of the field of interest at baseline. The right-side image shows that same field at dpa10. Annotation is as follows: asterisks indicate ablated astrocytes, arrows indicate replacement astrocyte processes, and arrow-heads indicate replacement astrocyte to-be. **c)** and **d)** Volumetric reconstruction depicting a field of interest, with the arrow-head indicating astrocyte chosen for laser-activation, from c) a dorsal view and d) a dorsolateral view of the replacement astrocyte. **e)** Single-optical section of the replacement astrocyte field at baseline, as depicted in b and d. **f)** Single-optical section of the original astrocyte field at baseline, as depicted in c. **g)** Single-optical section showing the original astrocyte and pre-capillary arteriole at the time of laser-activation, followed by **h)** a single-optical section showing return to baseline. **i)** Single-optical section showing the replacement astrocyte and pre-capillary arteriole at time of laser-activation. The precapillary arteriole constricts soon after astrocyte activation. **j)** Single-optical section showing return to baseline. **k)** Quantification of change in fluorescence over baseline fluorescence (Δf/f) for the duration of the experiment in astrocytes originally occupying an appositional vascular location. **l)** Quantification of change in diameter over baseline diameter (Δ diameter) for the duration of the experiment in astrocytes originally occupying an appositional vascular location. **m)** Quantification of change in fluorescence over baseline fluorescence (Δf/f) for the duration of the experiment in replacement astrocytes. **n)** Quantification of change in diameter over baseline diameter (Δ diameter) for the duration of the experiment in replacement astrocytes. n=5 astrocytes over 3 mice for both groups. Scale bars=20 µm

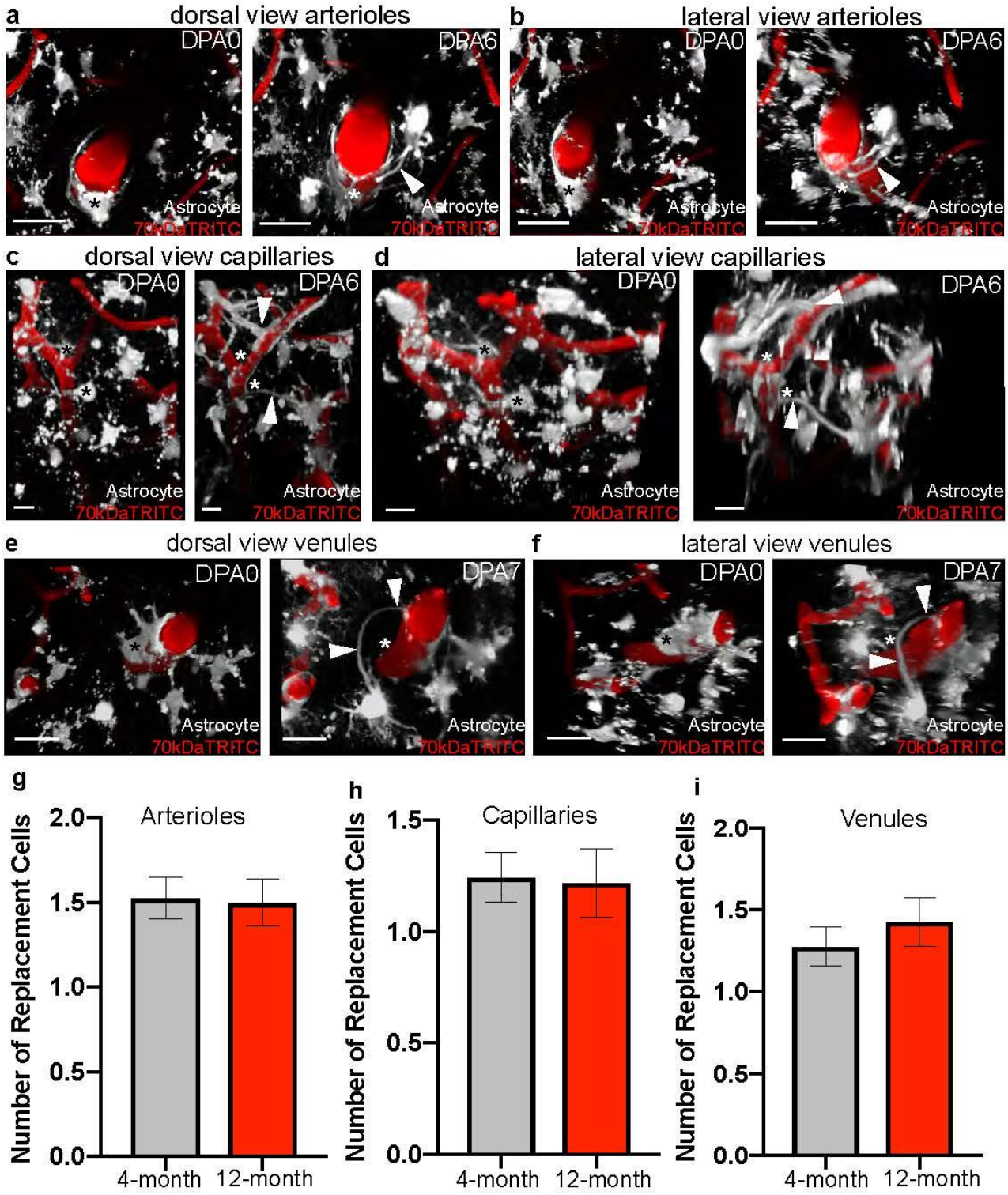

Figure 3-Gliovascular structural plasticity remains intact at levels of the vascular tree in aging- In order to determine if gliovascular structural plasticity remained intact in aging, we ablated astrocytes in 12-month-old Aldh1l1-eGFP mice making contact with Alexa 633 hydrazide positive penetrating arterioles, capillaries, and venules. We further compared the extent of replacement in old versus young mice as well. In all images, asterisks indicate the ablated astrocyte(s) and arrows demarcate replacement processes. **a)** and **b)** Volumetric

reconstruction showing astrocyte associations with a penetrating arteriole at dpa0 (left) and dpa6 (right), from a) a dorsal perspective and b) a dorsolateral perspective. Scale bar=25 µm. **c)** and **d)** Volumetric reconstruction showing the astrocytes and their association with a capillary at dpa0 (left) and dpa6 (right) from c) a dorsal view and d) a dorsolateral view. Scale bar=10 µm. **e)** and **f)** Volumetric reconstruction showing an ascending venule and astrocyte interactions with it at dpa0 (left) and dpa7 (right), from e) a dorsal view and f) a dorsolateral view. Scale bar=20 µm **g)** Average number of replacement astrocytes (the number of cells polarizing processes to vascular vacancies) in 4- versus 12-month-old mice at arterioles, Two-tailed Mann-Whitney test, p=0.9465, n=40cells/7 mice for 4-month data, n=40cells/6 mice for 12-month data. **h)** Average number of replacement astrocytes in 4-versus 12-month-old mice at capillaries, Two-tailed Mann Whitney test, p=0.6853, n=40 cells/4 mice for both 4- and 12-month-old mice. **i)** Average number of replacement astrocytes in 4-versus 12-month-old mice at venules, Two-tailed Mann Whitney test, p=0.3060, n=40 cells/7 mice for 4-month-old data, n=40cells/5 mice for 12-month-old data.

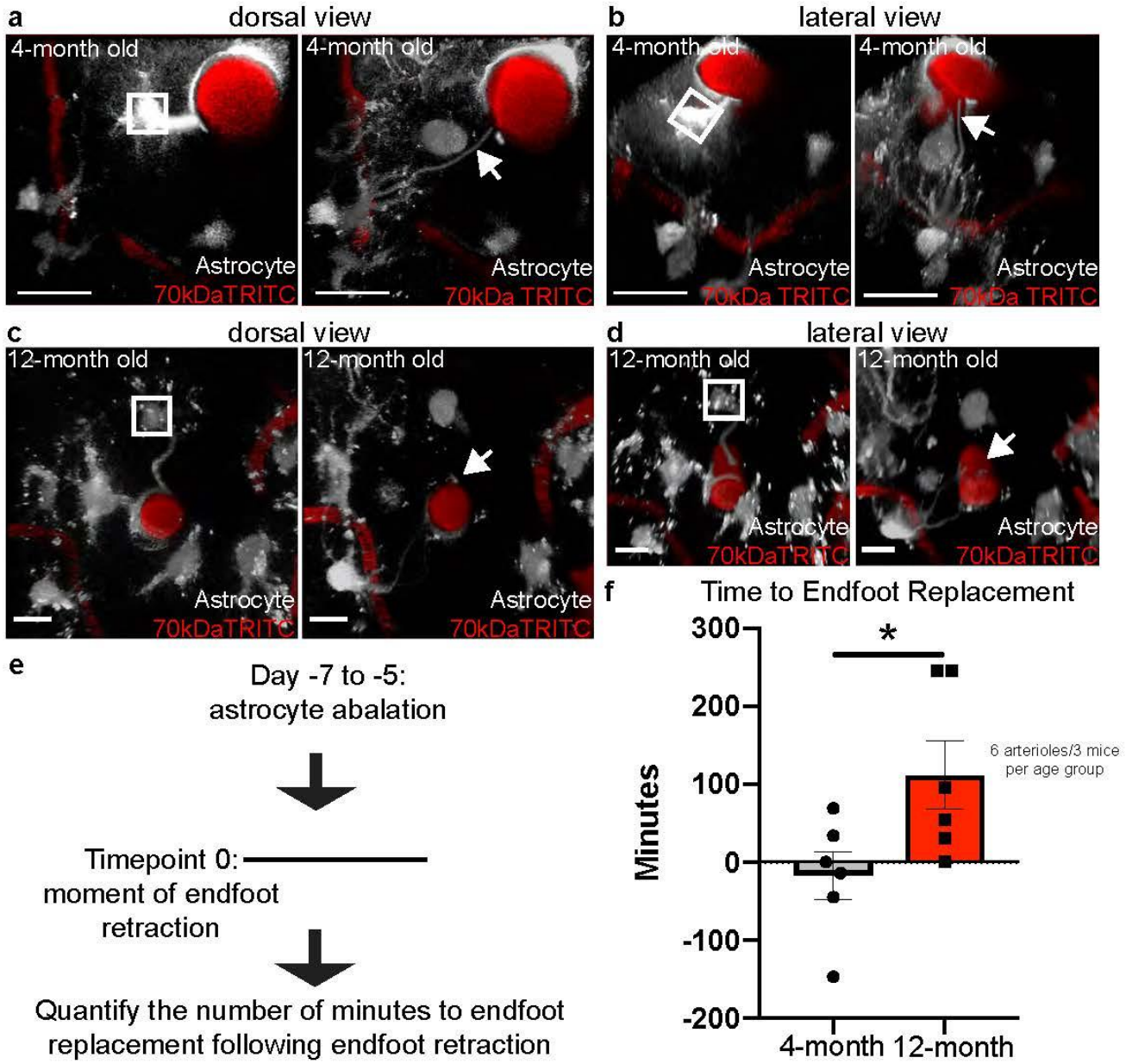

Figure 4-Aging significantly attenuates the kinetics of the gliovascular structural plasticity response- In order to determine if the kinetics of endfoot replacement significantly slowed as a result of aging, we ablated astrocytes at penetrating arterioles and acquired continual z-stacks to capture the exact time of endfoot replacement. White boxes indicate ablated astrocyte and arrows demarcate replacement processes (as in a and b) or lack thereof (as in c and d). **a)** and **b)** Volumetric reconstruction showing the penetrating arteriole in a 4-month-old mouse at baseline (left) and the exact moment of endfoot retraction (right), from a) a dorsal view and b) dorsolateral view of the same field. Scale bar=25 µm. **c)** and **d)** Volumetric reconstruction showing a penetrating arteriole in a 12-month-old mouse at baseline (left) and the near exact moment of endfoot retraction (right), in c) the dorsal view and d) the dorsolateral view. Scale bar=10 µm e) Schematic illustrating methodology to quantify the number of minutes to endfoot replacement. Right-side images in a-d represent time point zero, or the moment of endfoot retraction. Subsequent images were analyzed to determine the number of minutes until a process occupied an appositional vascular location, as depicted in right-side images of a and b. **f)** Average number of

minutes to endfoot replacement in 4- versus 12-month-old mice. n=6 cells/4 mice for both age groups, Two-tailed, unpaired t-test, p<0.0371.

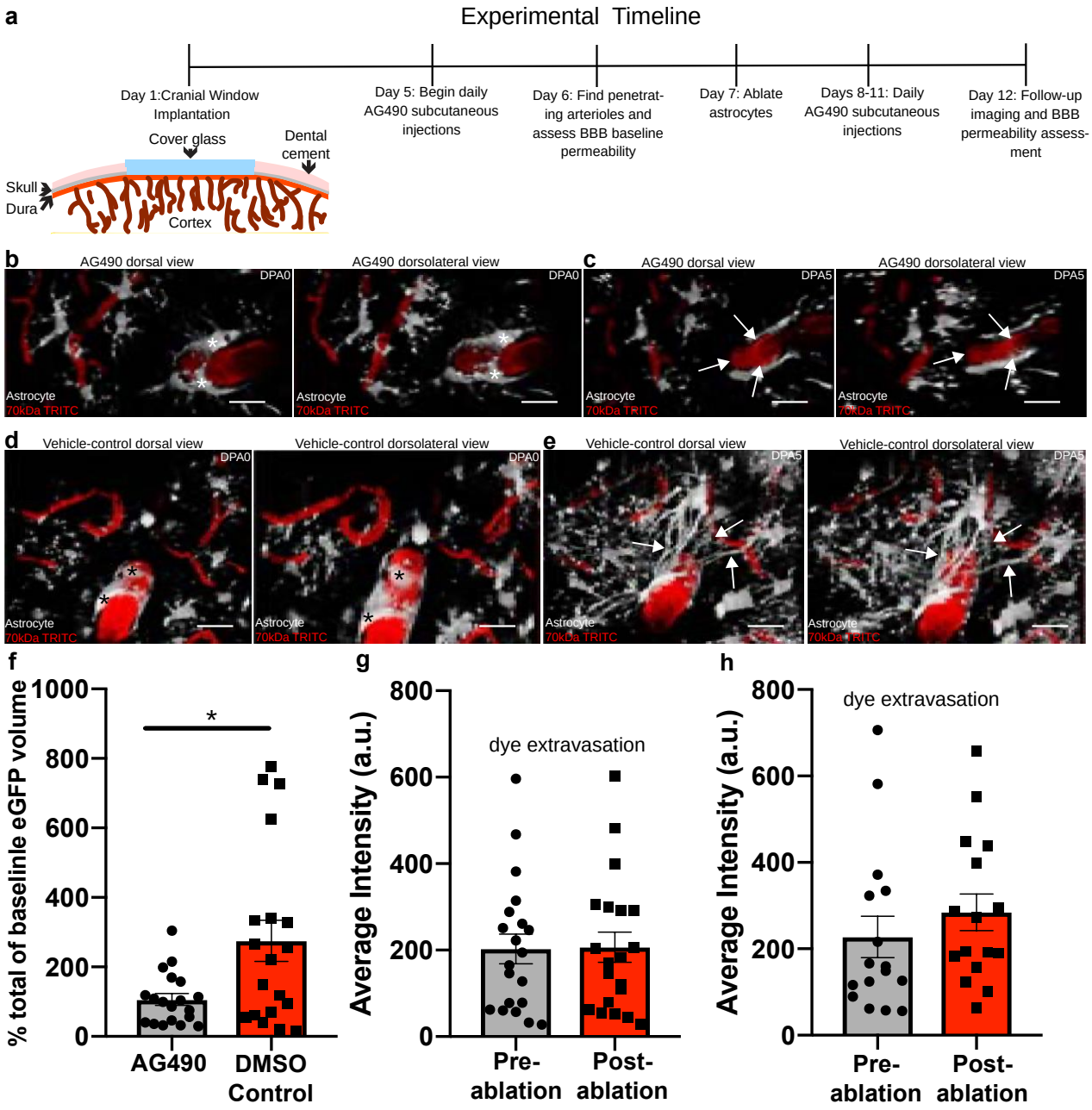

Figure 5-The pharmacological inhibition of EGFR/pSTAT3 significantly reduces the volumes of replacement astrocytes post-ablation-In order to determine if EGFR and pSTAT3 is necessary for gliovascular structural plasticity, we subcutaneously injected AG490. In all images, asterisks indicate ablated astrocyte(s) and arrows demarcate replacement processes, or lack thereof. **a)** Schematic illustrating the experimental timeline. **b)** and **c)** Volumetric reconstructions showing the dorsal view (left) and dorsolateral view (right) of astrocytes and

their interactions with a penetrating arteriole in AG490-injected mice at b) dpa0 and c) dpa5. Scale bar=20 µm **d)** and **e)** Volumetric reconstructions showing the dorsal view (left) and dorsolateral view (right) of astrocytes interacting with a penetrating arteriole in DMSO vehicle-injected control mice at d) dpa0 and e) dpa5. Scale bar=20 µm. **f)** Bar graph comparing percent increase in eGFP volume at dpa5 relative to baseline in AG490-injected mice relative to DMSO-injected control, n=19 penetrating arterioles/4 mice, Two-tailed Mann-Whitney test, p=0.0497. **g)** Bar graph comparing the average intensity of 3kDa TRITC extravasation pre-ablation versus post-ablation, n=20 penetrating arterioles/4 mice, Two-tailed Wilcoxin matched pairs signed-rank test, p=0.6215. **h)** DMSO vehicle-injected control group, n=16 penetrating arteriole/4 mice, Two-tailed Wilcoxin matched pairs signed-rank test, p=0.1167.

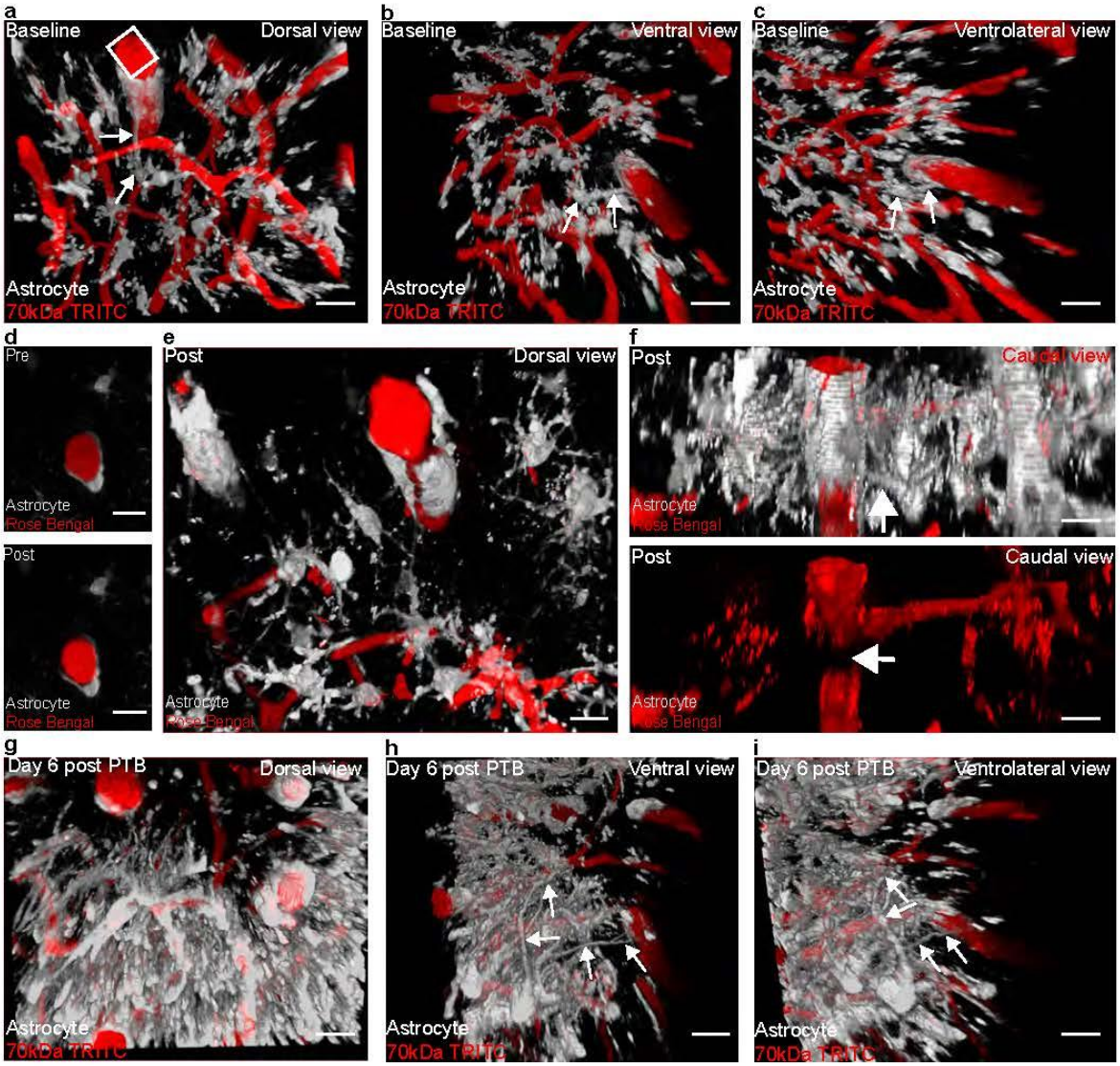

Figure 6-Gliovascular structural plasticity occurs following reperfusion post-focal photothrombotic stroke- In order to determine if gliovascular structural plasticity occurs following loss of astrocyte-vascular

coverage due to CNS insult, we turned to the Rose Bengal focal photothrombotic stroke method. Arrows in all images demarcate astrocyte processes either at baseline (as in a, b, c, and f) or replacement processes six days following reperfusion from focal-stroke (as in h-i). **a)** through **c)** Volumetric reconstruction showing a penetrating arteriole at baseline from a) dorsal view, b) a ventral view, and c) a ventrolateral view. **d)** Single optical section showing a penetrating arteriole following Rose Bengal injection (top) and immediately after laser-induced dye nucleation (bottom). **e)** and **f)** Volumetric reconstruction showing a penetrating arteriole immediately after Rose Bengal laser-induced dye nucleation from e) a dorsal view and f) a lateral view of that same field showing the penetrating arteriole after Rose Bengal injection (top) and (bottom) immediately after dye nucleation. The arrow in the bottom image demarcates where RBC buildup has occurred. **g)** Volumetric reconstruction showing a dorsal view of the previously occluded vessel six days later. Note that reperfusion occurred within the hour following Rose Bengal dye nucleation (data not shown) **h)** Volumetric reconstruction of the same field but from a ventral view and **i)** ventrolateral view. n=5 arterioles/5 mice. Scale bar in a-i=20 µm

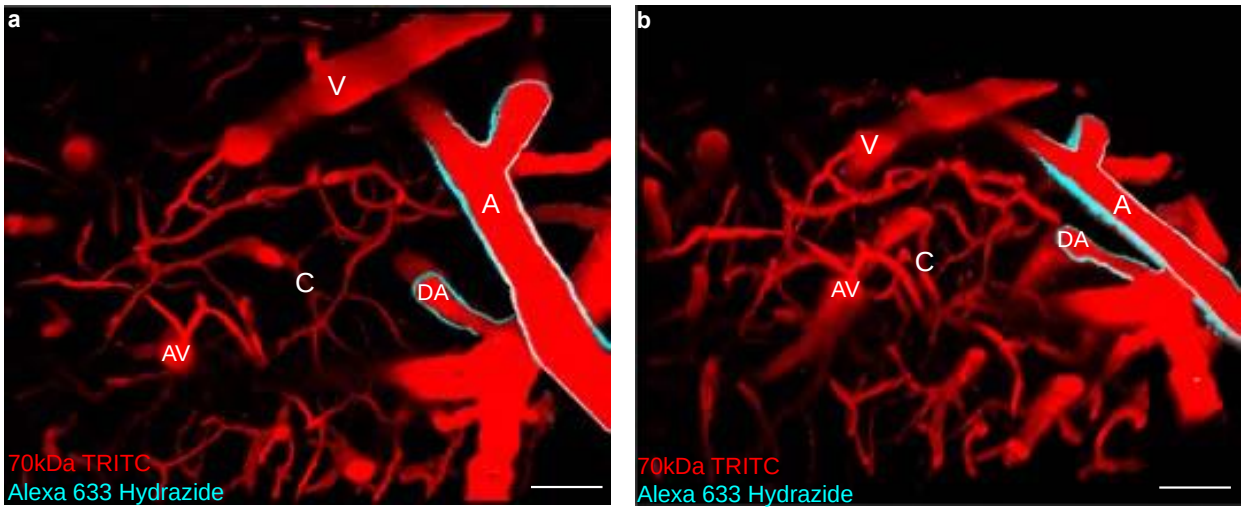

Supplementary Figure 1-Alexa 633 hydrazide positively selects for arterioles- In order to determine which vessel type we were ablating astrocytes at, we employed the use of Alexa 633 hydrazide to: positively select for arterioles and penetrating arterioles; size exclusion; and negative selection of venules, ascending venules, and capillaries (<10 µm). Volumetric reconstruction showing **a)** a dorsal view of all zones of the vascular tree and **b)** a dorsolateral view of the same field. Scale bar=25 µm. A- arteriole, DA- descending arteriole, V- venule, AV- ascending venule, C- capillary.

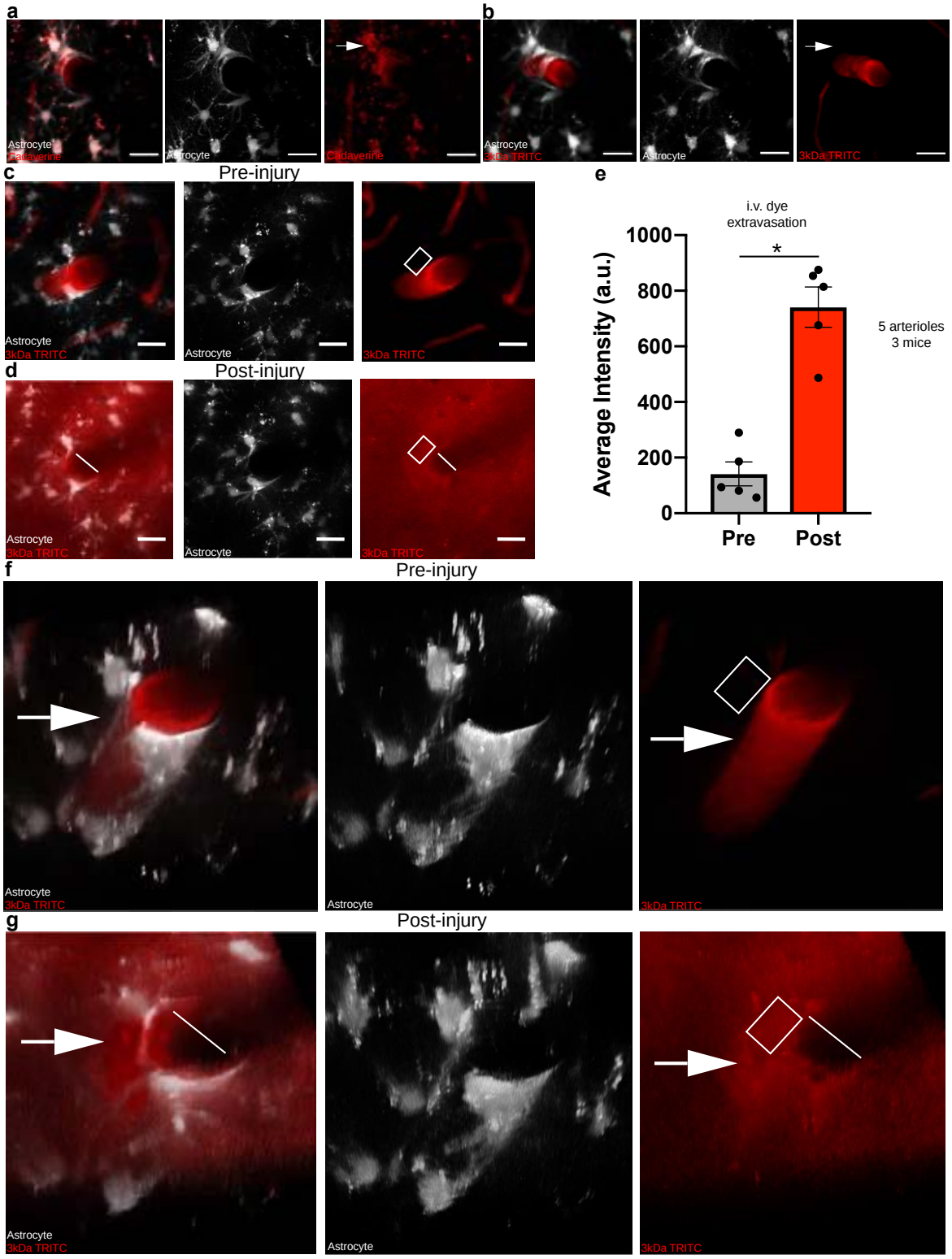

Supplementary Figure 2-Extravasation of 3kDa TRITC can be reliably detected *in vivo*- To measure breaches in BBB integrity, we employed the use of small molecular weight dyes and determined through laser-induced vessel injury that they can be reliably detected *in vivo*. **a)** Maximum intensity projections showing

cadaverine extravasation at baseline in Aldh1l1-eGFP mice (left, middle, and right). **b)** Maximum intensity projections showing that 3kDa TRITC does not extravasate at baseline in Aldh1l1-eGFP mice (left, middle, and right). Scale bar in a-b=20 µm **c)** Maximum intensity projections showing a penetrating arteriole at baseline without apparent 3kDa TRITC extravasation relative as opposed to **d)** obvious 3kDa TRITC dye extravasation following vessel injury. The white line indicates where the laser scanned across the vessel lumen, and the white box indicates where measurements were taken. Scale bar in c and d=20 µm. **e)** Comparison of the average intensity of 3kDa TRITC extravasation pre-vessel injury relative to post-injury. n=5 arterioles/3mice, Two-tailed paired t-test, $p<0.0021$. **f-g)** Volumetric reconstructions showing a dorsolateral view of the same images displayed in c and d.

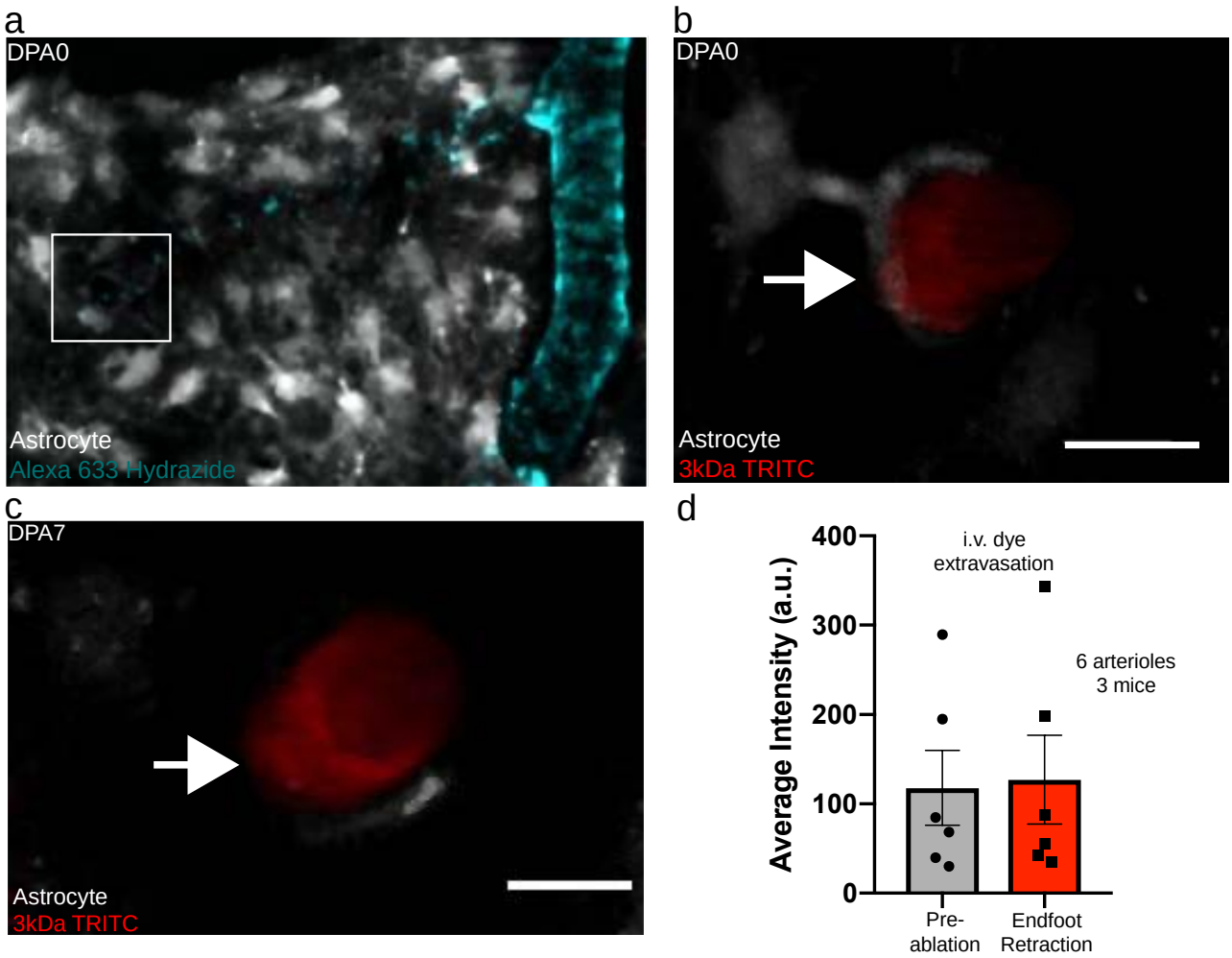

Supplementary Figure 3-Blood-brain barrier integrity is not compromised in 12-month-old mice a) Maximum intensity projection showing an Alexa-633 hydrazide positive arteriole in a 12-month-old Aldh1l1-EGFP mouse. White square indicates a penetrating portion of a branch from that arteriole, shown **b)** at a higher magnification at baseline, and **c)** at the same magnification at the exact moment of endfoot retraction on dpa7.

Scale bar in b and c = 10 µm. **d)** Comparison of the average intensity of 3kDa TRITC at baseline, prior to astrocyte ablation, relative to post-ablation. n=6 arterioles/3mice, Two-tailed paired t-test, p<0.3785.

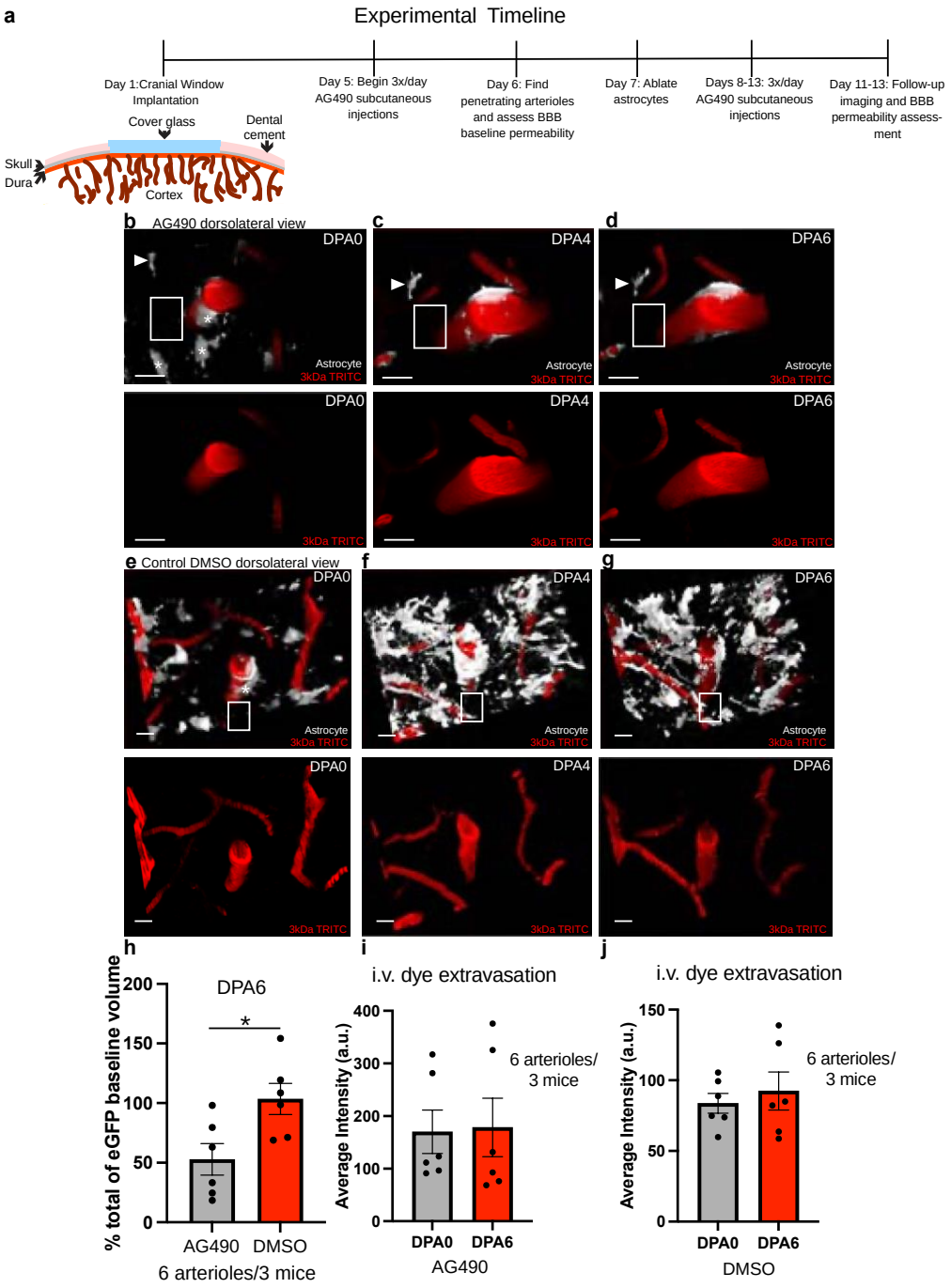

Supplementary Figure 4-Significant reductions in astrocyte volume at penetrating arterioles post-ablation is sufficient to maintain BBB integrity- In order to determine how BBB integrity would be impacted following a significant reduction in endfoot coverage post-astrocyte ablation, we adopted the experimental timeline outlined in **a)**. Following cranial window implantation, mice received 3 doses of AG490 daily beginning at day five post-operation. This injection continued through post-operation day 13. After ablating astrocytes on day seven post-operation, follow-up imaging would occur to assess endfoot plasticity volume for three days (days four to six post-ablation). **b)** Volumetric reconstruction at baseline depicting a dorsolateral view of the astrocyte-vascular landscape (top) or just vascular landscape (bottom) in AG490-injected mice. **c)** Same field as b, but day 4 post-ablation, and **d)** at day 6 post-ablation. Arrow-head indicates a reference astrocyte. Asterisks indicate ablated astrocytes. Scale bar in b-d= 20 µm. **e)** Volumetric reconstruction at baseline depicting a dorsolateral view of the astrocyte-vascular landscape (top) or just vascular landscape (bottom) in DMSO control-injected mice. Asterisk indicates the ablated astrocyte. **f)** Same field as e, but at day 4 post-ablation, and **g)** at day 6 post-ablation. **h)** Quantification of the percent change in astrocyte volume at dpa6 relative to dpa0 along arteriole locations where astrocytes were ablated. n=6 arterioles over 3 mice. Two-tailed unpaired t-test, $p< 0.0213$. **i)** Average intensity of 3kDa TRITC dye extravasation along arteriole locations where astrocytes were ablated at dpa6, relative to baseline in AG490-injected mice. n=6 arterioles/3 mice. Two-tailed paired t-test. $P<0.4104$. **j)** Average intensity of 3kDa TRITC dye extravasation along arteriole locations where astrocytes were ablated at dpa6, relative to baseline in DMSO-injected control mice. n=6 arterioles/3 mice. Two-tailed paired t-test. $p< 0.5861$. White boxes in b-e represent locations of ROI placement for BBB measurements. Scale bar in e-g=10 µm.

Chapter 4

Summary and Conclusion

Summary and Future Direction

Astrocytes extend processes called endfeet that intimately associate with nearly all ~400 miles of cerebrovasculature (1-2). Decades of research suggested this was necessary to ensure maintenance of blood-brain barrier integrity (3-7), and work from our lab further characterized disruption of astrocyte-vascular contact coinciding with blood-brain barrier deficits in a glioma model(8). Given that we had also characterized impaired gliovascular interactions in a vascular amyloidosis model (9), the initial aim of this dissertation was to extend our BBB findings in the glioma model to the vascular amyloidosis model. The results discussed in Chapter 1 revealed that the tight junction protein ZO1 was significantly reduced in regions of vascular amyloid deposition, and preliminary data further showed this was accompanied with extravasation of various molecular weight dyes. In order to elucidate what aspect of this blood-brain barrier phenotype was due solely to disrupted endfoot-vascular associations along with the normal process of biological aging, we turned to the 2Phatal single-cell ablation method (10). Interestingly, we found that, upon removal of astrocyte-vascular contact, surrounding astrocytes extend processed to re-innervate vacancies left by previously ablated astrocytes. We named this response gliovascular structural plasticity (GSP)- and given its novelty- we turned to characterizing GSP at all levels of the vascular tree, its physiological relevance to blood flow, the effects of normal biological aging on it, and elucidating its underlying mechanisms.

Chapter 3 revealed that GSP does indeed occur at levels of the vascular tree and that the extent of replacement does not differ between young and aged mice. GSP kinetics, however, are significantly reduced in aging. I was able to evaluate BBB integrity in aged mice during these periods of vascular vacancies, the results of which revealed no breaches to the BBB. As discussed, it is possible that the duration of time the arteriole surface lacked endfoot contact was too short to account for the half-life of tight junction proteins, and as such, we conclude that the focal ablation of an astrocyte is not sufficient to induce breaches in BBB integrity. Should future studies focally strip vessels of endfoot coverage for extended periods of time and determine that the BBB remains intact, these results would suggest that the observed BBB deficits in the glioma and vascular amyloidosis disease models exist independent of perturbed astrocyte-vascular interactions and/or lost trophic support from astrocytes.

Further inquiries regarding the role of astrocytes in the vascular amyloidosis model could therefore view amyloid deposition as the trigger leading to BBB deficits indirectly by how it induces reactivity from surrounding cells. Its deposition may result in alterations to underlying signaling mechanisms known to be necessary for BBB maintenance, such as the SSeCKS-Ang1-VEGF signaling axis highlighted in Chapter 1, which has been shown to be perturbed in astrocytes under conditions of hypoxia (4). Perhaps amyloid accumulation over time impairs blood flow or the free diffusion of oxygen to levels sufficient to induce hypoxia in surrounding astrocytes. Such onset would lead to the release of VEGF and subsequent ZO1 reductions. This hypothesis could thus be viewed in the dual gain and/or loss of function framework presented for astrocytes in AD in Chapter 1. Amyloid accumulation results in BBB deficits due to loss of astrocyte trophic support in the form of Ang1 or because of a toxic gain-of-function whereby astrocytes release VEGF resulting in subsequent tight junction dysregulation. Given that astrocytes have been shown to release VEGF-A in CNS inflammatory disease (11) and that they have highest mRNA expression of this molecule relative to other CNS cell types (12), future studies should specifically examine this isoform of VEGF.

Alternatively, amyloid in oligomeric form may induce VEGF release from astrocytes which in turn induces matrix metalloproteinase (MMP) 9 release from endothelial cells, subsequently leading to Claudin 5 disruption. Spampinato et. al not only showed this mechanism to be at play, but that oligomeric amyloid had no direct impact on BBB integrity (13). Given that BBB breaches have been shown to occur prior to amyloid deposition in humans, amyloid also may just simply exacerbate vascular deficits in both direct and indirect ways rather than representing the etiology of them.

I further demonstrated in Chapter 3 that replacement astrocyte endfeet are capable of vasoconstricting primary capillaries. This finding demonstrates that replacement endfeet inherently possess the ability to release vasoactive molecules, which perhaps isn't so surprising given that all astrocyte on average have 3.5 endfeet (14). Future experiments should determine if replacement astrocytes actually occupy synaptic contacts previously occupied by the ablated astrocyte, as this would have major implications for neurovascular coupling at primary

capillaries. It is known that astrocytes naturally exemplify dynamism at the synaptic interface (15-19), so it is conceivable to think they have the existing molecular machinery to occupy vacant synaptic contacts.

I also went on to show in Chapter 3 that the phosphorylation of signal transducer and activator of transcription 3 (pSTAT3) by Janus Kinase 2 (JAK2) and the epidermal growth factor receptor (EGFR) are necessary arbiters of the GSP response. Given that both are known to mediate reactive astrogliosis (20-21), this suggest that GSP could be thought of as a focal resolving reactivity gliosis response (22). As the name implies, resolving reactivity occurs when the signal inducing astrogliosis ceases. In the case of GSP, 2Phatal results where replacement processes appeared stable ten days following ablation at capillaries suggest a signal would cease once a vascular vacancy is occupied by surrounding astrocytes. Likewise, showing that GSP occurs specifically in locations of lost astrocyte-vascular contact following reperfusion post transient-focal photothrombotic stroke further suggest this. While there appeared to be a gliosis response due to stroke, GSP specifically occurred only in locations of lost astrocyte vascular contact, and this was stable up to six days post-stroke induction. Together, these studies support the idea that GSP can be thought of as a focal resolving reactivity gliosis response, and they also suggest that other molecules implicated in gliosis like β1-integrin (23) should be investigated as well.

In closing, years of research effort combined with this thesis reveal that astrocyte endfeet are functional domains worthy of deliberate investigation. Their contributions to normal brain physiology cannot be overstated. The future truly looks bright when considering the plethora of questions to be answered regarding astrocyte endfoot development and contribution to disease.

References

1. Zlokovic BV. Neurovascular pathways to neurodegeneration in Alzheimer's disease and other disorders. *Nat Rev Neurosci.* 2011;12:723–738.
2. Watanabe K, Takeishi H, Hayakawa T, Sasaki H. Three-dimensional organization of the perivascular glial limiting membrane and its relationship with the vasculature: a scanning electron microscope study. Okajimas folia anatomica Japonica. 2010; 87: 109-121
3. Obermeier B, Daneman R, & Ransohoff RM. Development, maintenance and disruption of the blood-brain barrier. Nat Medicine. 2013; 19: 1584-1596. Doi: 10.1038/nm.3407.
4. Lee SW, et al. SSeCKS regulates angiogenesis and tight junction formation in the blood-brain barrier. Nat Medicine. 2003;9:900-906.
5. Wang Y, Imitola J, Rasmussen S, O'Connor KC, & Khoury, SJ. Paradoxical dysregulation of the neural stem cell pathway sonic hedgehog-Gli1 in autoimmune encephalomyelitis and multiple sclerosis. Ann Neurol. 2008; 64: 417-427. Doi: 10.1002/ana.21457.
6. Alvarez JI, et. Al. The Hedgehog pathway promotes blood-brain barrier integrity and CNS immune quiescence. Science. 2011; 334: 1727-1731. Doi: 10.1126/science.1206936.
7. Daneman R, & Engelhardt B. Brain barriers in health and disease. Neurobiol Dis. 2017; 107: 1-3.doi: 10.1016/j.nbd.2017.05.008.
8. Watkins S, Robel S, Kimbrough IF, Robert SM, Ellis-Davies G, Sontheimer H. Disruption of astrocyte-vascular coupling and the blood-brain barrier by invading glioma cells. Nature Communications, 5, 4196. doi: 10.1038/ncomms5196
9. Kimbrough IF, Robel S, Roberson ED, Sontheimer H. Vascular amyloidosis impairs the gliovascular unit in a mouse model of Alzheimer's disease. Brain, 138(12). doi: 10.1093/brain/awv327.
10. Hill RA, Damisah EC, Chen F, Kwan AC, Grutzendler J. Targeted two-photon chemical apoptotic ablation of defined cell types in vivo. Nature Communications. 2017; 8, 15837. doi: 10.1016/j.bbrc.2016.08.088.
11. Argaw AT, Asp L, Zhang J, et al. Astrocyte-derived VEGF-A drives blood-brain barrier disruption in CNS inflammatory disease. *J Clin Invest*. 2012;122(7):2454-2468. doi:10.1172/JCI60842
12. Zhang Y, Chen K, Sloan SA, Bennett ML, Scholze AR, O'Keefe S, Phatnani HP, Guarnieri P, Caneda C, Ruderisch N, Deng S, Liddelow SA, Zhang C, Daneman R, Maniatis T, Barres BA, Wu JQ. An RNA-sequencing Transcriptome and Splicing Database of Glia, Neurons, and Vascular Cells of the Cerebral Cortex. *J Neurosci*. 2014; 34(36): 464-477. doi: 10.1111/jnc.14068.
13. Spampinato SF, Merlo S, Sano Y, Kanda T, Sortino MA. Astrocytes contribute to Aβ-induced blood-brain barrier damage through activation of endothelial MMP9. *Journal of Neurochemistry*. 2017; 142(3): 464-477. doi: 10.1111/jnc.14068.
14. Bindocci E, Savtchouk I, Liaudet N, Becker D, Carriero G, Volterra A. Three-dimensional Ca^{2+} imaging advances understanding of astrocyte biology. *Science*. 19 May 2017; 356(6339). doi: 10.1126/science.aai8185
15. Stogsdill, J. A., Ramirez, J., Liu, D., Kim, Y. H., Baldwin, K.T., Enustun, E., et al. (2017).Astrocytic neuroligins control astrocyte morphogenesis and synaptogenesis.Nature551,192–197. doi: 10.1038/nature2463824.
16. Theodosis, D. T. (2002). Oxytocin-secreting neurons: a physiological model of morphological neuronal and glial plasticity in the adult hypothalamus.Front.Neuroendocrinol.23, 101–135. doi: 10.1006/frne.2001.022625.
17. Procko, C., Lu, Y., and Shaham, S. (2011). Glia delimit shape changes of sensory neuron receptive endings in C. elegans. Development138, 1371–1381. doi:10.1242/dev.05830526.
18. Tatsumi, K., Okuda, H., Morita-Takemura, S., Tanaka, T., Isonishi, A., Shinjo, T., et al.(2016). Voluntary exercise induces astrocytic structural plasticity in the globus pallidus.Front. Cell. Neurosci.10:165. doi: 10.3389/fncel.2016.00165

19. Bellesi, M., de Vivo, L., Chini, M., Gilli, F., Tononi, G., and Cirelli, C. (2017). Sleep loss promotes astrocytic phagocytosis and microglial activation in mouse cerebral cortex.J.Neurosci.37, 5263–5273. doi: 10.1523/JNEUROSCI.3981-16.2017
20. Herrmann, J.E., Imura, T. Song, B., Qi, J., Ao, Y., Nguyen, T.K., Korsak, R.A., Takeda, K.,Akira, S., Sofroniew, M.V. STAT3 is a Critical Regulator of Astrogliosis and Scar Formation after Spinal Cord Injury. The Journal of Neuroscience. 2008; 28(28):7231-7243. doi:10.1523/JNEUROSCI.1709-08.2008
21. Li, ZW., Li, JJ., Wang, L.et al.Epidermal growth factor receptor inhibitor ameliorates excessive astrogliosis and improves the regeneration microenvironment and functional recovery in adult rats following spinal cord injury.J Neuroinflammation11, 71 (2014).https://doi.org/10.1186/1742-2094-11-7129.
22. Sofroniew, M. V. (2020). Astrocyte Reactivity: Subtypes, States, and Functions in CNS Innate Immunity. Trends in Immunology,41(9), 758–770
23. Robel S, Mori T, Zoubaa S, Jürgen S, Sirko S, Faissner A, Goebbels S, Dimou L, & Götz M. Conditional deletion of β1-integrin in astroglia causes partial reactive gliosis. *Glia*. 16 April 2009: 57; 1630-1647. doi: 10.1002/glia.20876